[redacted]

MARTIN MARIETTA ENERGY SYSTEMS LIBRARIES
3 4456 0360998 6

CENTRAL RESEARCH LIBRARY
DOCUMENT COLLECTION

AEC RESEARCH AND DEVELOPMENT REPORT

ORNL-1940
Progress

Cy. 4A

CHEMISTRY DIVISION

SEMIANNUAL PROGRESS REPORT

FOR PERIOD ENDING JUNE 20, 1955

CENTRAL RESEARCH LIBRARY
DOCUMENT COLLECTION

LIBRARY LOAN COPY

DO NOT TRANSFER TO ANOTHER PERSON

If you wish someone else to see this document, send in name with document and the library will arrange a loan.

OAK RIDGE NATIONAL LABORATORY
OPERATED BY
UNION CARBIDE NUCLEAR COMPANY
A Division of Union Carbide and Carbon Corporation
UCC
POST OFFICE BOX P · OAK RIDGE, TENNESSEE

[redacted]

[redacted]

[redacted]

[redacted]

ORNL-1940

This document consists of 94 pages.
Copy 4 of 147 copies. Series A.

Contract No. W-7505-eng-26

CHEMISTRY DIVISION

SEMIANNUAL PROGRESS REPORT

for Period Ending June 20, 19[redacted]

E. H. Taylor, Director
M. A. Bredig, Associate Director

DECLASSIFIED

CLASSIFICATION CHANGED TO:
BY AUTHORITY OF: TID-1148
BY: G. Morrison 7/24/57

DATE ISSUED

OCT 10 1955

OAK RIDGE NATIONAL LABORATORY
Operated by
UNION CARBIDE NUCLEAR COMPANY
A Division of Union Carbide and Carbon Corporation
Post Office Box P
Oak Ridge, Tennessee

[redacted]

MARTIN MARIETTA ENERGY SYSTEMS LIBRARIES
3 4456 0360998 6

[redacted]

INTERNAL DISTRIBUTION

[redacted]

1. C. E. Center
2. logy Library
3. h Physics Library
4-6. Ce Research Library
7-12. Labo y Records Department
13. Laborat Records, ORNL R. C.
14. Reactor E imental Engineerin brary
15. C. E. Larson
16. L. B. Emlet (K-2
17. J. P. Murray (Y-12)
18. A. M. Weinberg
19. E. H. Taylor
20. E. J. Murphy
21. E. D. Shipley
22. S. C. Lind
23. F. C. VonderLage
24. W. H. Jordan
25. J. A. Swartout
26. F. L. Culler
27. A. H. Snell
28. A. Hollaender
29. M. T. Kelley
30. G. H. Clewett
31. K. Z. Morgan
32. T. A. Lincoln
33. A. S. Householder
34. C. S. Harrill
35. C. E. Winters
36. D. W. Cardwell
37. E. M. King
38. J. A. Lane
39. G. E. Boyd
40. M. A. Bredig
41. R. W. Stoughton
42. R. B. Briggs
43. G. W. Parker
44. C. J. Borkowski
45. G. H. Jenks
46. K. A. Kraus
47. H. A. Levy
48. R. S. Livingston
49. T. E. Willmarth
50. C. H. Secoy
51. C. J. Hochanadel
52. W. H. Baldwin
53. A. R. Brosi
54. R. N. Lyon
55. S. A. Reynolds
56. P. F. Thomason
57. E. G. Bohlmann
58. C. P. Keim
59. C. D. Susano
60. D. D. Cowen
61. P. M. Reyling
62. R. Livingston
63. G. H. Cartledge
64. E. R. Van Artsdalen
65. G. C. Williams
66. R. W. Johnson
67. S. D. Schiffman (K-25)
68. E. P. Wigner (consultant)
69. S. J. Cromer
M. J. Skinner
7 D. S. Billington
72. A. Charpie
73. H MacPherson (consultant)
74. J. L abbard
75. R. W. lson (consultant)
76. H. Eyrin onsultant)
77. V. Schomak (consultant)
78. J. W. Kenned onsultant)
79. G. T. Seaborg (sultant)
80. R. R. Dickison

[redacted]

[redacted]

EXTERNAL DISTRIBUTION

81[redacted] Argonne National Laboratory
89-9[redacted]tomic Energy Commission, Washington
97-100. [redacted]okhaven National Laboratory
101-104. du[redacted] Company, Wilmington
105-106. Knoll[redacted]omic Power Laboratory
107-112. General [redacted]ctric Company, Richland
113. Phillips P[redacted]eum Company (NRTS)
114-117. Los Alamos S[redacted]tific Laboratory
118. Mound Laborator[redacted]
119-121. New York Operatio[redacted]ffice
122. Patent Branch, Washi[redacted]n
123. Savannah River Operatio[redacted]Office, Augusta
124-138. Technical Information Servi[redacted]Oak Ridge
139-142. University of California Radia[redacted]Laboratory, Berkeley
143-144. Bettis Plant (WAPD)
145. Iowa State College
146. Division of Research and Medicine, A[redacted]RO
147. North American Aviation, Inc.

[redacted]

[redacted]

Chemistry Division progress reports previously issued in this series are as follows:

ORNL-65	March, April, May, 1948
ORNL-176	June, July, August, 1948
ORNL-229	September, October, November, 1948
ORNL-336	December, 1948, January and February, 1949
ORNL-286	Period Ending June 30, 1949
ORNL-499	Period Ending September 30, 1949
ORNL-607	Period Ending December 31, 1949
ORNL-685	Period Ending March 31, 1950
ORNL-795	Period Ending June 30, 1950
ORNL-870	Period Ending September 30, 1950
ORNL-1036	Period Ending December 31, 1950
ORNL-1053	Period Ending March 31, 1951
ORNL-1116	Period Ending June 30, 1951
ORNL-1153	Period Ending September 30, 1951
ORNL-1260	Period Ending December 31, 1951
ORNL-1285	Period Ending March 31, 1952
ORNL-1344	Period Ending June 30, 1952
ORNL-1432	Period Ending September 30, 1952
ORNL-1482	Period Ending December 31, 1952
ORNL-1587	Period Ending June 20, 1953
ORNL-1674	Period Ending December 20, 1953
ORNL-1755	Period Ending June 20, 1954
ORNL-1832	Period Ending December 20, 1954

[redacted]

[redacted]

CONTENTS

CHEMISTRY DIVISION PUBLICATIONS FROM DECEMBER 20, 1954 TO JUNE 20, 1955 vii

SUMMARY 1

INORGANIC AND PHYSICAL CHEMISTRY 5
- Anion-Exchange Studies 5
- Ultracentrifugation of Inorganic Systems 5
- Chemistry of Corrosion 6
  - Inhibition by the Pertechnetate Ion 6
  - Electrochemistry of Stainless Steel 10
- Emf Measurements at Elevated Temperatures 11
- Chemistry of Fused Salts 12
  - Electrical Conductance and Density 12
  - Self-Diffusion in Molten Salts 13
  - Cryoscopy 14
  - High-Temperature Calorimetry 17
- High-Temperature and Structural Chemistry 17
  - Miscibility of Liquid Metals with Salts 17
  - Molar Volume and Structure of Molten Alkali Halides 19

NUCLEAR CHEMISTRY 20
- Production and Identification of Long-lived Technetium Isotopes at Masses 97, 98, and 99 20
- Short-lived Fission Products 21
  - Radiations of 44-sec Rh^{104} and 15-sec Tc^{100} 21
  - Short-lived Isotopes of Rubidium 22
- Radioactivity of the Ce^{137} Isomers 27
  - Isomeric Transition in Ce^{137} 27
  - Electron Capture Decay of Ce^{137} 28
  - Discussion 28

ORGANIC CHEMISTRY 30
- Pinacol Rearrangement of Triphenylethylene Glycol 30
- Reaction of 2-Phenyl-2-*p*-tolylethyl-1-C^{14}-amine with Nitrous Acid – A Reinvestigation 32
- Pinacol Rearrangement of 1,2-Diphenyl-1-*p*-tolylethylene Glycol 33
- Isotope Fractionation Studies 36
  - Examination of the Isotope Effect in the Condensation of *o*-Benzoylbenzoic Acid-carboxyl-C^{14} to Anthraquinone-9-C^{14} 36
  - Study of C^{13} Isotope Fractionation in Brominative Decarboxylation of 3,5-Dibromo-4-hydroxybenzoic Acid 36

CHEMICAL PHYSICS 39
- X-Ray Diffractometer for Liquid Studies 39
- High-Speed Computation of the Absorption Correction Used in Diffraction Studies 40
- Neutron Diffraction Study of $Ca(OH)_2$ 43
- Surface Ionization of Alkali Metals and Halides on Tungsten and Platinum 44
- Paramagnetic Resonance Studies of Electric Discharge Products 44
- Paramagnetic Resonance Studies on Atomic Hydrogen 46
- Microwave Spectroscopy 46

[redacted]

[redacted]

CHEMISTRY OF SEPARATION PROCESSES 47
Fundamental Studies on Ion-Exchange Resins 47
Osmotic Coefficients of Strong-Base Anion Exchangers and the Structure of the Exchange Ion 47
Osmotic Coefficients of Multivalent Cation Forms of Strong-Acid Exchanger 48
Moisture Isotherms of Sulfonium-Type Anion Exchangers 50
Interaction Between Tributyl Phosphate Solvent and Monovalent Electrolyte Solutes 52
P^{32} in Neutron-irradiated KH_2PO_4 57
Distribution of Neptunium in the Purex Metal-Recovery Process 57
Metal-Recovery Flow Plan 58
Trial Material Balances of Neptunium Through Typical Plant Runs 58
Discussion 60

RADIATION CHEMISTRY 61
Radiation Studies on Nitrate Solutions 61
Effect of Acidity on the Decomposition of Nitrate Solutions 61
Effect of Temperature on the Reactor Decomposition of Nitrate Solutions 61
Effect of Acidity on Nitrite Formation in Concentrated Nitrate Solutions 63
Radiation Chemistry of Ceric Ion 64
Effect of Thallous Ion 64
Direct Action of Cobalt Gamma Radiation 65
Radiation Chemistry of Sulfuric Acid 65
Radiation Chemistry of Organic Substances 66
Gas-Phase Irradiation 68

REACTOR CHEMISTRY 70
Investigation of the Alkali or Alkaline-Earth Oxide–Uranium Trioxide–Carbon Dioxide–Water Phase Equilibria at High Temperature 70
Experimental 70
The Systems UO_3-H_2O and UO_2CO_3-H_2O 72
The System (MO or M_2O)-UO_3-CO_2-H_2O – General Discussion 72
The System Na_2O-UO_3-CO_2-H_2O 73
The System MgO-UO_3-CO_2-H_2O 73
The System Li_2O-UO_3-CO_2-H_2O 74
Summary and Conclusions 76
The Base-saturated Region of the System CuO-UO_3-SO_3-H_2O at 100°C 79
Experimental Methods 79
Data and Discussion 80

[redacted]

[redacted]

CHEMISTRY DIVISION PUBLICATIONS FROM DECEMBER 20, 1954 TO JUNE 20, 1955

UNCLASSIFIED PUBLICATIONS

Inorganic and Physical Chemistry

G. H. Cartledge, "The Pertechnetate Ion as an Inhibitor of Corrosion," *J. Am. Chem. Soc.* **77,** 2658 (1955).

M. H. Lietzke and J. V. Vaughen, "The Behavior of the Silver, Silver Chloride and the Mercury, Mercurous Chloride Electrodes at High Temperatures," *J. Am. Chem. Soc.* **77,** 876 (1955).

M. H. Lietzke, "The Hydrogen Electrode–Silver Chloride Electrode System at High Temperatures and Pressures," *J. Am. Chem. Soc.* **77,** 1344 (1955).

F. Nelson and K. A. Kraus, "Anion-exchange Studies. XII. Adsorption of Acids by Strong Base Anion-exchange Resins in Polyvalent Forms. Separation of Weak and Strong Acids," *J. Am. Chem. Soc.* **77,** 329 (1955).

F. Nelson and K. A. Kraus, "Anion Exchange Studies. XIII. The Alkaline Earths in Citrate Solutions," *J. Am. Chem. Soc.* **77,** 801 (1955).

F. Nelson, "Anion-exchange Studies. XIV. The Alkali Metals in Ethylenediaminetetraacetic Acid Solutions," *J. Am. Chem. Soc,* **77,** 813 (1955).

K. A. Kraus and G. E. Moore, "Anion-exchange Studies. XV. Separation of Protactinium and Iron by Anion-exchange in HCl-HF Solutions," *J. Am. Chem. Soc.* **77,** 1383 (1955).

K. A. Kraus, F. Nelson, F. B. Clough, and R. C. Carlston, "Anion Exchange Studies. XVI. Adsorption from Lithium Chloride Solutions," *J. Am. Chem. Soc.* **77,** 1391 (1955).

E. R. Van Artsdalen and I. S. Yaffe, "Electrical Conductance and Density of Molten Salt Systems: KCl-LiCl, KCl-NaCl and KCl-KI," *J. Phys. Chem.* **59,** 118 (1955).

A. S. Dworkin and D. J. Sasmor, "Low Temperature Specific Heats of Layered Lattices," *J. Tenn. Acad. Sci.* **30,** 32 (1955).

A. S. Dworkin, D. J. Sasmor, and E. R. Van Artsdalen, "The Low Temperature Heat Capacity and Entropy of Cadmium Iodide," *J. Am. Chem. Soc.* **77,** 1304 (1955).

D. Smith, A. S. Dworkin, and E. R. Van Artsdalen, "The Heats of Combustion and Formation of Boron Carbide," *J. Am. Chem. Soc.* **77,** 2654 (1955).

M. A. Bredig, J. W. Johnson, and Wm. T. Smith, Jr., "Miscibility of Liquid Metals with Salts. I. The Sodium–Sodium Halide Systems," *J. Am. Chem. Soc.* **77,** 307 (1955).

M. A. Bredig, H. R. Bronstein, and Wm. T. Smith, Jr., "Miscibility of Liquid Metals with Salts. II. The Potassium–Potassium Fluoride and Cesium–Cesium Halide Systems," *J. Am. Chem. Soc.* **77,** 1454 (1955).

J. W. Johnson, P. A. Agron, and M. A. Bredig, "Molar Volume and Structure of Solid and Molten Cesium Halides," *J. Am. Chem. Soc.* **77,** 2734 (1955).

M. A. Bredig, G. E. Klein, and B. S. Borie, Jr., "X-Ray Diffractometer for Highly Radioactive Materials," *Rev. Sci. Instr.* **26,** 610 (1955).

R. H. Busey, *A Combination Isothermal-Adiabatic Low-Temperature Calorimeter,* ORNL-1828 (Jan. 26, 1955).

Organic Chemistry

C. J. Collins and W. A. Bonner, "Molecular Rearrangements. III. The Mechanism of the Wagner–Meerwein Rearrangement in the 1,2,2-Triphenylethyl System," *J. Am. Chem. Soc.* **77,** 92 (1955).

[redacted]

[redacted]

W. A. Bonner and C. J. Collins, "Molecular Rearrangements. IV. Triple-labeling Experiments on the Isotope Position Isomerization of 1,2,2-Triphenylethyl Acetate," *J. Am. Chem. Soc.* **77,** 99 (1955).

R. M. Roberts, G. A. Ropp, and O. K. Neville, "The Action of Aluminum Chloride on Ethyl-β-C^{14}-benzene," *J. Am. Chem. Soc.* **77,** 1764 (1955).

M. T. Clark, E. C. Hendley, and O. K. Neville, "C^{14}-Tracer Studies in the Rearrangements of Unsymmetrical α-Diketones. V. Substituted Benzils," *J. Am. Chem. Soc.* **77,** 3280 (1955).

Chemical Physics

C. A. Burrus and W. Gordy (Duke University), B. Benjamin, and R. Livingston, "One-to-Two Millimeter Wave Spectra of TCl and TBr," *Phys. Rev.* **97,** 1661 (1955).

Chemistry of Separation Processes

B. Soldano and Q. V. Larson, "Osmotic Behavior of Anion and Cation Exchangers," *J. Am. Chem. Soc.* **77,** 1331 (1955).

B. Soldano and D. Chesnut, "The Osmotic Approach to Ion-exchange Equilibrium. I. Anion Exchangers," *J. Am. Chem. Soc.* **77,** 1334 (1955).

B. Soldano, Q. V. Larson, and G. E. Myers, "The Osmotic Approach to Ion-exchange Equilibrium. II. Cation Exchangers," *J. Am. Chem. Soc.* **77,** 1339 (1955).

B. Soldano, *J. Am. Chem. Soc.* **77,** 2918 (1955); review of book by A. Opler and N. K. Hiester, entitled *Tables for Predicting the Performance of Fixed Bed Ion Exchange and Similar Mass Transfer Processes*, Wiley and Sons, New York, 1955.

Radiation Chemistry

T. J. Sworski, "Yields of Hydrogen Peroxide in the Decomposition of Water by Cobalt γ-Radiation. II. Effect of Chloride Ion," *Radiation Research* **2,** 26 (1955).

T. J. Sworski, "A Mechanism for the Photo-Oxidation of Water by Ceric Ion," *J. Am. Chem. Soc.* **77,** 1074 (1955).

C. J. Hochanadel, J. A. Ghormley, and T. J. Sworski, "The Decomposition of Sulfuric Acid by Cobalt γ-Rays," *J. Am. Chem. Soc.* **77,** 3215 (1955).

CLASSIFIED PAPERS

G. W. Parker, G. E. Creek, P. M. Lantz, and W. J. Martin, *Preparation of Kilocurie Quantities of Xenon-135*, BNL-302, p 37–44 (December 1954).

J. Halperin, R. W. Stoughton, D. E. Ferguson, D. C. Overholt, and C. M. Stevens, "An Effective Capture Cross Section of Np^{239} for Thermal Pile Neutrons," *Nuclear Sci. Technol.* **1,** 209 (1955).

[redacted]

[redacted]

CHEMISTRY DIVISION SEMIANNUAL PROGRESS REPORT

SUMMARY

INORGANIC AND PHYSICAL CHEMISTRY

Continued work on the adsorbability of metal complexes from concentrated LiCl solutions and LiCl-HCl mixtures on a strong-base anion-exchange resin further demonstrated the much higher adsorbability of these complexes from LiCl solutions than from HCl solutions. The effect is believed to be due to the formation of less strongly adsorbed undissociated chloro-complex acids in the case of the HCl solutions.

Ultracentrifugation of Th(IV) in 1 *M* NaCl and in 1 *M* $NaClO_4$ solutions as a function of acidity confirmed the observation previously reported that aggregates of much higher degrees of polymerization are present in chloride media than in perchlorate media containing thorium hydrolyzed to the same extent. All solutions are polydisperse, and there is no indication of the existence of species of preferred stability.

As part of a general emf study in aqueous solution at elevated temperature, the potentials of the cell In, $In_2(SO_4)_3(m)$, Ag_2SO_4(sat.), Ag were measured from 15 to 70°C, with the $In_2(SO_4)_3$ concentration varying from 0.01 to 2.3 *m*.

Observations on carbon steel specimens inhibited by potassium pertechnetate have now extended over a period of 30 months, with no evidence of corrosion or exhaustion of the inhibitor from solution. Experiments in the presence of added electrolytes agree with electrode potentials in showing that a weak, reversible adsorption of the inhibitor is involved, rather than a firm binding of adsorbed particles. Further experiments with the perrhenate ion confirm the previous conclusion that it differs radically from the pertechnetate ion with respect to inhibition. The electrode potentials observed with electrolytic iron in perrhenate solutions are in agreement with the corrosion experiments. The electrode potential for the half-reaction

$$(Pt)TcO_2(c) + 2H_2O \rightleftharpoons TcO_4^-(aq) + 4H^+ + 3e$$

was determined in the absence of air, the E^0 value being -0.738 ± 0.003 v. Further studies on the electrochemistry of stainless steel showed that carbon monoxide acts differently from oxygen with respect to the corrosion and electrode potential of stainless steel in 0.1 *N* H_2SO_4 at 85°C. Experiments with radioactive iron also demonstrated the participation of Fe(III) ions in the electrode reaction associated with the ennobling process.

Density and electrical conductance data are presented for nearly all the molten pure alkali halides, with the exception of the fluorides. The heat of activation for equivalent conductance generally varies approximately linearly with temperature; the entropy of activation is in the range of −6 to −7 cal/mole·deg and is nearly independent of temperature. Reasonable theoretical interpretations account for these results. Data are presented for the self-diffusion coefficient of sodium ion in molten sodium nitrate. Freezing-point-depression measurements demonstrated that a number of halides, such as cadmium chloride and lead chloride, are incompletely dissociated in molten nitrates. The addition of chloride ion from neutral salts, for example, NaCl, $CaCl_2$, LiCl, etc., demonstrated for the first time the existence of the common-ion effect in molten salt solutions. It was shown that a chloro-cadmium complex containing at least four chlorines exists in molten sodium nitrate. Final calibrations are in progress with the high-temperature adiabatic heat-capacity calorimeter.

Equipment was constructed for the determination of vapor pressures and for the measurement of electrical conductance in liquid metal–fused salt solutions. One first result obtained seems indicative of a very slow rate of increase in conductivity with addition of potassium metal – much smaller than additive behavior would require. Careful extrapolation of molar volumes of the solid alkali halides permitted a more reliable evaluation of the expansion occurring in the alkali halides on melting. The data thus obtained suggest changes, varying in degree, in ionic coordinations to values lower than 6 in the lithium and sodium salts, that is, changes similar to the coordination decreases from 8 to approximately, or slightly more than, 6 in CsBr and CsI.

[redacted]

NUCLEAR CHEMISTRY

A hitherto "missing" technetium isotope was prepared in the 86-in. cyclotron and was identified by means of a mass spectrometer. This isotope may be of importance in connection with the problem of the existence of primordial technetium on the crust of the earth, since its half life appears to be long. The discovery of this isotope completes our knowledge of the nuclear chemistry of technetium, which program has been conducted during the past eight years.

The decays of Rh^{104}, Tc^{100}, Rb^{88}, and Rb^{89} were studied by scintillation spectroscopy. A brief description of the instruments and techniques used for the investigation of these short-lived nuclides is included.

In the decay of 44-sec Rh^{104}, the most energetic beta-ray component was found to have an energy of 2.41 ± 0.05 Mev. The principal gamma-ray transition of energy 0.556 ± 0.007 Mev is present in low intensity.

The decay of 15-sec Tc^{100} was found to include a 2.86 ± 0.05 Mev ground state beta-ray transition and a prominent 0.542 ± 0.008 Mev gamma ray.

Nuclear levels in Sr^{88} were studied by means of the gamma radiation following the decays of 17.8-min Rb^{88} and 104-day Y^{88}. Gamma rays of energies 0.908 ± 0.005, 1.39, 1.85 ± 0.008, 2.11, 2.68, 3.01, 3.24, 3.52, 3.68, and 4.87 Mev were resolved and fitted into a level scheme with the assistance of coincidence spectroscopy. Comparative half lives of the beta-ray transitions feeding the levels were determined from the gamma-ray intensities; parities were assigned to all levels, and possible spin assignments were made.

The decay of 15.4-min Rb^{89} was found to excite gamma-ray transitions in Sr^{89} with energies of 0.663, 1.05, 1.26, 1.55, 2.20, and 2.55 Mev. Some evidence was also obtained for gamma rays having energies of 1.95 and 2.7 Mev. A level scheme is proposed which is consistent with these gamma-ray energies and with coincidence experiments. The energy of the beta-ray transition from Rb^{89} to the ground state of Sr^{89} was determined to be 3.92 ± 0.10 Mev.

A cerium isotope with an 8.7-hr half life was assigned to Ce^{137} and was shown to decay by electron capture, with about 3% of the captures to a 445-kev level in La^{137}. The 34.5-hr decay period previously characterized as electron capture of Ce^{137} is an isomeric transition from a 255-kev level in Ce^{137}. Spin assignments consistent with the experimental data indicate that the transition between ground states of La^{137} and Ba^{137} should be allowed. However, the *K* or *L* electron capture half life of La^{137} was found to be greater than 10^5 years.

ORGANIC CHEMISTRY

The pinacol rearrangement of triphenylethylene glycol was studied by means of multiple-labeling and carrier techniques. The contribution of each of four reaction paths was calculated under a variety of reaction conditions. The phenyl/hydrogen migration ratios were shown to vary from 7.33 in concentrated sulfuric acid to 0.04 in dilute aqueous dioxane–hydrochloric acid mixtures.

A previously reported anomalous *p*-tolyl/phenyl migration ratio of less than 1 in the deamination of 2-phenyl-2-*p*-tolylethylamine was shown to be incorrect. New values for this ratio determined by two independent methods are 1.22 and 1.25.

The α- and β-forms of 1,2-diphenyl-1-*p*-tolylethylene glycol were shown to rearrange in formic acid to give yields of 88 and 12%, respectively, of *p*-tolyldesoxybenzoin and *p*-tolylbenzhydryl ketone. The yields of these same products are 85 and 15%, respectively, when concentrated sulfuric acid is used as the catalyst. Less than 5% secondary hydroxyl removal occurs under either of these conditions.

The "reverse isotope effect" in the ring closure of *o*-benzoylbenzoic acid-carboxyl-C^{14} reported by others was shown to be nonexistent. The isotope effect in the brominative decarboxylation of 3,5-dibromo-4-hydroxybenzoic acid has been determined and is consistent with the mechanism which was previously proposed.

CHEMICAL PHYSICS

The results of an experimental study of surface ionization of the alkali metals and of the potassium halides on tungsten and platinum are summarized.

The construction of an x-ray diffractometer designed specifically for studies on the structure of liquids, including fused salts, was completed. The instrument provides for simultaneous angular motion of the x-ray tube and the detector on arms moving about a horizontal axis lying in the liquid surface. This makes it possible to work with

liquids with a free surface where sample-holder absorption and scattering are eliminated.

A method of computing, by means of the Oracle, the absorption correction used in x-ray and neutron diffraction studies is described. The details of the crystal structure and of the thermal motion of the ions in $Ca(OH)_2$ were determined by neutron diffraction.

An analytical procedure was developed in which paramagnetic resonance was used for determining the number of unpaired electrons in samples containing free radicals. A free radical formed by condensing the products of electric discharges through water vapor and through hydrogen, with subsequent addition of oxygen, was found to be present in high concentration; the radical may be HO_2.

A cryostat was built and was used for studying the rate at which atomic hydrogen disappears in warmed samples of various acids where the initial atomic hydrogen was produced by gamma irradiation at liquid-nitrogen temperature.

CHEMISTRY OF SEPARATION PROCESSES

Investigations were continued into the nature of the exchange process; isopiestic measurements were made on several resins of differing structures containing exchanging ions of different size and shape.

Previously obtained osmotic coefficients for a variety of monovalent exchanger salts of the strong-base anion exchanger Dowex 1 were analyzed mathematically. The results served to confirm the previous conclusion that no generalization exists which would describe the concentration dependence of osmotic coefficients in terms of simple parameters dependent upon ion size and shape.

Osmotic coefficients of multivalent cation salt forms of the strong-acid exchanger Dowex 50 are, in general, found not to have the same concentration dependence as the monovalent salt forms of Dowex 50 and Dowex 1. Among the divalent cation forms there appears to be a qualitative relation between osmotic coefficient, that is, degree of dissociation, and the free energies of hydration of the cations.

Moisture isotherms of a number of monovalent anion salts of a strong-base sulfonium-type anion exchanger demonstrate that the degree of ionic association, in general, follows the same series that occurs with the salts of Dowex 1, indicating that no specific ionic interactions occur in either resin. The shape of the isotherms leads to the further conclusion that the positive sulfonium group is considerably more hydrated than the positive quaternary ammonium group of Dowex 1.

The Scatchard-Hildebrand theory was used to define the distribution of HCl between water and tributyl phosphate up to 9 *N* HCl in the aqueous phase. The presence of water in the organic phase is important, as it hydrates both the tributyl phosphate and the electrolyte. Thus hydrogen bonding plays a significant role in solvent extraction.

Neutron irradiation of KH_2PO_4 produced P^{32} that was found in orthophosphate, pyrophosphate, triphosphate, and two components that have not yet been identified.

A trial material balance of the distribution of Np^{237} in the current Purex metal-recovery program accounted for slightly more than 30% of that found in the dissolved metal. On the basis of numerous batch-type distribution experiments and valence determinations, it was expected that a relatively large portion of the neptunium would appear in the first column waste; however, only about 10% was found. Studies are in progress to account for this discrepancy.

RADIATION CHEMISTRY

In the reactor decomposition of U^{235}-enriched, concentrated thorium nitrate solutions, the yields of nitrogen and hydrogen were independent of temperature in the range 135 to 250°C. The nitrogen yield increased with increasing nitrate concentration but was independent of pH in the range 0.5 to 11. Extensive studies of the gamma-ray decomposition of concentrated nitrate solutions indicated reduction to nitrite by "direct action" on the nitrate. A sudden increase in nitrite yield in the pH range 11 to 13 was attributed to ionization of OH to O^-, which reduced the nitrate.

The radiation chemistry of Ce(IV)–Tl(I) mixtures in sulfuric acid solutions is under detailed investigation. The effect of nitrate ion on the radiation-induced reduction of Ce(IV) in this mixture unequivocally demonstrates nitrate ion reduction by direct action of radiation. The study of this mixture has also yielded an evaluation of

the radical yield in sulfuric acid solutions up to 20.0 *N* sulfuric acid.

The radiation decomposition of substituted butanes is under investigation. Mass spectrometric analysis of the gaseous decomposition products of tri-*n*-butyl phosphate showed about 17% isomerization of the butyl group. This is about the amount expected on the basis of positive butyl ions as intermediates. In irradiated tri-*n*-butyl phosphate very little fragmentation of the butyl group occurred, whereas in di-*n*-butyl carbonate considerable fragmentation occurred.

Results are presented of studies on the polymerization of carbon monoxide, hydrocyanic acid, and benzene by alpha particles in the absence and presence of noble gases.

REACTOR CHEMISTRY

Preliminary solubility data were obtained for the systems Na_2O-UO_3-CO_2-H_2O, Li_2O-UO_3-CO_2-H_2O, and MgO-UO_3-CO_2-H_2O up to approximately 1000 psi of CO_2 at 250°C. Some deductions about the solid phases in equilibrium with the solutions and tentative phase diagrams are presented. The solubility of UO_3 or UO_2CO_3 as a function of CO_2 gas pressure and temperature from 150 to 290°C is given as an order of magnitude.

A study was almost completed of the solid-liquid phase equilibria in the four-component system CuO-UO_3-SO_3-H_2O at 100°C in the region in which the liquid is base-saturated. Except for a small uranium-rich region, data are presented for the entire phase diagram from total salt concentrations as low as about 4% up to salt concentrations as high as about 25%.

INORGANIC AND PHYSICAL CHEMISTRY

ANION-EXCHANGE STUDIES

F. Nelson K. A. Kraus
D. J. Coombe

Work continued on the adsorbability of metal complexes from concentrated LiCl solutions and from HCl-LiCl mixtures with a strong-base anion-exchange resin. In addition, the activity coefficients of LiCl in the resin phase were determined for this resin over a wide range of LiCl concentration by a method similar to that used to measure activity coefficients of HCl.[1] As with HCl, only small differences were found between the activity coefficients of LiCl in the resin and solution phases.

The fact that many metals adsorb from LiCl solutions as much as a hundred times more strongly[2] than from HCl solutions of the same concentration probably does not result, therefore, from differences in activity coefficients in the resin phase in these two media. More probably, this large adsorbability difference is due to the formation of less strongly adsorbed undissociated acids by negative chloro-complexes in hydrochloric acid.

Distribution coefficients of Au(III), an element which shows this "lithium chloride effect," were determined as a function of acidity at constant total molality (m = 10) in LiCl-HCl mixtures. The data could be fitted reasonably well by assuming the equilibrium

$$(1) \qquad HAuCl_4 \rightleftharpoons H^+ + AuCl_4^-$$

with concentration quotient $K_b^m = \sim 0.1$ (25°C) at this ionic strength.

ULTRACENTRIFUGATION OF INORGANIC SYSTEMS

J. S. Johnson K. A. Kraus
R. W. Holmberg

The study[3] of polymerization of Th(IV) as a function of its hydrolysis in perchlorate and chloride media is essentially complete. The marked increase of polymerization in the presence of chloride over that found in perchlorate for the same degree of hydrolysis is confirmed. The results for perchlorate media agree with those of Hietanen.[4]

The results are summarized in Table 1. Values of the degree of polymerization, $N_{Z,z'}$, are taken from the slopes, S_e, of plots of log Z^*/x vs x^2 (ref. 5), where x is the radius, and Z^* is the refractive index gradient attributable to the presence of the thorium salt. The values listed in the table are evaluated at $x^2 = \sim 42$ and 48 by the equation

$$(1) \qquad N_{Z,z'} = \frac{4.606\, RT\, S_e/\omega^2}{M_2'(1 - \bar{v}_2 \rho)} ,$$

where R is the gas constant, T the absolute temperature, ω the angular velocity, M_2' the molecular weight of the monomer unit, $\bar{v}$ the partial specific volume, and ρ the density of the solution.

The values of $N_{Z,z'}$ do not represent exactly either the weight-average or the Z-average degree of polymerization. Briefly, for an uncharged system, Eq. 1 yields Z-average degrees of polymerization,[5] which stress heavier species more than the weight-average degree of polymerization N_w, the quantity used here for comparison with other work. On the other hand, the values of $N_{Z,z'}$ are only partially corrected for charge, by assuming a maximum charge in computing $M_2'(1 - \bar{v}_2\rho)$ and neglecting the rest of the charge effect.[6] This error tends to compensate for the first; that is, it decreases computed values of the degree of polymerization. The numbers listed in the table should be good approximations to weight-averages.

The differences in the values at the different radii for the same experiment indicated that the solutions are quite polydisperse. There is no indication of the existence of species of preferred stability, such as that found earlier for Bi(III), Zr(IV), and Hf(IV).[3,7]

The results in chloride media are higher than in perchlorate, for the same degree of hydrolysis.

---

[1] K. A. Kraus and G. E. Moore, *J. Am. Chem. Soc.* 75, 1457 (1953).

[2] K. A. Kraus *et al*, *J. Am. Chem. Soc.* 77, 1391 (1955).

[3] J. S. Johnson, K. A. Kraus, and R. W. Holmberg, *Chem. Semiann. Prog. Rep. Dec. 20, 1954*, ORNL-1832, p 8.

[4] S. Hietanen, *Acta Chem. Scand.* 8, 1626 (1954).

[5] W. D. Lansing and E. O. Kraemer, *J. Am. Chem. Soc.* 57, 1369 (1935).

[6] J. S. Johnson, K. A. Kraus, and G. Scatchard, *J. Phys. Chem.* 58, 1034 (1954).

[7] J. S. Johnson, K. A. Kraus, and R. W. Holmberg, *J. Am. Chem. Soc.* (in press).

TABLE 1. POLYMERIZATION OF Th(IV)

Initial Molarity of Th(IV)	Hydroxyl Number	Medium	Equilibrium Obtained	Temperature (°C)	$N_{Z,z}$'	N_w from Hietanen*
0.015	1.00	1 *M* $NaClO_4$	Yes	31.9	2.0–2.8	3.1
0.015	1.00	1 *M* NaCl	Yes	30.1	3.0–6.4	
0.015	1.44	1 *M* NaCl	No**	30.1	22–45	
0.0075	1.50	1 *M* NaCl	Yes	28.1	42–60	
0.015	1.55	1 *M* $NaClO_4$	Yes	31.6	1.6–4.2	3.9
0.015	1.94	1 *M* $NaClO_4$	Yes	31.1	4.0–4.9	4.9
0.015	2.00	1 *M* NaCl	No	25.2	34–58	
0.015	2.40	1 *M* $NaClO_4$	Probably no	30.3	5.6–12.0	6.5
0.015	2.40	1 *M* $NaClO_4$	Yes	2.7	3.4–7.8	
0.0075	2.41	1 *M* NaCl	No	25.2	31–120	

*Hietanen listed number-average degrees of polymerization. The weight-average degrees of polymerization N_w were computed from her results.

**Values of $N_{Z,z}$' for cases in which equilibrium was not attained are minimum.

The difference at hydroxyl number 1.5 and above is especially striking, polymers in chloride solution being about a factor of 10 larger, even though in some cases the initial Th(IV) concentration is lower in the chloride medium. Apparently, chloride ions must be complexed by the polymers and contribute to stability of the aggregates.

The results in perchlorate media agree with those of Hietanen[4] within the approximations of the treatment. Her values were obtained by interpretation of hydrolytic data by the continuous polymerization theory of Sillén.[8] This mechanism thus seems to give a good picture of the distribution in the range of hydrolysis of Th(IV) studied here. The agreement between centrifugation and potentiometric studies contrasts with the sharp differences in values obtained by the two methods in the case of Bi(III).[3] For hydroxyl numbers less than 0.5, Hietanen's interpretation does not agree so closely as an earlier interpretation of the hydrolytic data.[9] Apparently, in early stages, aggregation is not so simple as postulated by Hietanen [a Th^{4+} core with $Th(OH)_3$ links].

A single centrifugation carried out at reduced temperature indicates that the apparent heat of polymerization is positive.

CHEMISTRY OF CORROSION

G. H. Cartledge

Inhibition by the Pertechnetate Ion

Periodic observations were continued with specimens of carbon steel inhibited in concentrations of from 5×10^{-5} to 5×10^{-4} *f* $KTcO_4$. The two specimens started in January 1953 remained completely free of corrosion, and their beta activities have continued to be essentially constant ever since stable values were obtained early in the experiment. After about three months, during which the temperature was alternated between 23°C and near 100°C, the samples have stood at room temperature, exposed to air.

As previously reported,[10,11] the experiments show that inhibition by the pertechnetate ion is almost surely not dependent upon a film of reaction

[8] L. G. Sillén, *Acta Chem. Scand.* 8, 299, 318 (1954).

[9] K. A. Kraus and R. W. Holmberg, *J. Phys. Chem.* 58, 325 (1954).

[10] G. H. Cartledge, *Chem. Semiann. Prog. Rep. Dec. 20, 1953*, ORNL-1674, p 14.

[11] G. H. Cartledge, *J. Phys. Chem.* (in press).

products but, rather, upon the presence of an adequate concentration of dissolved inhibitor, which, however, is not consumed on long exposure. In previous discussions of adsorption theories there has been some confusion concerning the degree of reversibility of the adsorption. Most of the recent work has been done with radioactive Cr^{51} in the form of the chromate ion, and the results have been complicated by the possibility of irreversible reduction of part of the inhibitor to insoluble chromium(III) oxide. Accordingly, a series of experiments was conducted with the pertechnetate ion to establish definitely the extent to which the process responsible for inhibition by this ion is reversible in direction (not necessarily reversible in the thermodynamic sense).

Two types of experiments were conducted which involved the effects of added electrolytes upon the inhibiting property of the pertechnetate ion and upon the electrode potential of electrolytic iron in a pertechnetate solution. As shown previously,[12] inhibition by the pertechnetate was lost in the presence of sufficient concentrations of hydrogen ions or other electrolytes. For the present study, the sulfate ion was selected, since it is an excellent flocculating agent for hydrous iron oxide and could hardly be suspected of peptizing a protective film. For a second ion of different charge type, the perrhenate ion was chosen because of its close similarity to the pertechnetate ion in most respects.

The inhibiting concentrations of potassium pertechnetate are so small (from 5×10^{-5} / up) that the solutions have a low electrical conductivity. Even 10 ppm of added chloride ion is only 2.8×10^{-4} /. Since added electrolytes were shown to weaken or destroy the inhibiting power of the pertechnetate, this effect might be ascribed to the increase in conductivity of the solution, as well as to any specific action on the metal-solution interface, such as the competitive displacement of an adsorbed inhibitor. For this reason, parallel inhibition tests were conducted in two solutions of essentially equal conductivities but of different ionic types. One solution was 0.01 / potassium perrhenate, $KReO_4$, and the other was 0.005 / sodium sulfate. At 25°C, the equivalent conductance of 0.010284 / $KReO_4$ is 119.15 mho-cm^2 (ref. 13), and that of 0.005 / Na_2SO_4 is 117.28 mho-cm^2 (ref. 14). Neither solution by itself inhibits corrosion.

Each solution was made 3.6×10^{-4} / in technetium, and 1 × 2 cm emeried specimens of carbon steel (sample No. 102) were exposed at 100°C (23°C overnight). The metal in the sulfate solution became heavily smudged almost immediately, the solution became turbid, and rusting soon followed. The specimen in the perrhenate mixture remained bright during the first hour at 100°C, except for a few small blue-grey spots. After four days at 23°C there were a few small areas of localized rusting in the rhenium specimen, whereas the sulfate specimen showed much rust. After three weeks, the specimen in the TcO_4^--ReO_4^- mixture had much bright metal, some interference film, and a few very small pits. The specimen in the TcO_4^--SO_4^{--} mixture was dark all over, except for a large bare area that was deeply corroded and numerous other areas less deeply corroded. There was much more loose rust in suspension in this tube than in the one containing the perrhenate mixture. It was apparent that whereas the presence of the perrhenate interfered to some extent with the pertechnetate inhibition, such effect was far less prominent than that observed in the sulfate solution. It appears, then, that the disturbance caused by the presence of electrolytes is not due merely to the increase in conductivity, but also involves specific effects such as competition between different ionic species in adsorption at the interface. This result is in agreement with the data of Hackerman and Powers,[15] who showed that there is a corresponding competition between chromate and sulfate ions adsorbed on chromium.

In another series of experiments the electrode potential of iron was measured in dilute solutions of potassium pertechnetate, potassium perrhenate, sodium sulfate, and mixtures of these. A preliminary experiment[16] showed that the noble potential attained in potassium pertechnetate alone was debased by addition of sufficient concentrations of sodium sulfate. These experiments have been extended with results that completely substantiate the earlier conclusion that the inhibition and the

[12] G. H. Cartledge, *Corrosion* 11, 335t (1955).

[13] J. H. Jones, *J. Am. Chem. Soc.* 68, 240 (1946).

[14] *International Critical Tables*, vol VI, p 236, McGraw-Hill, New York, 1929.

[15] N. Hackerman and R. A. Powers, *J. Phys. Chem.* 57, 139 (1953).

[16] G. H. Cartledge, *Chem. Semiann. Prog. Rep. Dec. 20, 1954*, ORNL-1832, p 15.

electrode potential are both sensitive to the presence of competing ions, the sulfate ion being more effective than the perrhenate ion. It is clear that a weak and reversible adsorption of the pertechnetate ion is involved both in its inhibitory action and in the potential-determining processes at the electrode surface. Typical experiments are illustrated in Figs. 1 and 2. Fuller details and a discussion of the results are in the process of publication.[17]

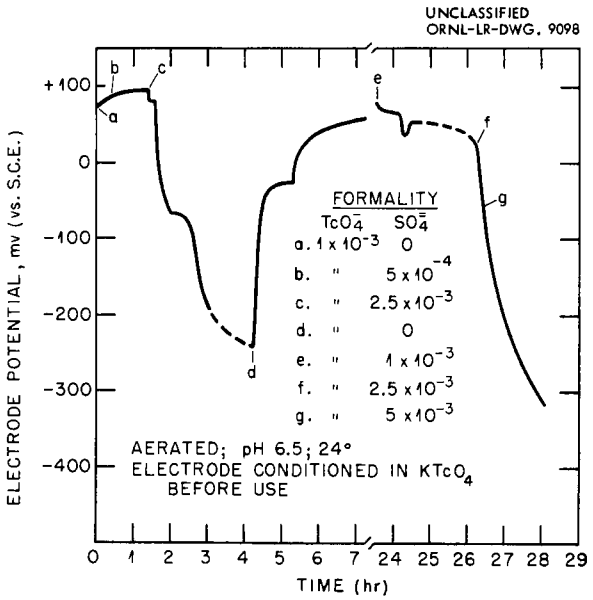

Fig. 1. Effect of Added Sulfate Ion Upon the Electrode Potential of Electrolytic Iron in Aerated Potassium Pertechnetate.

Two further studies of the perrhenate ion have been made. A single batch of the crystalline potassium salt obtained commercially was used in the experiments previously reported.[16,18] In order to eliminate the possibility that the failure to obtain inhibition was due to some impurity in the salt not revealed by its ultraviolet spectrum, other tests were made by using a very pure compound obtained from the University of Tennessee. When this salt was used at concentrations of 10^{-2} and 10^{-3} *f* with carbon steel at 100 and at 23°C, no inhibiting action was observed.

[17] G. H. Cartledge, *J. Phys. Chem.* (in press).

[18] G. H. Cartledge, *Chem. Semiann. Prog. Rep. Dec. 20, 1953*, ORNL-1674, p 14.

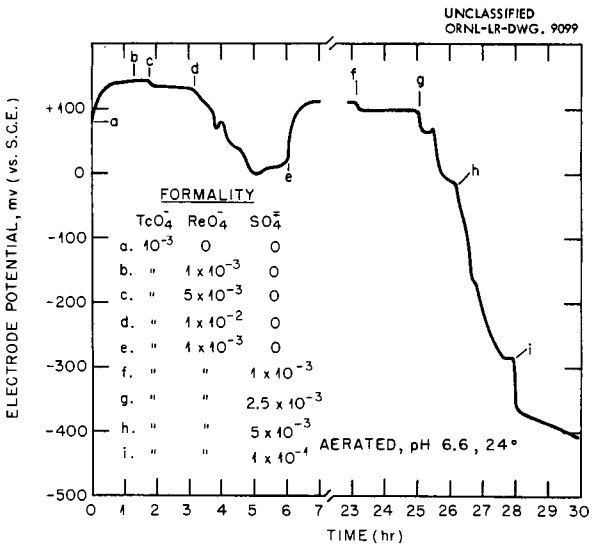

Fig. 2. Effect of Added Perrhenate and Sulfate Upon the Electrode Potential of Electrolytic Iron in Aerated Potassium Pertechnetate.

To supplement the tests for inhibition, the effect of the perrhenate ion upon the electrode potential of electrolytic iron was determined in the manner previously described for the pertechnetate ion. The iron half-cell was stirred by a stream of air, and the potential was measured against a saturated calomel half-cell (S.C.E.) of the Beckman type at 24°C. When the iron electrode was immersed in 1.0×10^{-3} *f* $KReO_4$ having a pH of 6.35, the potential soon became approximately steady at 230 mv negative to the S.C.E. This value was intermediate between the values previously observed in 5×10^{-4} *f* Na_2SO_4 and in 1×10^{-3} *f* $KTcO_4$. Addition of sodium sulfate to the perrhenate solution in amount sufficient to make it 1×10^{-3} *f* in sulfate caused a shift to –375 mv in 9 min, and an increase of the sulfate concentration to 1×10^{-2} *f* gave a further rapid debasing to –460 mv. In the corresponding measurements with potassium pertechnetate, 10^{-3} *f* sulfate had only little effect on the potential, and even 10^{-2} *f* sulfate caused much less debasing than that observed here. These observations are in harmony with the results of the preceding study in that they indicate a slight, easily reversed adsorption of the perrhenate ion at the interface, but without the production of inhibition against dissolved oxygen.

A similar measurement was then made with a

stream of nitrogen, freed from oxygen by hot copper, passing through the solution. The electrolyte was 1×10^{-3} *f* potassium perrhenate, and the potentials of two electrodes were measured. The details of the changes in potential of one of the electrodes are shown in curve I, Fig. 3. The two electrodes behaved in exactly the same manner, and at no point did their potentials differ by more than 35 mv; at most points they were within 10 mv of each other. Initially, the solution contained air, and the electrode potential was similar to that observed in the preceding experiment. After the nitrogen had been passing for 2 min, the potentials debased rapidly, with an inflection at –425 mv and a halt at –660 mv. From the normal potential for the $ReO_2(c)$-ReO_4^- electrode,[19] it may be calculated that ReO_2 should begin to form at about –300 mv (S.C.E.) under the prevailing conditions and that hydrogen at 1 atm could form at –570 mv. Experience in attempting to prepare ReO_2 electrodes by electrolyzing potassium perrhenate with platinum cathodes has shown that little ReO_2 is deposited unless hydrogen is being rapidly evolved. It is therefore possible that the halt at –660 mv indicated the beginning of reduction, since the electrodes appeared unchanged until potentials in the neighborhood of –700 mv were reached. At point b the electrodes were slate-grey in color, and the solution was clear and colorless.

[19] W. M. Latimer, *Oxidation Potentials*, 2d ed., p 244 Prentice-Hall, New York, 1952.

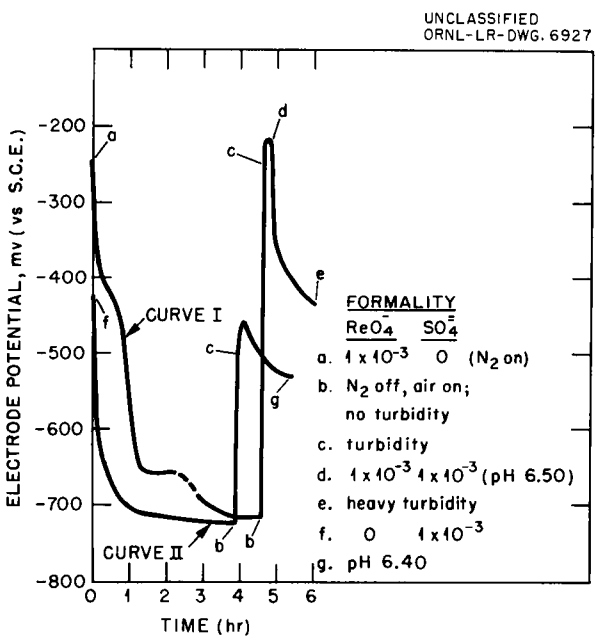

Fig. 3. Electrode Potential of Electrolytic Iron in Potassium Perrhenate or Sodium Sulfate.

At the time indicated by point b, the nitrogen was replaced by air. In 3 min the potential rose 470 mv, and in 5 min the electrodes were apparently steady at –215 and –225 mv, respectively. Addition of sufficient sodium sulfate to bring the concentration to 1×10^{-3} *f* again caused an immediate and extensive debasing, as shown in Fig. 3. Turbidity in the solution and browning of the electrodes were observed at point c, and the solution was very turbid at the end of the experiment.

In another experiment the potentials of two iron electrodes were measured in 1×10^{-3} *f* sodium sulfate alone – first in nitrogen and then in air (curve II, Fig. 3). It will be seen that the potential fell rapidly to –720 mv (S.C.E.) and then remained almost constant; the two electrodes were always within 20 mv of each other. There was no halt such as was observed in the perrhenate experiment. When air was admitted after almost 4 hr, the potentials rose very rapidly to a maximum of about –450 mv, after which slow debasing and obvious corrosion ensued. From the previous measurements in aerated sodium sulfate, it is known that the potential would have continued to fall as corrosion proceeded. Such an abrupt and temporary ennobling which follows admission of air to a corroding system has been repeatedly observed. It is doubtless due to the rapid oxidation of adsorbed or dissolved hydrogen to unstable peroxy products, such as HO_2 or hydrogen peroxide itself.

The results again demonstrated the extreme lability of the electrode interface, as shown in the preceding study. It is seen, however, that perrhenate ions, in contrast to pertechnetate ions, have no ennobling effect except in the presence of oxygen. In air, the potential is above the thermodynamic potentials for the reduction of either hydrogen ions or perrhenate ions, but the reduction of oxygen is not eliminated, as the corrosion experiments demonstrated. In the absence of air, the potential fell to the same value as was obtained in sodium sulfate.

The bearing of these results upon the theory of the inhibitory mechanism is discussed in papers now in the process of publication.

In connection with the studies of electrode potentials in the presence of $TcO_2(c)$ and TcO_4^-, it became apparent that the electrode reaction

$$(Pt)TcO_2(c) + 2H_2O \rightleftharpoons TcO_4^-(aq) + 4H^+ + 3e$$

is very sensitive to the presence of oxygen. Since the value of the standard potential for this electrode given in the literature[20] was obtained without exclusion of air, a series of determinations was made in nitrogen, the resulting value being 44 mv less noble than the reported value.

Six TcO_2 electrodes were prepared by cathodic reduction of potassium pertechnetate on platinum, and two were prepared on gold. The electrodes were immersed in solutions of potassium pertechnetate of varying concentration and were adjusted to varying pH values by addition of low concentrations of sulfuric acid. Nitrogen freed from oxygen was passed continuously through the solutions. Potential measurements were made by means of a vibrating-reed electrometer and a Brown recorder, the reference electrode being a saturated calomel half-cell. The pH was determined initially and was checked at the end of a series of measurements by using a Beckman model G pH meter. The potassium pertechnetate concentration was determined by measurement of the adsorption spectrum. The average value of the standard electrode potential based on the eight electrodes was −0.738 ± 0.003 v, which gives the following revised diagram for the different potentials in acid solution:

$$\begin{array}{ccccccc} & & & -0.738 & & & \\ & & \overline{\phantom{TcO_2 \xrightarrow{-0.8} TcO_3 \xrightarrow{-0.7}}} & & & & \\ Tc & \xrightarrow{-0.272} & TcO_2 & \xrightarrow{-0.8} & TcO_3 & \xrightarrow{-0.7} & TcO_4^- \\ & & \underline{\phantom{Tc \xrightarrow{-0.272} TcO_2 \xrightarrow{-0.8} TcO_3 \xrightarrow{-0.7} TcO_4^-}} & & & & \\ & & & -0.472 & & & \end{array}$$

Further details of the measurements and calculations are in the process of publication.[21]

Electrochemistry of Stainless Steel

G. H. Cartledge F. A. Posey

Uhlig[22] has shown that carbon monoxide inhibits the corrosion of 18-8 stainless steel in hydrochloric acid under certain conditions. The inhibition was found to disappear with rise of temperature, and pitting was noted at 60°C in 3.1 *N* acid. At 90°C the corrosion rate reported was 194.5 g/dm²/day. The inhibition observed at the lower temperatures was ascribed to an activated adsorption of carbon monoxide resembling the adsorption of oxygen. In view of the details of the ennobling process, as disclosed in the work previously reported,[23] it was of interest to determine, under the milder conditions of these experiments, whether carbon monoxide could act like oxygen in inducing the recovery of the electrode potential from the value maintained in the state of continuing corrosion.

The experimental procedures previously described for working in a hydrogen atmosphere were followed. Carbon monoxide from a cylinder was purified by passage through a trap at dry-ice temperature to remove iron pentacarbonyl, and then through chromous chloride and a water scrubber. The metallic specimens were type 347 stainless steel, sample S-300, as used in the experiments with hydrogen or air.

Experiments were done at temperatures between 45 and 85°C in 0.1 *N* sulfuric acid at pH 1.25 and in a 0.1 *N* sulfate mixture at pH 1.50. The electrodes were activated by a brief cathodizing treatment in dilute sodium hydroxide. The several experiments may be summarized as follows:

1. The base potential established in a hydrogen atmosphere, where corrosion was rapid, was ennobled only slightly upon passage of carbon monoxide.
2. This observation was confirmed at all temperatures between 45 and 85°C.
3. When air was admitted after stabilization in carbon monoxide, ennobling set in promptly but proceeded more slowly than when air followed hydrogen.
4. The corrosion in carbon monoxide at 85°C was not stopped but was lower than it was in an atmosphere of hydrogen. There was no indication of reaching a "critical recovery potential" in carbon monoxide at any temperature in the range studied.
5. It appears that carbon monoxide is in competition with the hydrogen liberated at the interface under the condition of these experiments but

[20] J. W. Cobble, Wm. T. Smith, Jr., and G. E. Boyd, *J. Am. Chem. Soc.* 75, 5777 (1953).

[21] G. H. Cartledge and Wm. T. Smith, Jr., *J. Phys. Chem.* (in press).

[22] H. H. Uhlig, *Ind. Eng. Chem.*, 32, 1490 (1940).

[23] G. H. Cartledge, *Chem. Semiann. Prog. Rep. Dec. 20, 1954*, ORNL-1832, p 15; *Chem. Semiann. Prog. Rep. June 20, 1954*, ORNL-1755, p 13.

that, unlike oxygen, it is unable to block the local-action currents sufficiently to inhibit the corrosion or to ennoble the potential.

A further study is in progress to determine the nature of the ennobling process that occurs after the electrode potential rises above the critical recovery potential at about −295 mv S.C.E. There were indications that Fe(III) ions from the solution were involved in the process by a redox type of interaction, since Cr(III) ions were ineffective. Accordingly, experiments were done in which radioactive $Fe^{55,59}$ was added to the sulfuric acid solution while four electrodes were at the corroding potential below −300 mv S.C.E. There were four similar electrodes in the solution. Two of them were kept at −324 mv S.C.E. by the passage of sufficient current to prevent the ennobling to take place. The other two electrodes ennobled promptly when 1 mg of irradiated iron in the form of sulfate was added. After a time, all four electrodes were removed, thoroughly washed in water, and counted. The average count on the electrodes which ennobled was 171 counts/min on a 2π gas-flow proportional counter. The average count on the specimens held at a low potential was 48 counts/min. To determine whether the iron pickup is reversible, an electrode was first conditioned in the radioactive iron solution overnight at 60°C and then raised to 85°C for 1 hr. The total count on the two sides of the electrode was 466 counts/min. The electrode was then returned to the active solution and was cathodized for 48 min with a current of about 1 ma. It was then washed and again counted, showing a total of 82 counts/min. Since these experiments were done in air, they furnish additional evidence that both oxygen and ferric ions are involved in the interfacial changes associated with the ennobling process.

EMF MEASUREMENTS AT ELEVATED TEMPERATURES

M. H. Lietzke J. M. Chilton

As part of a general emf study in aqueous solutions at elevated temperatures, the potentials of the cell In, $In_2(SO_4)_3(m)$, Ag_2SO_4(sat.), Ag were measured from 15 to 70°C, with the $In_2(SO_4)_3$ concentration varying from 0.01 to 2.3 m. Above about 70°C irreversible hydrolytic reactions occurred which made interpretation of the measurements difficult or impossible in the absence of extra acid. Since the tendency to hydrolyze increased with decreasing concentration at any given temperature, the lower limit of the useful concentration range became higher as the temperature was raised from 15 to 70°C. The Oracle is being used to calculate the activity coefficients, partial molal heat contents, and partial molal heat capacities of $In_2(SO_4)_3$ over the temperature and concentration range indicated. An effort will be made to extrapolate the potentials to infinite dilution by using the extended Debye-Hückel equation, so that values of $E^0(t)$ may be obtained at 5-deg intervals from 15 to 70°C. The work will be described in detail in a paper to be submitted to the *Journal of the American Chemical Society.*

Some typical values for the relative activity coefficients, that is, the ratios of activity coefficients at any given molality to those obtained at the minimum feasible molality at any given temperature, are given in Table 2.

TABLE 2. RELATIVE ACTIVITY COEFFICIENTS

Molality	At 15°C	At 30°C	At 50°C	At 70°C
0.05	0.249	0.235		
0.1	0.144	0.132		
0.5	0.0479	0.0439	0.0330	
1.0	0.0583	0.0462	0.0291	0.0148
2.3	0.185	0.125	0.0610	0.0239
m_{min}	0.01	0.01	0.1	0.5

Equipment is being assembled and tested preliminary to a series of measurements involving the use of the hydrogen electrode at high temperatures and pressures. An attempt will be made to measure the activity of hydrochloric and sulfuric acid solutions up to 250°C by using silver chloride and silver sulfate reference electrodes. Preliminary results with the cell Ag, AgCl(sat.), HCl(m), H_2 up to 200°C indicated close agreement at 0.01 and 0.1 m between measured emf's and those obtained by extrapolating the data of Harned and Ehlers[24] to get the E^0 values and by using the Debye-Hückel theory (with the room-temperature "distance of closest approach" parameter) to correct for the activity coefficients.

[24] H. S. Harned and R. W. Ehlers, *J. Am. Chem. Soc.* 54, 1350 (1932); 55, 652 (1933); 55, 2179 (1933).

CHEMISTRY OF FUSED SALTS

Electrical Conductance and Density

I. S. Yaffe E. R. Van Artsdalen

The determination of density and electrical conductance has been completed for almost all the molten pure alkali halides, with the exception of the fluorides. The data are recorded in Table 3. The temperature dependence of equivalent conductance can be expressed approximately by the equation

$$(1) \qquad \Lambda = Ae^{-\Delta H^{\ddagger}/RT} .$$

However, the activation energy, $\Delta H^{\ddagger}$, is, in general, somewhat temperature dependent. This is shown clearly in Fig. 4, where $\Delta H^{\ddagger}$ is plotted as a function of temperature. It is observed that the sign of the temperature dependence is related to the cation, while the magnitude of the dependence is determined by the anion. It is believed that at least two different effects are responsible for this temperature dependence of heat of activation. Expansion of the liquid lattice with rising temperature would be expected to decrease somewhat the potentials restricting migration of ions. This effect should tend to lower the heat of activation as the temperature rises. However, an opposing effect, the result of like-ion repulsion, which increases with rising temperature, tends to increase these potentials. The actual sign of the temperature coefficient of the heat of activation will depend upon which of the two effects is the larger.

The entropy of activation for electrical conductance is given by the equation

$$(2) \quad \Lambda = 5.19 \times 10^{18}(D + 2)d^2 e^{\Delta S^{\ddagger}/R} e^{-\Delta H^{\ddagger}/RT}$$

described previously,[25,26] where D is the dielectric constant of the fused salt, d is half the distance the conducting ion must migrate in going from one equilibrium position to the next nearest one, and $\Delta S^{\ddagger}$ is the entropy of activation. Unfortunately, there are no values available for the dielectric constants of molten salts. An estimate of $D = 3$ has been used to calculate the entropy of activation for electrical conductance of the alkali halides, and the results at 850°C are listed in Table 3. There are some indications that the dielectric constant of molten salts may be higher, perhaps in the range of 15. When D in Eq. 2 is chosen equal to 15, the computed values of $\Delta S^{\ddagger}$ are approximately 2.5 cal/mole·deg more negative than those listed in Table 3; $\Delta S^{\ddagger}$ becomes about 0.1 to 0.2 cal/mole·deg more negative for a rise of 100°C.

[25] E. R. Van Artsdalen and I. S. Yaffe, *J. Phys. Chem.* 59, 118 (1955).

[26] A. S. Dworkin *et al.*, *Chem. Semiann. Prog. Rep. June 20, 1954*, ORNL-1755, p 20.

TABLE 3. DENSITY AND CONDUCTANCE OF ALKALI HALIDES

	Measured Range (°C)	Density, $\rho = a - b \times 10^{-3}t$ (g/cc)		Standard Deviation (g/cc)	Specific Conductance, $\kappa = -a + b \times 10^{-3}t - c \times 10^{-6}t^2$ (mho·cm^{-1})			Standard Deviation (mho·cm^{-1})	$-\Delta S^{\ddagger}$ at 850°C (cal/mole·deg)
		a	b		a	b	c		
LiCl	620 to 800	1.7660	0.4328	0.0001	−0.528	11.25	4.554	0.008	6.3
NaCl	800 to 1040	1.9911	0.54299	0.0007	0.1697	6.2594	1.9531	0.006	6.4
NaBr	750 to 960	2.9518	0.8169	0.0003	0.4392	5.6318	1.5721	0.002	6.3
NaI	675 to 915	3.3683	0.94909	0.0004	0.8202	5.9403	1.9764	0.002	6.4
KCl	790 to 930	1.9767	0.5831	0.0003	1.749	7.383	3.000	0.003	6.7
KBr	740 to 950	2.7333	0.82525	0.0005	3.2261	10.124	4.8276	0.004	6.9
KI	725 to 920	3.0985	0.95573	0.0003	1.7100	6.408	2.9652	0.003	7.4
RbCl	730 to 925	2.8799	0.88321	0.0002	1.8097	6.1759	2.1985	0.002	6.2
RbBr	700 to 920	3.4464	1.0718	0.0005	3.0305	9.1039	4.5096	0.002	7.3
RbI	660 to 905	3.6403	1.1465	0.0004	1.9114	6.6335	3.0021	0.002	7.1
CsCl	650 to 900	3.4782	1.0650	0.0006	1.8023	5.6282	1.7652	0.003	6.2
CsI	640 to 865	3.9179	1.1834	0.0002	1.3313	3.9581	1.3054	0.003	6.7

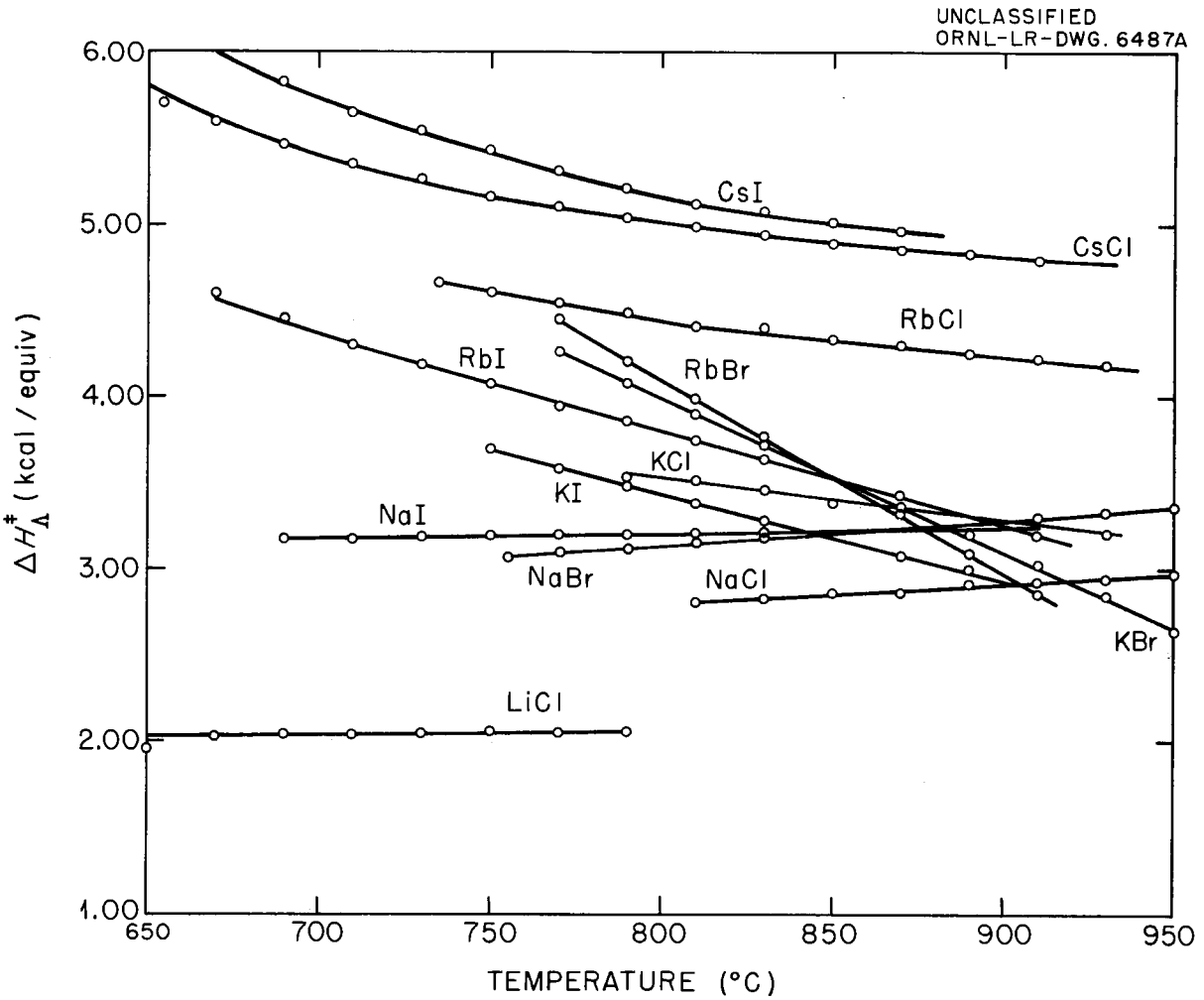

Fig. 4. Heat of Activation ($\Delta H^{\ddagger}$) for Conduction in Alkali Halides.

The fact that $\Delta S^{\ddagger}$ is a small negative number and differs but little among these salts indicates that the conduction process is analogous for all alkali halides and that the activated complex is similar and involves about the same degree of ordering in all cases. However, there is a hint that $\Delta S^{\ddagger}$ becomes more negative as the size of the anion increases. This may reflect a slightly lesser degree of order in the larger anion lattice.

Self-Diffusion in Molten Salts

A. S. Dworkin D. Brown
E. R. Van Artsdalen

Experimental results for the self-diffusion coefficient for the sodium ion in molten sodium nitrate are shown in Fig. 5 for the temperature range 315 to 375°C. The self-diffusion coefficient of Na^+ in $NaNO_3$ may be expressed by the equation

$$D = 1.29 \times 10^{-3} e^{-4970/RT} .$$

Over this limited temperature range $\Delta H^{\ddagger}$ appears to be constant. These data may be combined with those for equivalent conductance of silver nitrate in the manner described previously[27] to arrive at an estimate of a transport number for sodium ion in pure sodium nitrate. The results indicate a value of about 0.85 to 0.9 for this transport number. There is some question whether the Nernst-Einstein

[27] D. Brown *et al.*, *Chem. Semiann. Prog. Rep. Dec. 20, 1954*, ORNL-1832, p 23.

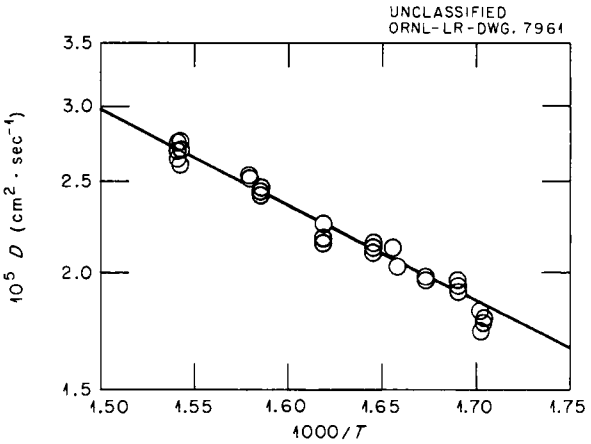

Fig. 5. Self-Diffusion of Na^+ in Molten $NaNO_3$.

equation, which is used in calculating the transport number, is, in fact, applicable under these circumstances. Although this equation is known to hold in dilute aqueous solutions, at best it is only a good approximation. Further work is in progress to determine its applicability in the case of molten salts. In the first place, a theoretical investigation is being made of the approximations involved in deriving the equation. Secondly, determination of the self-diffusion coefficients of both anion and cation in several salts is under way and will give an experimental test of the use of the Nernst-Einstein equation. Results of this study will be reported later; beyond all these points lies the problem of interpretation of separate and distinguishable transport numbers for the two ions of a single, pure 1-1 molten electrolyte.

Cryoscopy

J. E. Sutherland E. R. Van Artsdalen

Freezing-point-depression studies in molten salts can be used to elucidate the dissociation equilibria involved in fused salt solutions.[28,29] Freezing-point-depression measurements have yielded unequivocal information showing that certain halides which are prone to partial dissociation in aqueous solution are likewise much less than completely dissociated in molten nitrates.

[28] E. R. Van Artsdalen, *J. Tenn. Acad. Sci.* **29**, 122 (1954).

[29] A. S. Dworkin *et al.*, *Chem. Semiann. Prog. Rep. June 20, 1953*, ORNL-1587, p 26; *Chem. Semiann. Prog. Rep. Dec. 20, 1953*, ORNL-1674, p 26.

Figure 6 shows the freezing-point depression of sodium nitrate caused by the addition of the four salts, zinc chloride, cadmium chloride, cupric chloride, and lead chloride. The theoretical slopes for complete dissociation and for no dissociation whatever are shown as dotted lines designated as 1X and 3X, respectively. It is evident that these salts are more highly dissociated, the lower the concentration, and approach complete dissociation at infinite dilution.

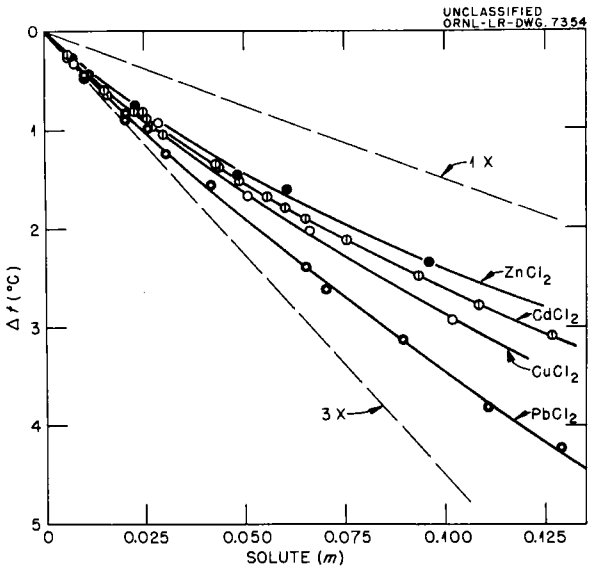

Fig. 6. Freezing-Point Depression of $NaNO_3$.

It seemed reasonable to expect that the addition of excess chloride ion should repress the dissociation of these salts, thereby exhibiting in molten salt solutions the common-ion effect, which is so well known in aqueous solutions. Furthermore, under these circumstances the formation of complex anions, MCl_n^{m-}, was anticipated. Therefore, a very detailed study was made in the case of cadmium chloride, and a somewhat less thorough study was made with lead chloride. The results with cadmium chloride are shown in Figs. 7 and 8. In solutions containing excess chloride, as NaCl, CsCl, etc., the freezing-point depression, Δt, is the additional depression caused by cadmium chloride. The common-ion effect is amply demonstrated for the first time by these data which also show that the cation exerts a negligible influence at low concentration. Figures 7 and 8 also prove

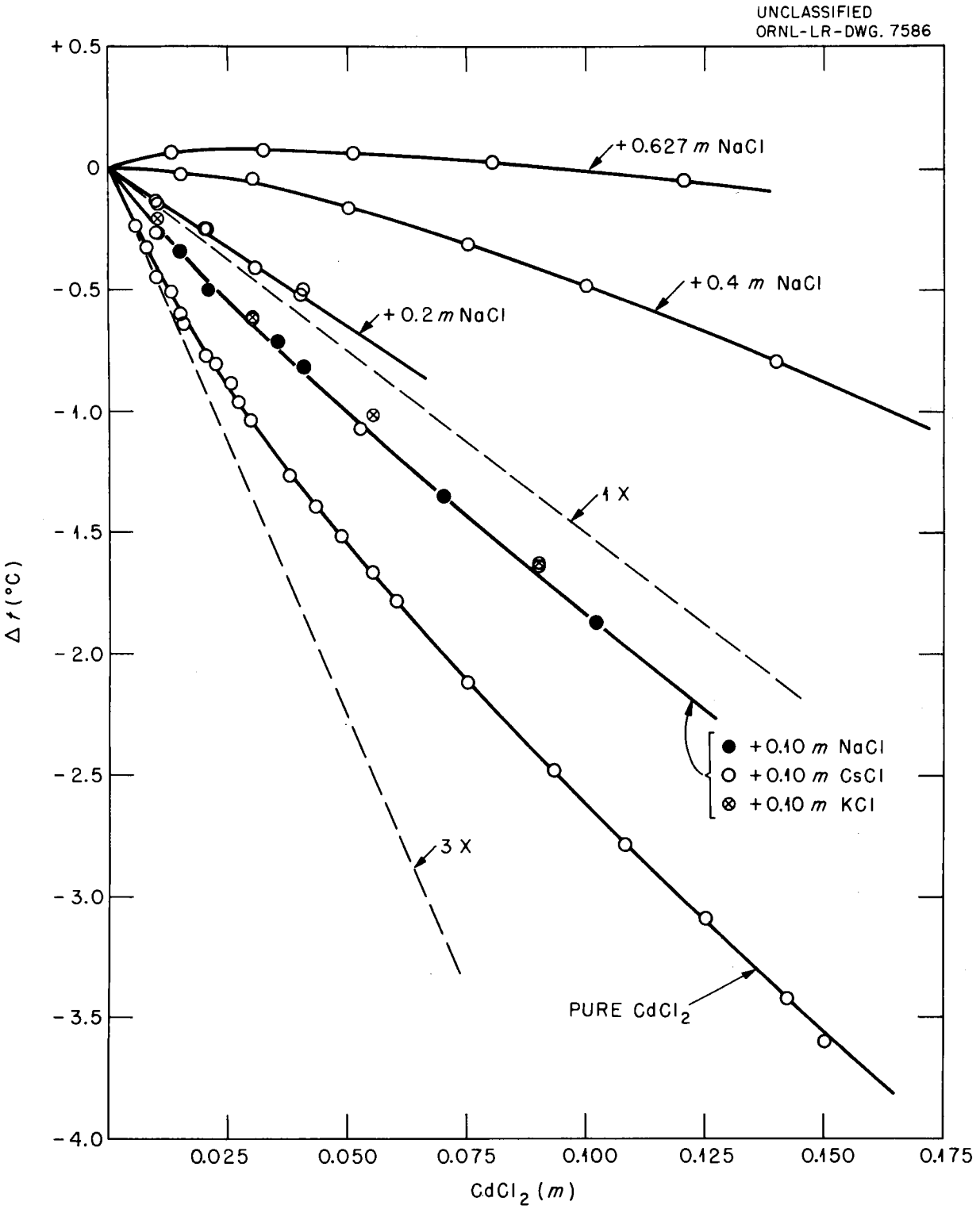

Fig. 7. Freezing-Point Depression by $CdCl_2$ in $NaNO_3$ – Effect of Added Chlorides.

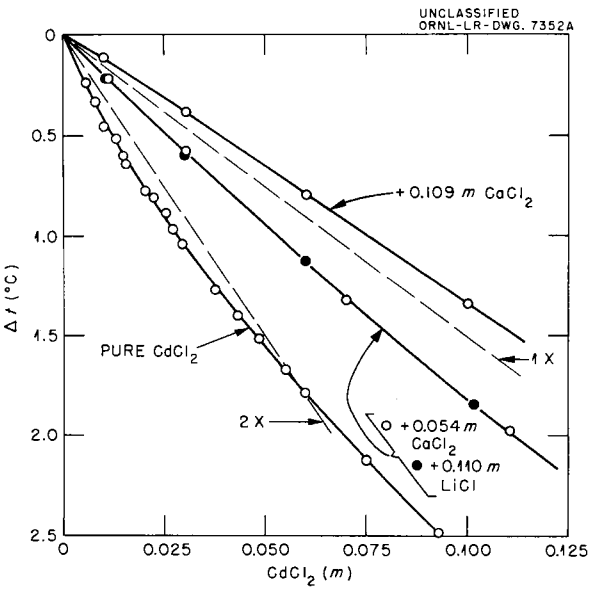

Fig. 8. Freezing-Point Depression by $CdCl_2$ in $NaNO_3$ – Effect of Added Chlorides.

that one or more complex chloro-cadmium anions exist. Thus the addition of 0.2 *m* NaCl causes some association of $CdCl_2$ with excess Cl^-, since the slope of the depression curve at this concentration is less than that which would be produced by a single particle per formula weight. The curve with 0.627 *m* NaCl shows that a complex exists that contains at least four chlorines, for example, $CdCl_4^{--}$. Thus, additions of $CdCl_2$ less than 0.095 *m* actually caused a rise in the freezing point which can be explained only on the assumption that, on the average, more than one Cl^- is removed per $CdCl_2$ dissolved.

The following reactions may be postulated:

$$CdCl_2 \rightleftharpoons CdCl^+ + Cl^- \qquad K_2$$

$$CdCl^+ \rightleftharpoons Cd^{++} + Cl^- \qquad K_1$$

$$CdCl_2 + Cl^- \rightleftharpoons CdCl_3^- \qquad K_3$$

$$CdCl_3^- + Cl^- \rightleftharpoons CdCl_4^{--} \qquad K_4$$

However, calculations of the equilibrium constants from experimental data seem to show that the chloro-cadmium complex ions containing odd numbers of chlorines are not very important thermodynamically, although it is reasonable to expect them to be involved kinetically. Therefore, the following equations can be written to express the equilibria:

$$CdCl_2 \rightleftharpoons Cd^{++} + 2Cl^- \qquad K_{12}$$

$$CdCl_2 + 2Cl^- \rightleftharpoons CdCl_4^{--} \qquad K_{34}$$

The equilibrium constants, K_{12} and K_{34}, are defined in the usual manner. In freezing $NaNO_3$ (i.e., at ~300 to 306°C, depending on concentration), $K_{12} = 0.0031 \pm 0.0004$, and $K_{34} = 4.4 \pm 0.8$.

Similar results were obtained with lead chloride and are plotted in Fig. 9, which shows that lead chloride is more completely dissociated and does not complex with excess chloride ion so readily as cadmium chloride. This is comparable with the known chemical behavior of these two compounds in aqueous solutions.

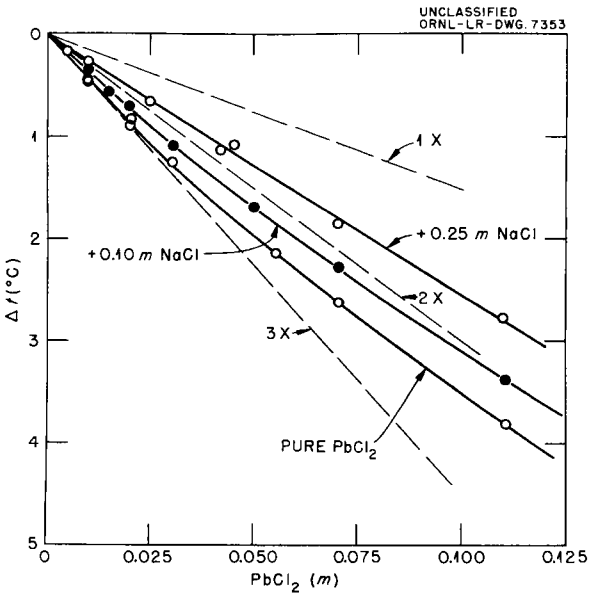

Fig. 9. Freezing-Point Depression of $NaNO_3$ by $PbCl_2$.

Some measurements have been made by using solutions of these salts dissolved in potassium nitrate as solvent. Although the measurements are incomplete, it can be said that the behavior in molten potassium nitrate is analogous to that in molten sodium nitrate. It may be possible to obtain useful information concerning the thermal stability of these complex ions by studying them in several molten nitrates which have somewhat different freezing points. Unfortunately, potassium

nitrate is not so well behaved a solvent (anomalies in heat of fusion, solid-solution formation, etc.) as sodium nitrate, but it appears that cadmium chloride is a little more dissociated in freezing potassium nitrate (334°C) than in freezing sodium nitrate (306°C).

This work is being continued vigorously, and attempts are being made to develop rigorous treatment of the equilibria which are involved. A more detailed discussion and theoretical treatment of complex-ion equilibria in molten salts will be presented in a paper at the Ion Pair Symposium of the fall meeting of the American Chemical Society and will be published later as a part of the symposium.

High-Temperature Calorimetry

D. J. Sasmor E. R. Van Artsdalen

The high-temperature adiabatic calorimeter has been used to temperatures of about 900°C. It is currently being calibrated with synthetic sapphire as the known calorimetric standard. A few experimental difficulties have developed, and a number of improvements have been made in circuitry and operation. Previous difficulties experienced with faulty heater windings were traced to electrical breakdown of the insulating ceramic beads, which were of a very inferior grade. This difficulty has been eliminated with the use of high-quality insulators. The calibration makes it appear that the over-all accuracy is better than ±1% in the determination of heat capacity. It is anticipated that refinements in sensitivity of temperature measurement will improve this figure somewhat.

HIGH-TEMPERATURE AND STRUCTURAL CHEMISTRY

Miscibility of Liquid Metals with Salts

M. A. Bredig H. R. Bronstein
J. W. Johnson

Work on the determination of phase equilibria which is discussed in detail in two recent publications[30,31] was interrupted temporarily in order to focus the effort on the design of apparatus for the study of some of the more significant physical and thermodynamic properties of these solutions, namely, electrical conductance and vapor pressure.

Metal Vapor Pressure Measurements. – A change from the combination boiling and sampling apparatus[32] to one without provision for sampling, employing four separate simple chambers connected to a common pressure manifold, was made for the following reasons:

1. Very little alkali metal was actually found retained in the cooled part of the older type of tank during boiling, as shown by a comparison of analyzed samples with the known amounts of salt added.
2. All four chambers of the new assembly can be charged with alkali metal, and its boiling points at various pressures can be determined in quadruplicate. This gives rapid information on the scatter in temperature readings.
3. In measurements on salt-metal solutions, one chamber can be reserved for pure alkali metal as a continuous reference point.
4. The three other chambers can be loaded with different amounts of salt; the differences in boiling temperatures as a function of concentration may thus be determined three times as rapidly as with one chamber.
5. An improved design incorporates more effective baffling and a "cold finger" which also permits, if desired, reading of the temperature of the condensing vapor.
6. Liquid phase equilibria studies were found to be considerably less difficult with the older sampling type of chamber than with individual capsules described in the publications.[30,31] Thus it seems advisable to restrict the use of that apparatus to such solubility studies.

Electrical Conductance. – One way of obtaining information on the state and mobility of the electron which the metal introduces into its solution in molten salt is the determination of electrical conductance changes associated with that dissolution. The literature shows examples of a decrease from the equivalent conductance of the pure salts, as, for instance, in the systems $CdCl_2$-Cd, $BiCl_3$-Bi, and $CaCl_2$-Ca. This effect has been attributed to the formation of comparatively simple, diatomic complex cations such as $(Cd{:}Cd)^{++}$ or $Cd^{++}(e^-)_2Cd^{++}$. Formation of such ions, similar to the mercurous ion $Hg^{++}(e^-)_2Hg^{++}$, whose existence both in crystals and aqueous solutions is well established,

[30] M. A. Bredig, J. W. Johnson, and Wm. T. Smith, Jr., *J. Am. Chem. Soc.* 77, 307 (1955).

[31] M. A. Bredig, H. R. Bronstein, and Wm. T. Smith, Jr., *J. Am. Chem. Soc.* 77, 1454 (1955).

[32] J. W. Johnson and M. A. Bredig, *Chem. Semiann. Prog. Rep. Dec. 20, 1954*, ORNL-1832, p 27.

appears plausible for transition metals such as cadmium. This is not the case for metals which form ions of noble gas type of structure and of relatively small polarizability, such as Ca^{++}, Na^{+}, or K^{+}. Indeed, solid calcium subchloride, CaCl, is said[33] to exhibit a crystal structure in which only giant metal ions $(Ca_n)^{n+}$ are discerned, rather than diatomic Ca^{++} ions. While data of the electrical conductance in solid CaCl are not available, *F*-center colored crystals of the alkali halides are said to contain, in anion vacancies, electrons which at only slightly elevated temperature (200°C) are mobile enough to contribute to the conductance of the crystal.[34] While additive behavior with respect to electrical conductance, which would correspond to an increase by 5000% of the conductance of the pure salt for every mole per cent of alkali metal added, is not likely, a decrease and, as a result, a minimum in conductance is not anticipated either. However, because of the presumed small free paths of conduction electrons in the presence of halide ion potential barriers, a pronounced negative deviation from additivity would seem probable.

An apparatus for the determination of electrical conductance has been designed and constructed (see Fig. 10). It incorporates all the features required in working with the highly volatile and reactive alkali metals. A stainless steel tank with a capacity of approximately 4 liters and containing a volume of approximately 1 liter of molten salt is heated in a 5-in.-ID tube furnace from the bottom and is cooled near the top. Through the tank lid various auxiliary equipment can be introduced without breaking the protective atmosphere of 40-psi argon gas. A conductance cell made of impervious high-fired beryllia, 3½ in. long and ⅝ in. OD, with a capillary 1/16 in. in diameter, can be introduced, together with a stainless steel wire electrode whose relative positions can be adjusted from the outside. A special loading device permits injection of liquid alkali metal into the molten salt, and a mechanical stirrer facilitates uniform distribution of the solute in the solvent. A sampler similar to the one used in the earlier vapor-pressure apparatus[32] allows taking a representative sample of the solution. The electrical resistance of the

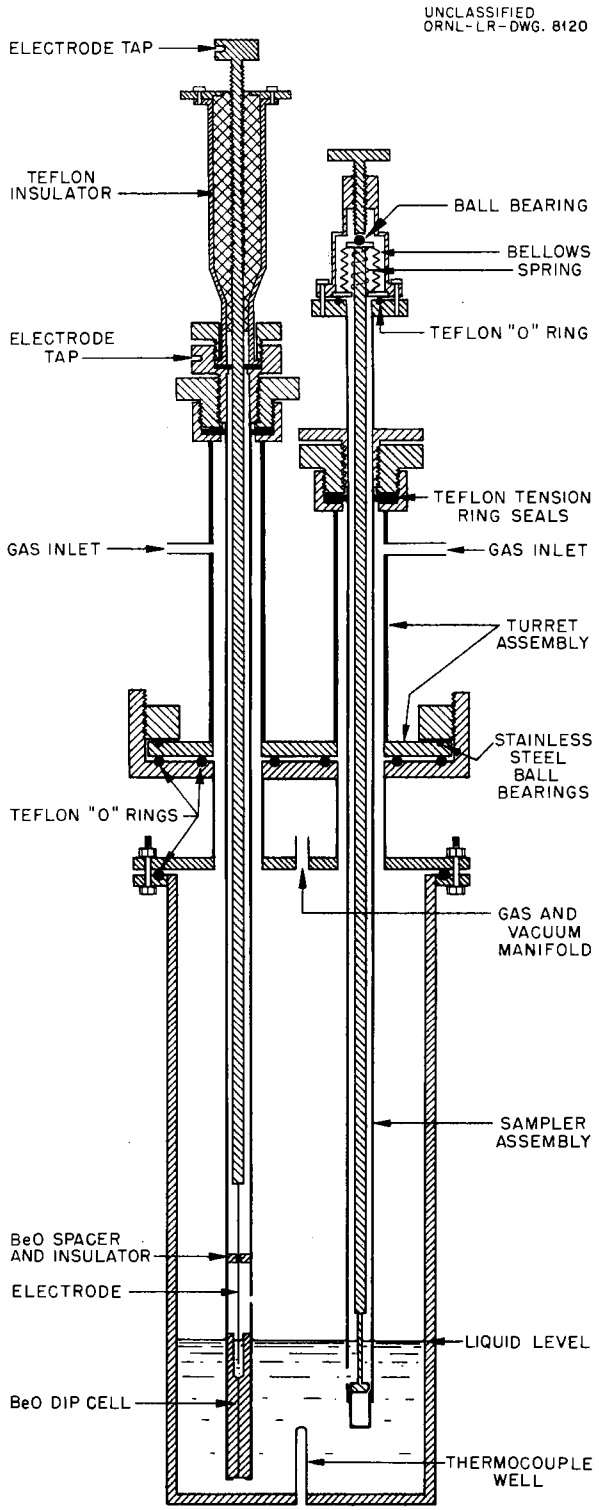

Fig. 10. Electrical Conductance Cell for Fused-Salt–Metal Solutions.

[33] P. Ehrlich and L. Gentsch, *Naturwiss.* 41, 211 (1954).

[34] F. Seitz, *Modern Theory of Solids*, p 459 McGraw-Hill, New York, 1940.

cell is measured with a Jones bridge, using alternating current adjustable between 1000 to 2000 cps. The conductivity of pure molten KCl was measured with an accuracy of ±0.1% by using a cell constant determined by measuring the resistance of a 1 demal aqueous KCl solution.

A few difficulties in the operation of the apparatus must still be overcome, the principal one being a slight porosity of the insulating beryllia cell. One test with a solution of 0.45 mole % potassium metal in molten KCl gave an increase of 5 to 10% in electrical conductance. However, this figure may be considerably in error, as the cell constant was found to be changed after the test by at least 15%. A change in conductance of the salt, if any, resulting from the presence of the small amount of metal added seems, however, to have been an effect smaller, by far, than additivity would require (2500%). Possibilities of reducing the porosity of the present cell, or of replacing it by one made of a single crystal of magnesium oxide, are being investigated.

Molar Volume and Structure of Molten Alkali Halides

M. A. Bredig J. W. Johnson

A preliminary discussion of molar volume and structure of molten alkali halides was presented some time ago.[35] A recent careful re-examination of density data of the literature led to the conclusion that it is possible by a straight-line plot of the logarithm of the molar volume V vs a function $(t + t^2)$, where t denotes °C, to derive molar volumes at the melting points for all the alkali halides. These are accurate to approximately ±1 cc and may thus be compared with the molar volumes of the liquid salts at the melting temperatures, which are known with somewhat greater accuracy. The results of these computations which are qualitatively similar, but which are considered to be more reliable than the earlier ones, are given in Table 4. Large volume expansions associated with melting in some of the salts, notably LiF (31%) and NaF (26%), when compared with the small expansion (17.5%) in KCl and with the corresponding small coordination change from 6 in the crystal to 5.8 in molten KCl, as obtained by x-ray diffraction,[36] suggest that a change in the average coordination number, usually a decrease of varying degree, may occur in many of these salts. This assumption is similar to the one proposed for cesium bromide and cesium iodide,[37] where there is undoubtedly a lowering from 8 in the crystal to probably an average of slightly more than 6 in the melt, that is, a change to a liquid "structure" similar to that of CsCl.

Details of these considerations are being reported in a paper that has been submitted for publication.[38] They will be examined further in the light of x-ray and neutron diffraction measurements, preparations for which are described in the section of this report entitled "Chemical Physics."

TABLE 4. VOLUME EXPANSION OF ALKALI HALIDES ON MELTING

Salt	Melting Point (°C)	Molar Volume (cc) at Melting Point		Valume Expansion (%)
		Solid	Liquid	
LiF	845	11.0	14.4	30.9
LiCl	610	22.6	28.2	24.8
LiBr	550	27.8	34.1	22.7
LiI	470	36.3	43.3	19.3
NaF	995	17.0	21.5	26 ± 2
NaCl	800	30.6	37.7	23.2
NaBr	750	36.3	44.2	21.8
NaI	662	45.4	54.7	20.3
KF	856	26.0	31.0	19 ± 2
KCl	772	41.7	49.0	17.5
KBr	735	48.3	56.2	16.4
KI	685	58.6	67.8	15.7
RbF	775	31.2	36.9	18 ± 3
RbCl	717	47.7	53.8	12.9
RbBr	680	54.0	61.0	12.8
RbI	640	65.8	74.1	11.1
CsF	703	36.6	41.8	14 ± 3
CsCl	645	54.8	60.3	10.0
CsBr*	636	53.4	67.7	26.8
CsI*	621	63.2	81.2	28.5

*Simple cubic structure at melting point.

[35] M. A. Bredig, J. W. Johnson, and W. T. Smith, *Chem. Quar. Prog. Rep. Dec. 31, 1952*, ORNL-1482, p 32–35.

[36] K. Lark-Horovitz and E. P. Miller, *Phys. Rev.* 49, 418 (1936); *Phys. Rev.* 51, 61 (1937).

[37] M. A. Bredig and P. A. Agron, *Chem. Semiann. Prog. Rep. June 20, 1954*, ORNL-1755, p 23–26.

[38] J. W. Johnson and M. A. Bredig, paper to be given at the meeting of the American Chemical Society, September 1955, at Minneapolis, Minnesota, and to be published in *J. Am. Chem. Soc.*

NUCLEAR CHEMISTRY

PRODUCTION AND IDENTIFICATION OF LONG-LIVED TECHNETIUM ISOTOPES AT MASSES 97, 98, AND 99

G. E. Boyd Q. V. Larson
J. R. Sites[1] C. R. Baldock[1]

The properties of the "missing" beta-unstable technetium isotope at mass 98 have recently become of considerable interest; it now appears[2] that the technetium isotopes at masses 97 and 99 are also unstable and decay with half lives of less than 10^6 years. If, therefore, primordial technetium is detected on the crust of the earth, presumably it will be found because the half life of Tc^{98} exceeds 10^8 years.

Arguments based on shell theory have suggested[3,4] that the spin of Tc^{98g} may be very high, so that its beta decay can be highly forbidden and can occur with an extremely long half life. On the other hand, because the odd proton in Tc^{98} may be either $g^+_{9/2}$ or $p^-_{1/2}$ and the odd neutron either $d^+_{5/2}$ or $g^+_{7/2}$, application of Nordheim's rules[5] leads to the prediction of either a low (1^+ or 2^-) or a high spin (4^- or 6^+, 7^+) ground state. Since approximately 1.8 Mev is available for beta disintegration, in the former instance the decay of Tc^{98} should be "allowed" with a half life of 10 ± 5 min. However, exhaustive searches by the senior author for a short-lived Tc^{98} produced by 14-Mev deuteron irradiation[6] of electromagnetically enriched Mo^{98} (95.0%) and separated by rapid chemistry have failed to reveal any hitherto unassigned technetium activity in this half-life range. Additional attempts to detect a very short-lived Tc^{98} formed by the irradiation of 100-mg quantities of carefully purified fission-product TcO_2 with 80-Mev x rays[7] were also unsuccessful. It was concluded that it was unlikely that Tc^{98g} possessed a low spin and was short-lived. Alternatively, measurements of the decay of the radiations from numerous other technetium sources for periods as long as seven years indicated that the half life of Tc^{98} was either extremely long or that, fortuitously, it decayed with a period and radiations nearly identical with one of the previously known technetium activities and hence had been overlooked.

To resolve this possible ambiguity, a large piece of molybdenum metal was bombarded[8] with 22-Mev protons from the ORNL 86-in. cyclotron for a time sufficient to produce approximately 10 μg of Tc^{98}. After 270 days, to allow for the complete decay of the shorter-lived technetium isotopes and to reduce the amount of 60-day Tc^{95m} formed, the complete target was processed chemically, and the technetium fraction was separated and purified by anion-exchange chromatography. An aliquot was electroplated on an iridium strip which subsequently was heated at 400°C in a stream of hydrogen gas to produce an adherent layer of technetium metal. Approximately 1 μg of technetium was present on the iridium strip employed as a filament source in a 60-deg mass spectrometer of 8-in. radius. Technetium ions produced both by electron bombardment and by thermal ionization appeared at a temperature consistent with that observed in previous analyses on fission-product Tc^{99g}. The prominent ions were those at masses 97, 98, and 99 (Fig. 11), with the indicated relative abundances taken from several other measurements. These masses were positively identified by employing ions formed by electron bombardment, together with a section of the mass-time dispersion curve. Known ion peaks used were Ir^{++} at 95.5 and 96.5; Pt^{++} at 97, 97.5, and 98; and Rh^+ at 103. A check dispersion-curve section was made with thermally produced ions by using Sr^+ at 86, 87, and 88, and Rh^+ at 103.

These results appear to be of interest for a number of reasons, some of which may include the following:

1. Weighable quantities of three long-lived technetium isotopes were produced, and Tc^{95}, Tc^{97},

[1] Stable Isotope Research and Production Division.

[2] G. E. Boyd, *Phys. Rev.* 95, 113 (1954).

[3] G. E. Boyd, *Record Chem. Progr. (Kresge-Hooker Sci. Lib.)* 12, 67 (1951).

[4] E. Segrè *Nuovo cimento* 9, 1008 (1952).

[5] L. W. Nordheim, *Revs. Mod. Phys.* 23, 322 (1951).

[6] These bombardments were conducted on the 60-in. cyclotron at the Department of Terrestrial Magnetism, Carnegie Institution of Washington. The hospitality and interest of Drs. M. A. Tuve, P. H. Abelson, and Dean Cowie are gratefully acknowledged.

[7] Thanks and appreciation are expressed to Drs. S. K. Allison and B. C. Cook for making the University of Chicago betatron available for these irradiations. J. W. Cobble assisted with these experiments.

[8] Assistance with the special target problem and with the high-current bombardment was generously afforded by J. A. Martin and F. Green of ORNL.

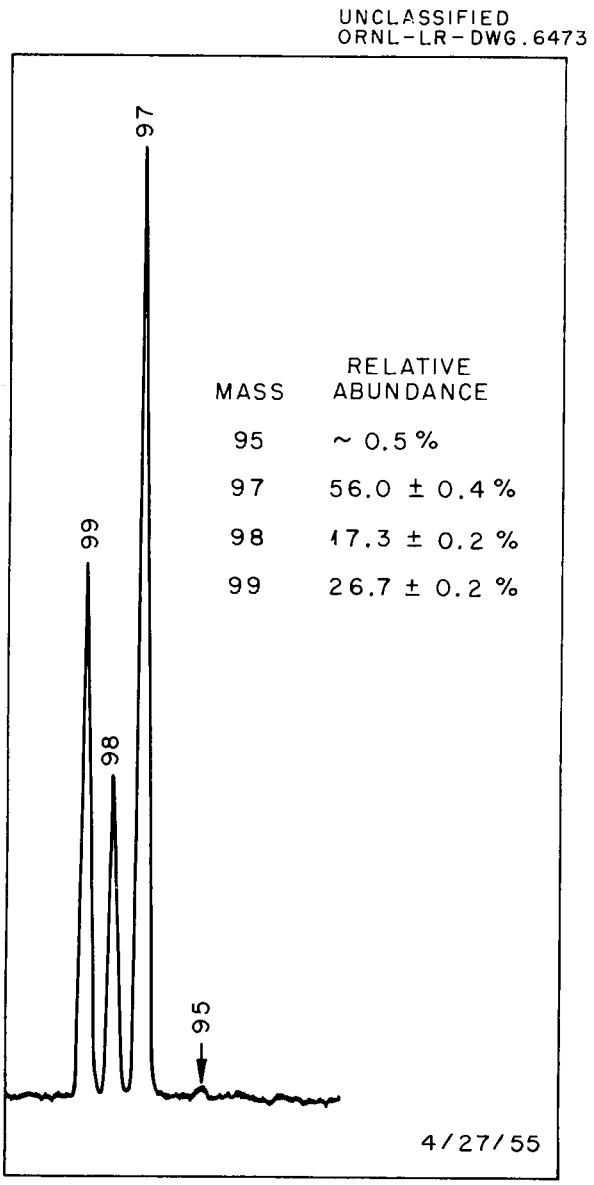

Fig. 11. Mass Spectrogram of Technetium Produced by the Irradiation of Molybdenum Metal with 22-Mev Protons.

and Tc^{98} have been seen on a mass spectrometer for the first time.

2. The "missing" isotope, Tc^{98}, has been observed and hence must be long-lived.

3. The occurrence of a long-lived isomer of Tc^{100} seems to be excluded.

4. The relative abundance of the 60-day Tc^{95m} found suggests that as little as 5×10^{-9} g of technetium can be estimated mass spectrometrically.

SHORT-LIVED FISSION PRODUCTS

Radiations of 44-sec Rh^{104} and 15-sec Tc^{100}

G. E. Boyd E. Eichler
G. D. O'Kelley Q. V. Larson

The radioactive decay of the "shielded" fission-product isotopes Rh^{104} and Tc^{100} were studied by scintillation spectroscopy. Gamma-ray spectra were observed by using NaI(Tl) crystals, 1 in. high and 1.5 in. in diameter, mounted on type 5819 or 6292 photomultiplier tubes after the method of Borkowski and Clark.[9] A hollow-crystal beta spectrometer[10] was prepared from a piece of anthracene scintillator ½ in. high and 1 in. in diameter. The pulse-height distributions from these scintillation spectrometers were displayed on a Du Mont model 329 oscilloscope, using a logarithmic sweep unit designed by Fairstein.[11] A polaroid camera served to record the spectra.

Sources of 44-sec Rh^{104g} were prepared by irradiating pure rhodium foil in the pneumatic transfer tube of the ORNL Graphite Reactor. Usually, the radiations were studied with the Rh^{104g} in equilibrium with the 4-min Rh^{104m}. The energy of the principal gamma-ray transition was measured as 0.556 ± 0.007 Mev, and the ground-state beta-ray transition was found to have an energy of 2.41 ± 0.07 Mev. The beta-ray energy was determined by visual inspection of the pulse-height distributions, comparing them with many distributions from standard sources of P^{32} and Pr^{144}. Because of the low beta branching to the first excited state at 0.556 Mev, preliminary attempts to measure the beta-ray spectrum coincident with the 0.556-Mev gamma ray were unsuccessful.

While this work was in progress, Bunker *et al.*[12] reported a study of Rh^{104g} in which gamma rays of energy 0.556 and 1.24 Mev were found, together with beta-ray groups of energies of about 2.5, 1.9, and 0.7 Mev. The values for the gamma-ray and

[9] C. J. Borkowski and R. L. Clark, *Rev. Sci. Instr.* 24, 1046 (1953).

[10] W. H. Jordan, p 207, esp p 218, Vol. 1 of *Annual Review of Nuclear Science*, L. F. Curtis (Chairman), Annual Reviews, Stanford, Calif., 1952.

[11] E. Fairstein, *Instrumentation and Controls Quar. Prog. Rep. Jan. 20, 1952*, ORNL-1335, p 13.

[12] M. E. Bunker, J. P. Mize, and J. W. Starner, *Bull. Am. Phys. Soc.* 30, No. 3, 59 (1955).

beta-ray transition energies to the ground state of Pd^{104}, as reported here, agree well with those of Bunker *et al.*

Sources of 15.8-sec Tc^{100} were prepared by using pure TcO_2. Irradiations were performed in the pneumatic transfer tube of the ORNL Graphite Reactor, where it was possible to discharge the sample from the reactor and mount it in the appropriate spectrometer in about 20 sec. The radiations were studied as in the case of Rh^{104}.

The most energetic beta-ray group, which is believed to be the ground-state transition, was found to have an energy of 2.86 ± 0.06 Mev, in surprisingly good agreement with the earlier absorption measurement[13] of 2.8 ± 0.2 Mev. A gamma ray of energy 0.542 ± 0.008 Mev was seen, which is probably the gamma ray from the first excited state of Ru^{100}. Further work on this decay scheme is in progress.

Short-lived Isotopes of Rubidium

G. D. O'Kelley E. Eichler N. H. Lazar[14]

The rate of decay of short-lived fission products is an important consideration in many reactor design studies. Gamma radiation from these nuclides is especially important in cases where a continuous processing of reactor fuel is envisioned, where reactor fuel is continuously circulated, or where the limits of safe approach to a reactor after operation must be determined. Ergen[15] has stressed the need for precise data on Kr^{88} and Rb^{88} in shielding calculations, and, more recently, Clark[16] has indicated the need for more complete data on the decay of Rb^{89}, Rb^{90}, and Rb^{91} as well. Data on the radiations and decay schemes of Rb^{88} and Rb^{89} are reported below.

Decay of 17.8-min Rb^{88}. – Levels in Sr^{88} excited by the decay of 17.8-min Rb^{88} and 104-day Y^{88} were studied by means of gamma-ray scintillation spectroscopy. Both single-crystal and coincidence spectroscopy experiments were performed by using 3 × 3 in. cylindrical NaI(Tl) crystals as scintillators, and the pulse-height spectra were recorded on a 20-channel analyzer.

[13] G. E. Boyd, Q. V. Larson, and G. W. Parker, *Phys. Rev.* 86, 1051 (1952).

[14] Physics Division.

[15] W. K. Ergen, *Hard Gamma Emitters Among Fission Fragments*, ANP-59 (May 3, 1951).

[16] F. H. Clark, *Decay of Fission Product Gammas*, NDA-27-39 (Dec. 30, 1954).

Figure 12 shows the gamma-ray spectrum obtained from a Y^{88} source placed 9.3 cm from the top face of a 3 × 3 in. NaI(Tl) crystal whose upper edge had been beveled at an angle of 45 deg to the axis of the cylinder to increase the photopeak detection efficiency. The area of the peak at 2.76 Mev, when corrected for coincident summing of the 0.098- and 1.85-Mev gamma rays,[17] indicated that the intensity of the 2.76-Mev crossover gamma ray is $5 \pm 3 \times 10^{-3}$ times that of the 1.85-Mev transition. The relative intensities of the 0.908- and 1.85-Mev gamma rays were also determined. In correcting the intensities for coincident summing, the ratio $I(1.85)/I(0.908)$ was found to be 1.09 ± 0.05, where the error is primarily an estimate of the uncertainty in the detection efficiencies involved.

[17] N. H. Lazar and E. D. Klema, *Phys. Rev.* 98, 710 (1955).

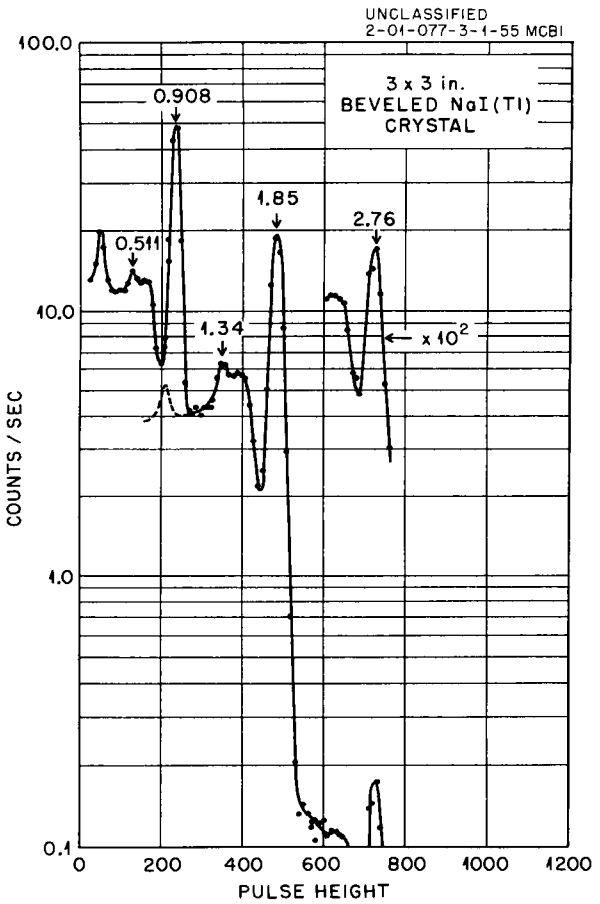

Fig. 12. Gamma-Ray Spectrum of Y^{88}.

The gamma-ray spectrum from Rb^{88} obtained with the beveled-crystal spectrometer is shown in Figs. 13 and 14. In the analysis up to 2.8 Mev, the spectral shapes obtained in the same spectrometer from sources of Y^{88} and Na^{24} were employed as guides. Above 2.8 Mev the spectrum from the 4.44-Mev gamma ray from the $N^{15}(p,\alpha\gamma)C^{12}$ reaction was used for estimating the relative height of the full-energy and pair peaks.[18]

The peak at a pulse height of 120 was caused by annihilation radiation, largely due to pairs produced in the lead detector shield. A bulge at a pulse height of approximately 280 was seen to decay with a much longer half life than that of Rb^{88} and was attributed to the 1.076-Mev gamma ray in the decay of 19-day Rb^{86}. No other impurities were found when the decay of some samples was followed for periods as long as five half lives of Rb^{88}.

With the previously used small NaI(Tl) crystals,[19] the peak at 1.39 Mev would have been difficult to detect because of the pair peak at 1.34 Mev from the 1.85-Mev gamma ray. Besides the gamma rays at 0.908 and 1.85 Mev discussed in the decay of Y^{88}, peaks due to gamma rays at 2.11 and 2.68 Mev are seen in Fig. 13, and gamma rays at 3.01, 3.23, 3.52, 3.68, and 4.87 Mev are resolvable in Fig. 14. The relative intensities of these gamma rays are given in Table 5.

Spectra were obtained in coincidence with the gamma rays at 0.908, 1.85, 2.11, and 2.68 Mev. Calculations of the expected coincidence peak intensities, based on the intensities obtained from

[18]The authors wish to acknowledge the assistance of H. B. Willard, J. K. Bair, and H. O. Cohn in performing the Van de Graaff experiment.

[19]S. Thulin, *Arkiv Fysik* 9, 108 (1955).

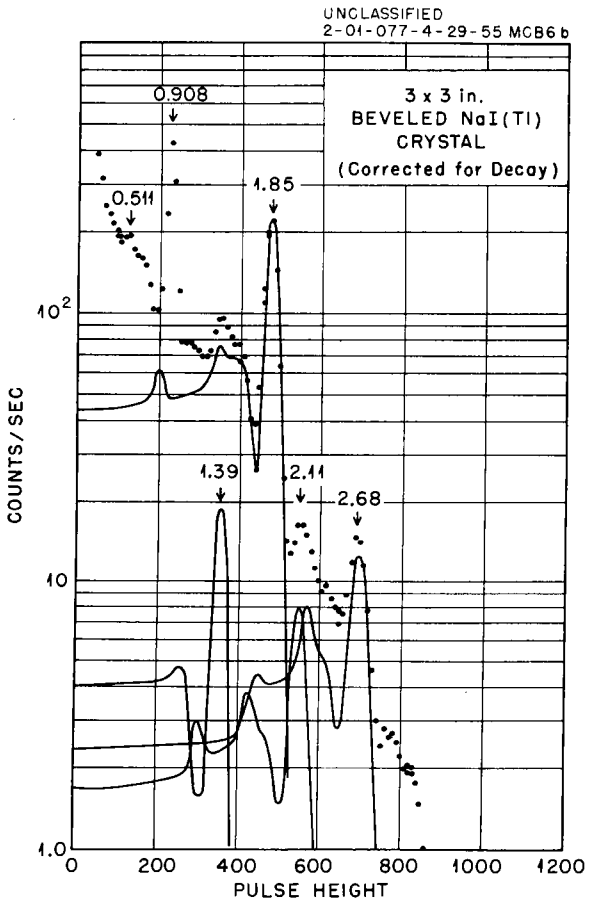

Fig. 13. Gamma-Ray Spectrum of Rb^{88} – Low-Energy Region.

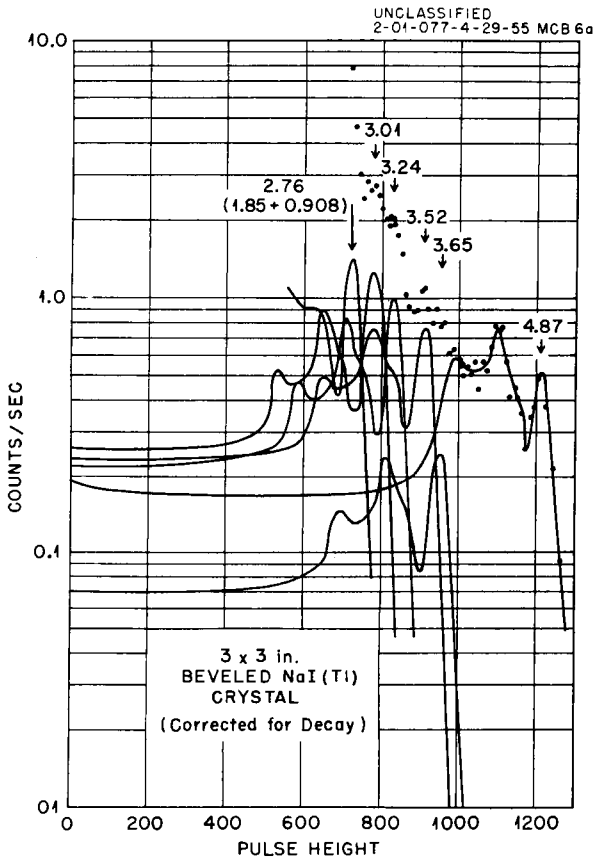

Fig. 14. Gamma-Ray Spectrum of Rb^{88} – High-Energy Region.

TABLE 5. ENERGIES AND INTENSITIES OF GAMMA RAYS FROM Rb^{88}

Energy (Mev)	Intensity Relative to 1.85-Mev Gamma Ray
1.850 ± 0.008	1.000
0.908 ± 0.005	0.631 ± 0.050
1.39 ± 0.03	0.062 ± 0.015
2.11 ± 0.03	0.045 ± 0.007
2.68 ± 0.05	0.107 ± 0.010
3.01 ± 0.05	0.014 ± 0.005
3.24 ± 0.03	0.014 ± 0.002
3.52 ± 0.05	0.011 ± 0.002
3.65 ± 0.05	0.004 ± 0.002
4.87 ± 0.05	0.014 ± 0.003

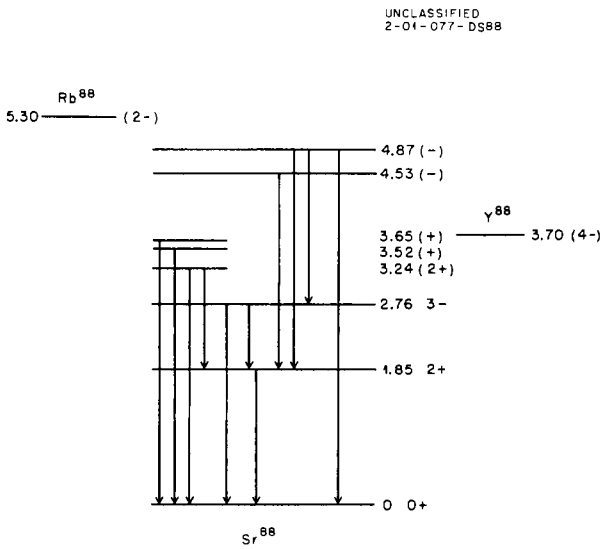

Fig. 15. Proposed Decay Scheme for the Levels of Sr^{88}.

the single-crystal data, were found to agree with the experimental measurements. The gamma-gamma coincidence and gamma-ray intensity data are consistent with the decay scheme shown in Fig. 15.

From the gamma-ray intensities it is apparent that less than 1% of them bypass the 1.85-Mev state. Thus it is possible to measure the intensity of the ground-state beta transition by an absolute measurement of the number of 1.85-Mev gamma rays and beta rays emitted from a sample of Rb^{88}. From such an experiment the ground-state beta transition was found to occur in 75.9 ± 5.0% of the total beta transitions.

Comparative half lives for all the beta transitions from Rb^{88} were calculated from the gamma-ray intensities, with the assumption that 76% of all beta transitions are to the ground state of Sr^{88}; the results are listed in Table 6. The log *ft* value of 7.9 for the beta-ray group to the first excited state is in good agreement with the proposed 2+ spin, but the transition to the 2.76-Mev level is slower than expected for an allowed decay. Odd parity was assigned to the 4.87- and 4.54-Mev states, since the comparative half lives of the beta transitions to these levels correspond to those expected for allowed transitions.

TABLE 6. INTENSITIES AND COMPARATIVE HALF LIVES OF THE BETA-RAY TRANSITIONS OF Rb^{88} COMPUTED FROM THE GAMMA-RAY INTENSITIES

(Transitions labeled by final states)

Beta-Ray Groups	Intensity	Logarithm of Comparative Half Life
β_0	0.759	7.5
$\beta_{1.85}$	0.043	7.9
$\beta_{2.76}$	0.136	6.7
$\beta_{3.24}$	0.017	7.3
$\beta_{3.32}$	0.0025	7.9
$\beta_{3.68}$	0.00083	8.1
$\beta_{4.53}$	0.025	5.2
$\beta_{4.87}$	0.017	5.0

Even parity is assigned to the states at 3.25, 3.52, and 3.68 Mev, again using as a guide the comparative half lives of the beta transitions feeding them. A spin of 2+ can be assigned to the 3.25-Mev level, from the intensities of the 3.25- and 1.39-Mev gamma rays.

An attempt was made to identify the first few excited states of $_{38}Sr^{88}_{50}$, with proton configurations predicted from the single-particle model. The single-particle states available for the twenty-ninth through the fiftieth protons are $f_{5/2}$, $p_{3/2}$,

$p_{1/2}$, and $g_{9/2}$; ${}_{40}Zr^{90}_{50}$, with two more protons, appears to fill the $p_{1/2}$ shell,[20] and so a reasonable assignment for the last ten protons in the ground state of Sr^{88} is $(f_{5/2})^6(p_{3/2})^4$. If one of the $p_{3/2}$ protons is excited into the $p_{1/2}$ orbital, the resulting coupling would very likely yield a 2+ state. If the proton is excited to the $g_{9/2}$ orbital, it might couple to the resulting hole to yield the 3– excited state. Pertinent configurations might be $(p_{3/2})^{-1}(p_{1/2})_{2+}$ and $(p_{3/2})^{-1}(g_{9/2})_{3-}$. Since the neighboring nucleus ${}_{39}Y^{89}_{50}$ is known to have a $g_{9/2}$-$p_{1/2}$ isomeric transition with an energy of 0.913 Mev, it is tempting to try to explain the slowness of the 0.908-Mev transition, compared with the single-particle estimates, by the $g_{9/2}$-$p_{1/2}$ proton orbital change between the initial and final states.

Decay of Rb^{89}. – The radiations from the decay of Rb^{89} were investigated by using the same single-crystal and coincidence spectroscopy techniques that were used for the Rb^{88} work.

Sources of 15.4-min Rb^{89} were "milked" from the 3.2-min Kr^{89} parent. Irradiations were performed in the pneumatic tube rabbit sketched in Fig. 16. The fission source consisted of enriched uranium, approximately 0.3 mg/cm^2 thick and 1.6 cm in diameter, over which a 3.12 mg/cm^2 aluminum foil was placed to eliminate the heavy xenon fission fragments. When the apparatus was assembled in the micarta rabbit, the stainless steel gas cell was sealed at the top by the rubber disk, and at the bottom by the rubber gasket and aluminum absorber foil. A typical irradiation time in the ORNL Graphite Reactor was 3 min, the approximate half life of the desired Kr^{89} parent nuclide.

After irradiation, the sample was ejected from the reactor core and dropped into a shielded holder for another 3 min to permit the higher-mass krypton isotopes of shorter half life to decay out. At this point a needle, made of two concentric stainless steel tubes sealed at the top, was forced downward until the rubber disk covering the gas cell was punctured and the needle chuck engaged the rabbit cap. Simultaneously, air was drawn down the inner tube of the needle and, after sweeping the gas cell, passed into the jacket of the needle through the four gas inlet holes. Air and radioactive gas traveled up the needle jacket, through

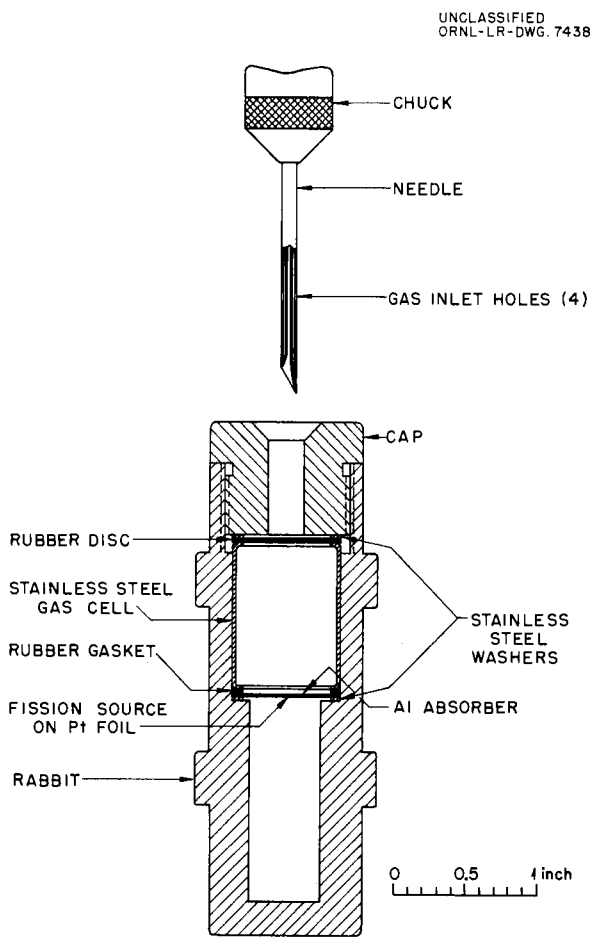

Fig. 16. Apparatus for Production and Fast Removal of Krypton Fission Gas.

a trap of glass wool refrigerated with dry ice and acetone, and into an evacuated collection cell. For another 3-min period the krypton gas was allowed to decay, the rubidium recoil atoms being collected on a negatively charged strip of metal foil. In experiments where larger amounts of Rb^{89} activity were desired, the gas cell in the rabbit was longer and was closed at the bottom. Enriched uranium was deposited on a larger platinum foil to which the aluminum absorber was cemented, the foil "sandwich" then being rolled into a cylinder and inserted in the gas cell, where it formed a liner.

Following collection, the Rb^{89} activity was usually radiochemically purified, since some krypton activity usually contaminated the collecting foil and since straggling in the aluminum absorber

[20] K. Ford, private communication.

caused a small amount of Cs^{138} contamination in the gamma-ray spectra.

Figure 17 shows a typical gamma-ray spectrum of Rb^{89} obtained with a 3 × 3 in. NaI(Tl) crystal and a 20-channel pulse-height analyzer. Peaks can be resolved at 0.25, 0.663, 1.05, 1.26, 1.44, 1.55, 1.87, 1.95, 2.20, 2.55, and 2.74 Mev. The peak at 1.44 Mev exhibited a longer half life than that for Rb^{89}, and is attributed to Cs^{138} contamination. These results are preliminary, and the existence of the weak lines at 1.87, 1.95, and 2.74 Mev must be further investigated. It is possible that the peak at 1.87 Mev is due to the 1.85-Mev gamma ray of Rb^{88}.

A sample of Rb^{89} was placed inside a $4\frac{3}{4}$-in. NaI(Tl) crystal, with the results shown in Fig. 18. In addition to the 0.663-, 1.05-, and 1.26-Mev gamma rays, lines due to coincident summing appear at 2.28 ± 0.04 and 3.22 ± 0.06 Mev. From this experiment it is concluded that the 1.05- and 1.26-Mev gamma rays are in coincidence, as are the 1.05- and 2.20-Mev gamma rays. Gamma-gamma coincidence measurements have confirmed these conclusions from the large-crystal data and have also established that the 2.55-Mev transition is not in coincidence with the 1.05-Mev gamma ray. Other measurements have also shown that the 2.55- and 0.663-Mev transitions are in coincidence as well.

These gamma-ray data can be used to build up a consistent decay scheme with levels at 1.05, 2.31, 2.55, and 3.25 Mev above the ground state of Sr^{89}. Although the principal gamma-ray transitions are fitted into this scheme, the presence of other gamma radiation in low intensity must be checked before this decay scheme study is complete.

The energy of the ground-state beta-ray transition in Rb^{89} was measured by using a hollow-crystal anthracene scintillation spectrometer and a single-channel analyzer. Calibration of the spectrometer was accomplished with the internal conversion electrons from a Cs^{137} source at 0.625 Mev and a Bi^{207} source at 0.98 Mev. Fermi analysis of several beta-ray spectra from different irradiations showed the ground-state transition to be 3.92 ± 0.10 Mev, where the error is estimated to be

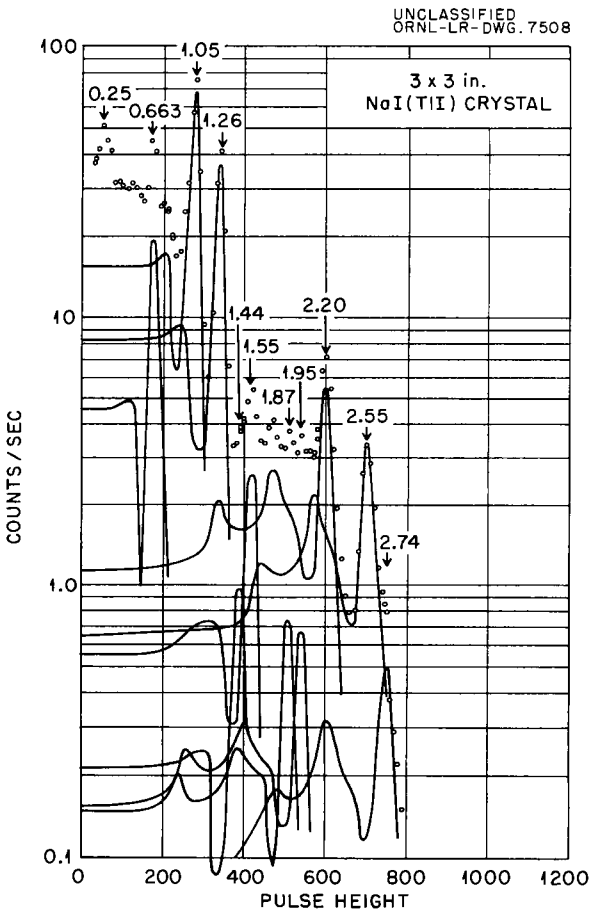

Fig. 17. Gamma-Ray Spectrum of Rb^{89}.

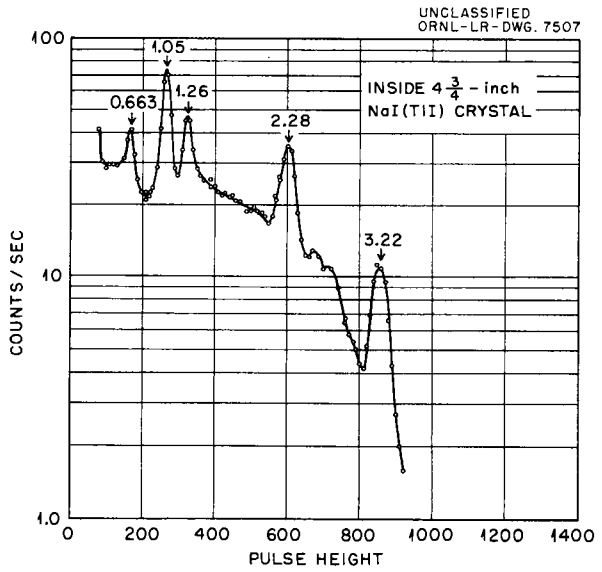

Fig. 18. Gamma-Ray Spectrum of Rb^{89} Inside a $4\frac{3}{4}$-in. NaI(Tl) Crystal.

chiefly due to the large extrapolation from the last calibration at 0.98 Mev to the end point.

RADIOACTIVITY OF THE Ce^{137} ISOMERS

A. R. Brosi B. H. Ketelle

A radioactive decay period of 36 hr was assigned to Ce^{137} by Chubbock and Perlman,[21] who reported decay by electron capture through a 280-kev level in La^{137}. Stover[22] confirmed the work of Chubbock and Perlman but found the gamma energy to be 240 kev. In a search for an isomeric transition in Ce^{137}, Hill[23] confirmed the mass assignment of the 36-hr period by the use of enriched isotopes and found the *K/L* conversion ratio of a 257-kev gamma ray to be about 4. Keller and Cork,[24] who also used enriched isotopes, confirmed the mass assignment and gave an energy of 253.4 kev for the gamma ray. They found a *K/L* conversion ratio of about 10. In the present work the *K* conversion coefficient, as well as the *K/L* conversion ratio, has been measured. This has led to a new assignment of the 36-hr decay period and to the discovery of a new radioactive species which has been assigned to Ce^{137}.

Isomeric Transition in Ce^{137}

A mixture of Ce^{137}, Ce^{139}, and Ce^{141} was produced by bombardment of a BaF_2 target with 48-Mev alpha particles in the Berkeley 60-in. cyclotron. The cerium fraction from the target was identified and purified with a cation-exchange column.[25] The conversion-electron spectrum of a source prepared from this material was measured with a thin-magnetic-lens spectrometer.

The intensity of the *K* conversion peak of the 255-kev gamma was measured relative to the *K* conversion peak of the 166-kev gamma of Ce^{139}. A NaI scintillation spectrometer was used to measure the relative intensities of the unconverted 255- and 166-kev gammas. From these intensity ratios and the published[26] *K* conversion coefficient (0.2 ± 0.05) of the 166-kev gamma, a *K* conversion coefficient of 5.5 ± 1.5 was found for the 255-kev gamma ray. This conversion coefficient and the *K/L* conversion ratio of 2.3 ± 0.2 indicate that the 255 kev gamma is emitted in an *M*4 transition.[27,28]

An *M*4 isomeric transition in Ce^{137} is expected from the systematics of energy-level spacings.[29] X-ray–gamma-ray coincidence measurements show that the 255-kev gamma is not coincident with capture x rays and thus support the conclusion that it is emitted from an isomeric level. This conclusion is confirmed by the fact that the x rays associated with the 34.5-hr period are cerium rather than lanthanum x rays. This was shown by using a xenon-filled proportional counter, in conjunction with a linear amplifier and a pulse analyzer. Both the $K\alpha_1$ and the $K\beta$ x rays of cerium are critically absorbed by xenon, whereas only the $K\beta$ x rays of lanthanum are critically absorbed. Escape of the fluorescent $K\alpha$ and $K\beta$ x rays of xenon results in pulse-height peaks at about 5 and 9 kev when either cerium or lanthanum x rays are counted. However, the ratio of the intensity of the peak at 5 kev to the peak at 9 kev should be about 10 times greater for cerium than for lanthanum *K* x rays. A comparison of the pulse-height spectra of Ce^{139} and Ce^{137} shows that the *K* x rays emitted with a 34.5-hr half life are those of cerium. The conversion electrons and unconverted gamma of the 255-kev transition also decay with a 34.5 ± 0.5 hr half life.

Cerium samples enriched in Ce^{136} have been used to confirm the mass assignment of the 34.5-hr decay period. One sample was enriched to 30% Ce^{136} and another to 6% Ce^{136}. Both were bombarded for the same period at the same neutron flux in the ORNL Graphite Reactor. The samples were measured with a scintillation spectrometer, and the 255-kev gamma-ray activities per microgram of each of the cerium isotopes in the samples are shown in Table 7. These data show that the yields of the 34.5-hr isomer per microgram of Ce^{136} are the same in the two samples and therefore that the isomeric transition is in Ce^{137}.

[21] J. B. Chubbock and I. Perlman, *Phys. Rev.* 74, 982 (1948).

[22] B. J. Stover, *Phys. Rev.* 81, 8 (1951).

[23] R. D. Hill, *Phys. Rev.* 82, 449 (1951).

[24] H. B. Keller and J. M. Cork, *Phys. Rev.* 84, 1079 (1951).

[25] B. H. Ketelle and G. E. Boyd, *J. Am. Chem. Soc.* 69, 2800 (1947).

[26] C. H. Pruett and R. G. Wilkinson, *Phys. Rev.* 96, 1340 (1954).

[27] M. E. Rose *et. al.*, *Phys. Rev.* 83, 79 (1951).

[28] M. E. Rose, privately distributed *L* conversion coefficients.

[29] M. Goldhaber and R. D. Hill, *Revs. Mod. Phys.* 24, 179 (1952).

TABLE 7. NEUTRON CAPTURE YIELDS REFERRED TO ISOTOPIC ASSAYS

	255-kev counts/min/μg				445-kev counts/min/μg			
	Ce^{136}	Ce^{138}	Ce^{140}	Ce^{142}	Ce^{136}	Ce^{138}	Ce^{140}	Ce^{142}
Isotopic enrichment No. 1	9.8	430	4.5	71	30.8	1340	14.2	220
Isotopic enrichment No. 2	10.1	6	0.8	21	31.0	18.3	2.4	64

Electron Capture Decay of Ce^{137}

When a mixture of stable cerium isotopes is bombarded with slow neutrons, a 445-kev gamma ray and x rays which decay with an 8.7-hr half life are produced. Chemical separation of cerium from rare-earth impurities shows that the activity is associated with a cerium isotope. The data in Table 7 show that the amount of the 445-kev gamma emitter formed is proportional to the amount of Ce^{136} bombarded and therefore that the transition must occur in the decay of Ce^{137}. The 445-kev gamma is in prompt coincidence with K x rays which are not critically absorbed in the xenon proportional counter. These facts show that Ce^{137} decays by electron capture, with at least some of the captures to a 445-kev level in lanthanum.

Decay curves of the x rays and the 445-kev gamma ray show that the 8.7-hr electron capture process is the daughter of the 34.5-hr isomeric transition. When the parent and daughter are in equilibrium, the relative number of 255- and 445-kev transitions indicates that 3% of the electron captures are to the 445-kev level in La^{137}. An approximate K conversion coefficient of 0.02 for the 445-kev transition was computed from intensity ratios, which indicates an $M1$ or $E2$ transition.

Approximate cross sections of Ce^{136} for reactor neutrons have been computed from the yields. The values give 20 barns for capture to the ground state and 2 barns for capture to the isomeric state of Ce^{137}. These cross sections are known within a factor of 2 and are in reasonable agreement with 25 barns ±100% given by Pomerance[30] for the thermal-neutron absorption cross section of Ce^{136}.

Discussion

On the basis of the single-particle model,[31] an isomeric transition between $h_{11/2}$ and $d_{3/2}$ levels

UNCLASSIFIED
ORNL-LR-DWG. 7386

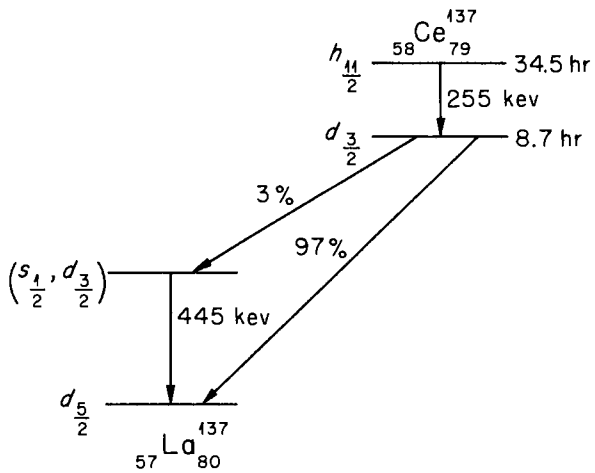

Fig. 19. Cerium-137 Decay Scheme.

is probable in Ce^{137}. In the 79 neutron isotopes of tellurium, xenon, and barium, the single-particle predictions have been verified, and isomeric transitions from $h_{11/2}$ levels to $d_{3/2}$ levels are known. In the case of Ce^{137} the K conversion coefficient and the K/L conversion ratio indicate an $M4$ transition for the decay of the 255-kev isomeric state. Therefore, the isomeric state is shown as an $h_{11/2}$ level in the decay scheme proposed for Ce^{137} in Fig. 19. Although it seems quite clear that the isomeric transition is to a $d_{3/2}$ level, it is not so certain that the ground state of Ce^{137} is a $d_{3/2}$ level. The ground states of many of the odd neutron isotopes near the end of the 82-neutron shell are $s_{1/2}$ levels. The systematics of energy-level spacing[32] do not lead to a definite prediction concerning the ground state of Ce^{137}. However,

[30] H. S. Pomerance, *Phys. Rev.* 88, 412 (1952).
[31] M. G. Mayer, *Phys. Rev.* 78, 16 (1950).
[32] M. Goldhaber and R. D. Hill, *Revs. Mod. Phys.* 24, 179 (1952).

no experimental evidence for a $d_{3/2}$-$s_{1/2}$ transition following decay of the isomer was found. The fact that electron capture to the 445-kev level and to the ground state of La^{137} is allowed can also be used as an argument against an $s_{1/2}$ ground state for Ce^{137}.

Of the single-particle levels available for assignment to the ground state of La^{137}, only $d_{5/2}$ fits the experimental observations. Since the spin of Ba^{137} is known to be $d_{3/2}$, a transition between the ground states of La^{137} and Ba^{137} should be allowed. However, no evidence of K or L x rays which could be attributed to electron capture decay of La^{137} was found. Because of the high x-ray counting efficiency of the detectors used in this work, the lower limit for the K or L electron capture half life for La^{137} must be increased from 400 years[33] to 10^5 years. The long half life of La^{137} may mean that the energy available for the transition is very low. On the other hand, this may be another case where the probability of a transition is reduced because it occurs between a state with a mixed configuration and a pure single-particle state.[34]

The authors wish to express appreciation to G. B. Rossi for arranging the cyclotron bombardment and to members of the Stable Isotope Research and Production Division for samples of enriched cerium isotopes and for isotopic assays.

[33] J. B. Chubbock and I. Perlman, *Phys. Rev.* 74, 982 (1948).

[34] A. De-Shalit and M. Goldhaber, *Phys. Rev.* 92, 1211 (1953).

ORGANIC CHEMISTRY

PINACOL REARRANGEMENT OF TRIPHENYLETHYLENE GLYCOL

C. J. Collins

The studies of the pinacol rearrangement of C^{14}-labeled triphenylethylene glycol (I*a*, I*b*, I*c*) in the presence of five different acid catalysts are now complete:

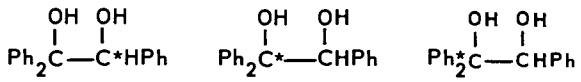

I*a* I*b* I*c*

Given in Chart 1 are the four possible reaction paths for this transformation. Given in Table 8 are the expected radioactivity distributions from paths through which benzhydryl phenyl ketone might be formed. Glycols I*a* and I*c* were rearranged in the presence of each of the following: (1) cold, concentrated sulfuric acid; (2) refluxing oxalic acid dihydrate; (3) refluxing formic acid; (4) refluxing dilute sulfuric acid; (5) refluxing dioxane–hydrochloric acid mixtures. These catalysts were selected because they are, in general, the ones which had been used previously to effect rearrangement of triphenylethylene glycol and its derivatives:

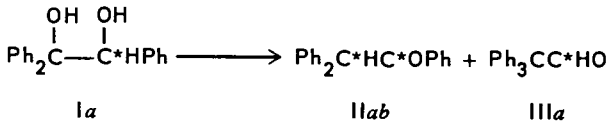

I*a* II*ab* III*a*

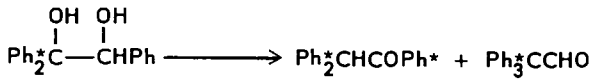

I*c* II*cd* III*c*

For those experiments in which the extent of C^{14} migration was to be determined, the products II*ab* and II*cd* were purified by crystallization from

CHART 1

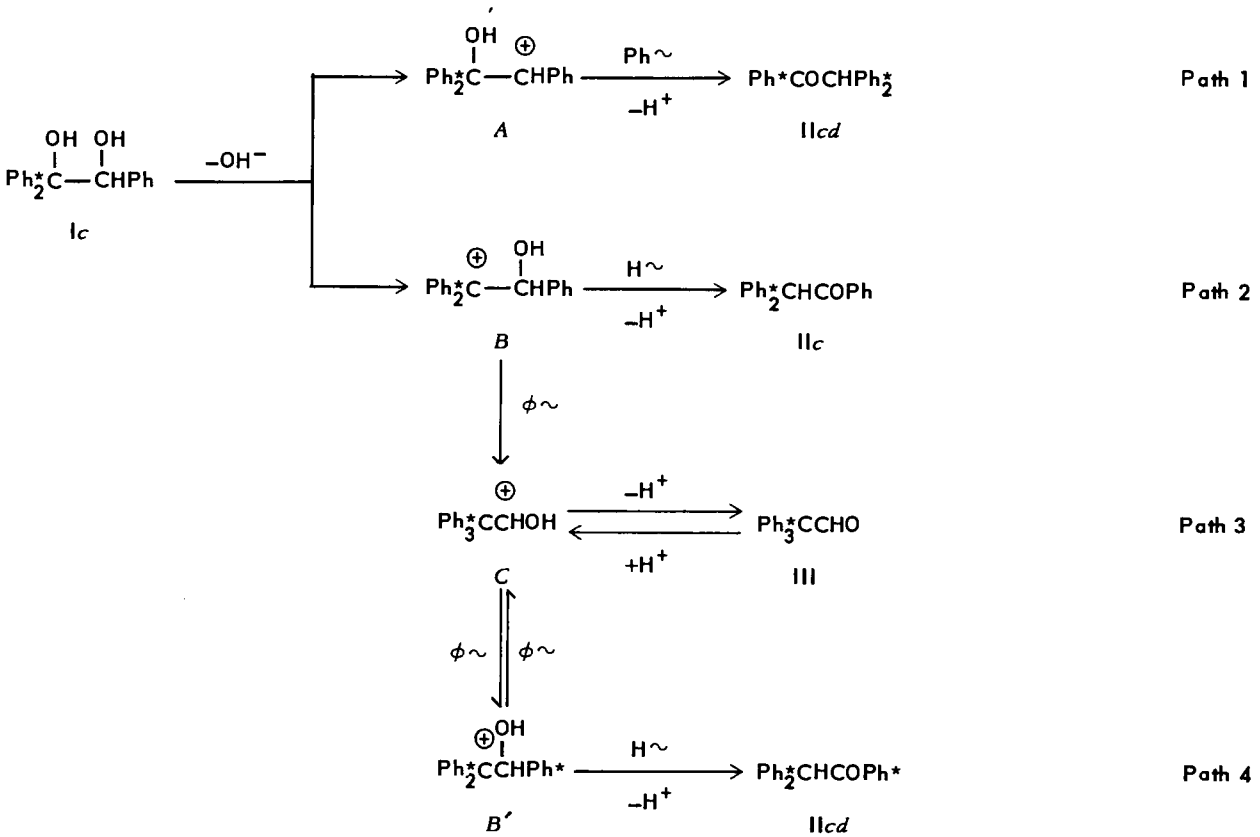

TABLE 8. EXPECTED RADIOACTIVITY DISTRIBUTIONS FROM REACTION PATHS THROUGH WHICH BENZHYDRYL PHENYL KETONE MIGHT BE FORMED

Reactant	Path Through Which Product Is Formed	Product	C^{14} Rearrangement (%)
$Ph_2C(OH)-C^*H(OH)Ph$ (Ia)	Path 1	$PhCOC^*HPh_2$	100
	Path 2	Ph_2CHC^*OPh	0
	Path 4	Ph_2CHC^*OPh	0
$Ph^*_2C(OH)-CH(OH)Ph$ (Ic)	Path 1	$Ph^*COCHPh^*_2$	50
	Path 2	$Ph^*_2CHCOPh$	0
	Path 4	$Ph^*_2CHCOPh^*$	33.3

ethanol and then oxidized with permanganate to benzophenone and benzoic acid:

$$\text{II}ab \xrightarrow{KMnO_4} Ph_2C^*{=}O + PhC^*OOH$$

$$\text{II}cd \xrightarrow{KMnO_4} Ph^*_2C{=}O + Ph^*COOH$$

The benzophenone fractions were converted quantitatively to their 2,4-dinitrophenylhydrazones, and the latter were assayed for radioactivity content. The molar radioactivities of these derivatives were taken as a direct measure of the amount of C^{14} migration attending the particular reaction studied. The results of these experiments are given in Table 9. It was necessary to use glycol I*a* instead of I*b* in these experiments because of the rather large error introduced into the migration calculations by the oxidative isotope effect during the action of permanganate on ketone II*b* (labeled in the benzhydryl portion of the molecule). Preliminary experiments in which I*b* was used erroneously indicated the amount of rearrangement of the chain-label to be 8 to 13% of the total reaction for each acid catalyst employed. It was shown independently that ketone II is stable to the action of acid by demonstrating that no C^{14} rearrangement took place in a sample of benzhydryl phenyl-C^{14} ketone (II*d*) which had been dissolved in concentrated sulfuric acid for 24 hr.

For those experiments in which the yields of ketone (II) and aldehyde (III) were to be determined by the isotopic dilution method, the reaction product from glycol I*b* was diluted to a given volume with ether and then divided into two equal portions. To one portion was added a weighed amount of nonradioactive ketone II. The solution was concentrated to dryness, the concentrate was then twice crystallized from ethanol, and the product was assayed for radioactivity. To the other portion a weighed amount of nonradioactive triphenylacetaldehyde (III) was added. The solution was concentrated to dryness and the concentrate was dissolved in alcohol and treated with an excess of 2,4-dinitrophenylhydrazine hydrosulfate. The derivative was twice crystallized from dioxane-ethanol solutions and then assayed for radioactivity. From the molar radioactivities of the diluted ketone (II*ab*) and of the diluted derivative of the aldehyde (III), the yields of II and III under each set of conditions were calculated with high accuracy. The results of these yield determinations are given in Table 10. Although, ideally, both the yield data and the migration data should be determined for each catalyst by using the product from a single experiment, this procedure was not practical. Because of the high degree of duplicability of the ring-label rearrangements (Table 9), the author has assumed that the yield data for II and III are similarly invariant.

From the foregoing data, therefore, the contribution of each path to the total reaction has been calculated when glycol I is subjected to rearrangement under the conditions employed in the present experiments. These contributions are given in Table 11; also given are the ratios, for each acid catalyst, of phenyl/hydrogen migration (to the tertiary carbon atom). These were obtained simply

TABLE 9. REARRANGEMENT OF C^{14} LABEL WHEN GLYCOLS I*a* AND I*c* ARE REARRANGED UNDER THE INFLUENCE OF VARIOUS ACID CATALYSTS

Experiment No.	Reactant	Catalyst Used	Molar Radioactivity of $Ph_2C^*{=}O$ or $Ph_2^*C{=}O$[a]		C^{14} Migration (%)
1	I*a*	Cold conc H_2SO_4	0.036 ± 0.001	0.025 ± 0.01[b]	2.5 ± 1.0[c]
2	I*a*	Cold conc H_2SO_4	0.015 ± 0.001		
3	I*c*	Cold conc H_2SO_4	0.693 ± 0.002	0.702 ± 0.008	29.8 ± 0.8
4	I*c*	Cold conc H_2SO_4	0.703 ± 0.001		
5	I*c*	Cold conc H_2SO_4	0.717 ± 0.002		
6	I*c*	Cold conc H_2SO_4	0.696 ± 0.002		
7	I*a*	Oxalic acid dihydrate, reflux	0.039 ± 0.0008	0.039 ± 0.001	3.9 ± 0.1
8	I*c*	Oxalic acid dihydrate, reflux	0.791 ± 0.001	0.804 ± 0.01	19.6 ± 1.0
9	I*c*	Oxalic acid dihydrate, reflux	0.817 ± 0.001		
10	I*a*	Formic acid, reflux	0.047 ± 0.001	0.047 ± 0.001	4.7 ± 0.1
11	I*c*	Formic acid, reflux	0.782 ± 0.001	0.789 ± 0.008	21.1 ± 0.8
12	I*c*	Formic acid, reflux	0.797 ± 0.003		
13	I*a*	Dilute H_2SO_4	0.045 ± 0.001	0.039 ± 0.006	3.9 ± 0.6
14	I*a*	Dilute H_2SO_4	0.033 ± 0.001		
15	I*c*	Dilute H_2SO_4	0.928 ± 0.005	0.930 ± 0.002	7.0 ± 0.2
16	I*c*	Dilute H_2SO_4	0.931 ± 0.003		
17	I*c*	Dioxane-water-HCl, reflux	0.995 ± 0.004	0.995 ± 0.004	0

[a]Taken as the fraction of the original radioactivity of the glycols I*a* or I*c*.
[b]Uncertainty expressed as the average deviation from the mean value of two or more determinations.
[c]Uncertainty expressed as the average deviation from the averages of the mean values given in column 4.

TABLE 10. YIELDS OF BENZHYDRYL PHENYL KETONE (II) AND OF TRIPHENYLACETALDEHYDE (III) AS DETERMINED BY THE ISOTOPE DILUTION METHOD WHEN TRIPHENYLETHYLENE GLYCOL (I) IS TREATED WITH VARIOUS ACID CATALYSTS

Catalyst	Yield of II (%)	Yield of III (%)	Total (%)
Cold conc H_2SO_4	100.1 ± 1.0	0.77 ± 0.04	100.9
Oxalic acid dihydrate	69.5 ± 0.5	29.9 ± 0.1	99.4
Formic acid	101.6 ± 0.6	0.98 ± 0.08	102.6
Dilute H_2SO_4	84.9 ± 0.4	16.5 ± 0.2	101.4
Dioxane-water-HCl	93.6 ± 0.9	3.9 ± 0.1	97.5

by dividing the sum of the contributions of paths 3 and 4 by the contribution of path 2 for each reaction. For simplicity, the aldehyde yields were used in calculating the data of Table 11; the yields were taken as zero in the reactions in which concentrated sulfuric and formic acids were used as catalysts.

REACTION OF 2-PHENYL-2-*p*-TOLYLETHYL-1-C^{14}-AMINE WITH NITROUS ACID – A REINVESTIGATION

B. M. Benjamin C. J. Collins

The reported anomalous observation[1] that the *p*-tolyl group migrates at a rate slower than that of

[1]L. S. Ciereszko and J. G. Burr, Jr., *J. Am. Chem. Soc.* 74, 5431 (1952); P. S. Bailey and J. G. Burr, Jr., *J. Am. Chem. Soc.* 75, 2951 (1953).

TABLE 11. CONTRIBUTIONS OF PATHS 1, 2, 3, AND 4 TO THE TOTAL REACTION WHEN TRIPHENYLETHYLENE GLYCOL IS REARRANGED WITH VARIOUS ACIDIC CATALYSTS

Catalyst	Contribution of Path (%)				ϕ/H Migration Ratio
	1	2	3	4	
Concentrated H_2SO_4	2.5	11.7	0	85.8	7.33
Oxalic acid	2.7	29.9	29.9	37.5	2.25
Formic acid	4.7	39.0	0	56.3	1.44
Diluted H_2SO_4	3.2	67.4	16.5	12.9	0.435
Dioxane-water-HCl	0	96.1	3.9	0	0.0406

the phenyl group in the deamination of 2-phenyl-2-*p*-tolylethyl-1-C^{14}-amine has been reinvestigated. Implicit in the experimental method employed[1] by the previous investigators is the assumption (see Chart 2) that compounds II and III are oxidized by permanganate to terphthalic acid in identical yields. This assumption is not valid. The foregoing experiments have been repeated, and the methods used by Burr and his collaborators have been duplicated as closely as possible. The data thus obtained were not consistent, since the values for the molar radioactivities of the terphthalic acid fractions were not duplicable, and the sum of the molar radioactivities of the benzoic and terphthalic acid fractions was usually much less than the activity of the amine (I). In one experiment in which the sum of the molar radioactivities of the benzoic and terphthalic acid fractions most nearly accounted for the radioactivity of the amine (I) (98% of the original activity of I), a *p*-tolyl/phenyl migration ratio of 1.22 was calculated. This value is in fair agreement with that of Curtin and Crew,[2] who stated this same ratio to be 1.28 in the deamination of 2-phenyl-2-*p*-tolylethanolamine. An alternate method was also employed, consisting in a determination of the yields of the products (II and III, Chart 2) by the isotopic dilution technique. The yields of the two alcohols are 43.4 and 34.8%, respectively. This corresponds to a *p*-tolyl/phenyl ratio of 1.25; 4-methyl stilbene was present in the reaction mixture in trace amounts (1.6%, indicated by dilution technique).

[2]D. Y. Curtin and M. C. Crew, *J. Am. Chem. Soc.* 76, 3719 (1954).

[3]A. McKenzie, R. Roger, and W. B. McKay, *J. Chem. Soc.* 2597 (1932).

PINACOL REARRANGEMENT OF 1,2-DIPHENYL-1-*p*-TOLYLETHYLENE GLYCOL

B. M. Benjamin C. J. Collins

McKenzie and co-workers[3] reported that the action of acidic reagents on the α-form of 1,2-diphenyl-1-*p*-tolylethylene glycol (I) resulted in the formation primarily of *p*-tolyldesoxybenzoin (II). This was in contradiction to earlier work[4] in which mainly *p*-tolylbenzhydryl ketone (III) was isolated from the reaction mixture. It is expected that both II and III are obtained in the reaction by the different paths indicated in Chart 3.

Both the α- and the β-forms of the glycol, labeled in the chain, were prepared and subjected to conditions for rearrangement. Nonradioactive samples of II and III were synthesized, and weighed portions of these were added to aliquots of the reaction mixtures. The compounds were then crystallized to constant radioactivity.

The yields of II and III could not be determined precisely when concentrated sulfuric acid was used in the rearrangements, probably because sulfonation was taking place. Roughly, the yields of II and III were 85 and 15%, respectively. The C^{14} distribution in the products indicated that 98% tertiary hydroxyl removal and 2% secondary hydroxyl removal occurred.

When the rearranging medium was formic acid, a good material balance was obtained. Both the α- and the β-forms of the glycol gave the same results, as shown in Table 12. The C^{14} distribution in the two ketones indicated that the tertiary hydroxyl group was removed 95% of the time.

[4]A. McKenzie, A. K. Mills, and J. R. Myles, *Ber.* 63, 904 (1930).

CHART 2

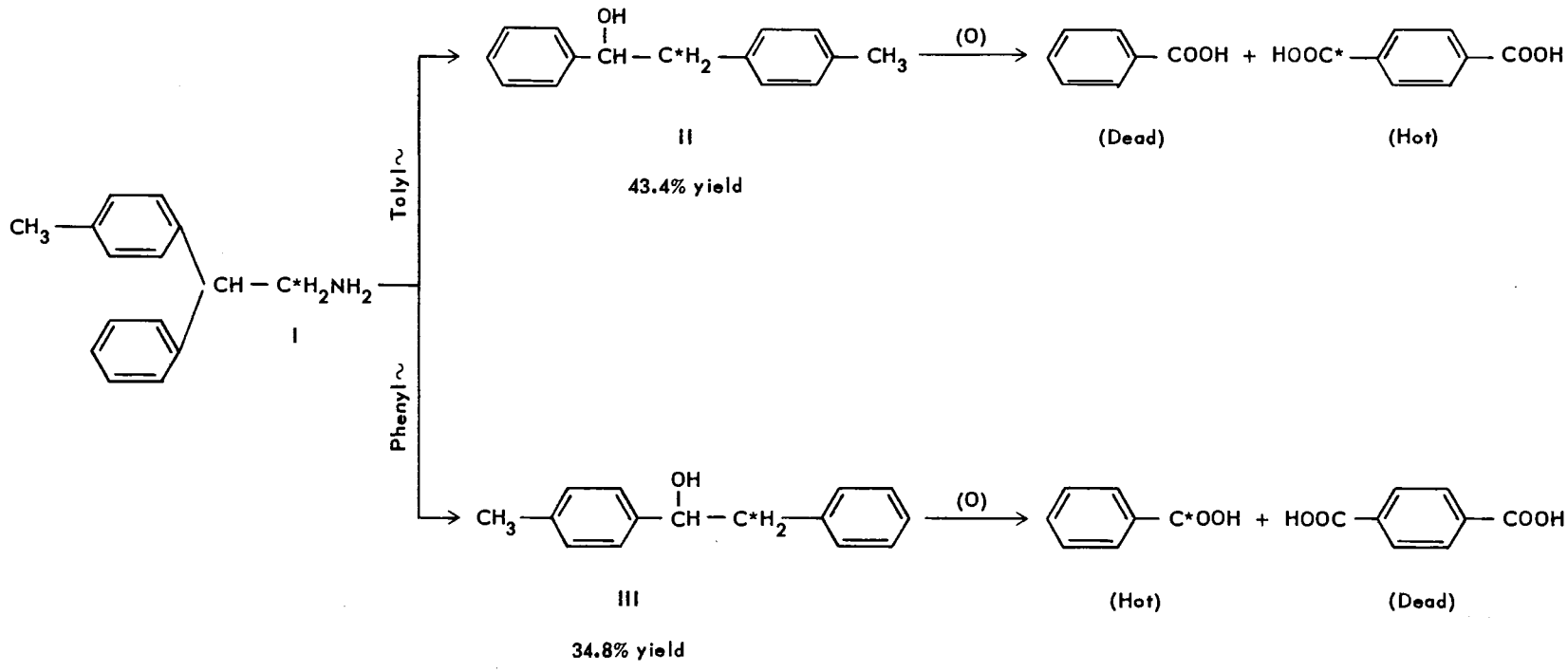
CH3
CH — C*H2NH2
I
Tolyl~
Phenyl~
OH
CH — C*H2
CH3
II
43.4% yield
(O)
COOH + HOOC*
COOH
(Dead)
(Hot)
CH3
OH
CH — C*H2
III
34.8% yield
(O)
C*OOH + HOOC
COOH
(Hot)
(Dead)

CHART 3

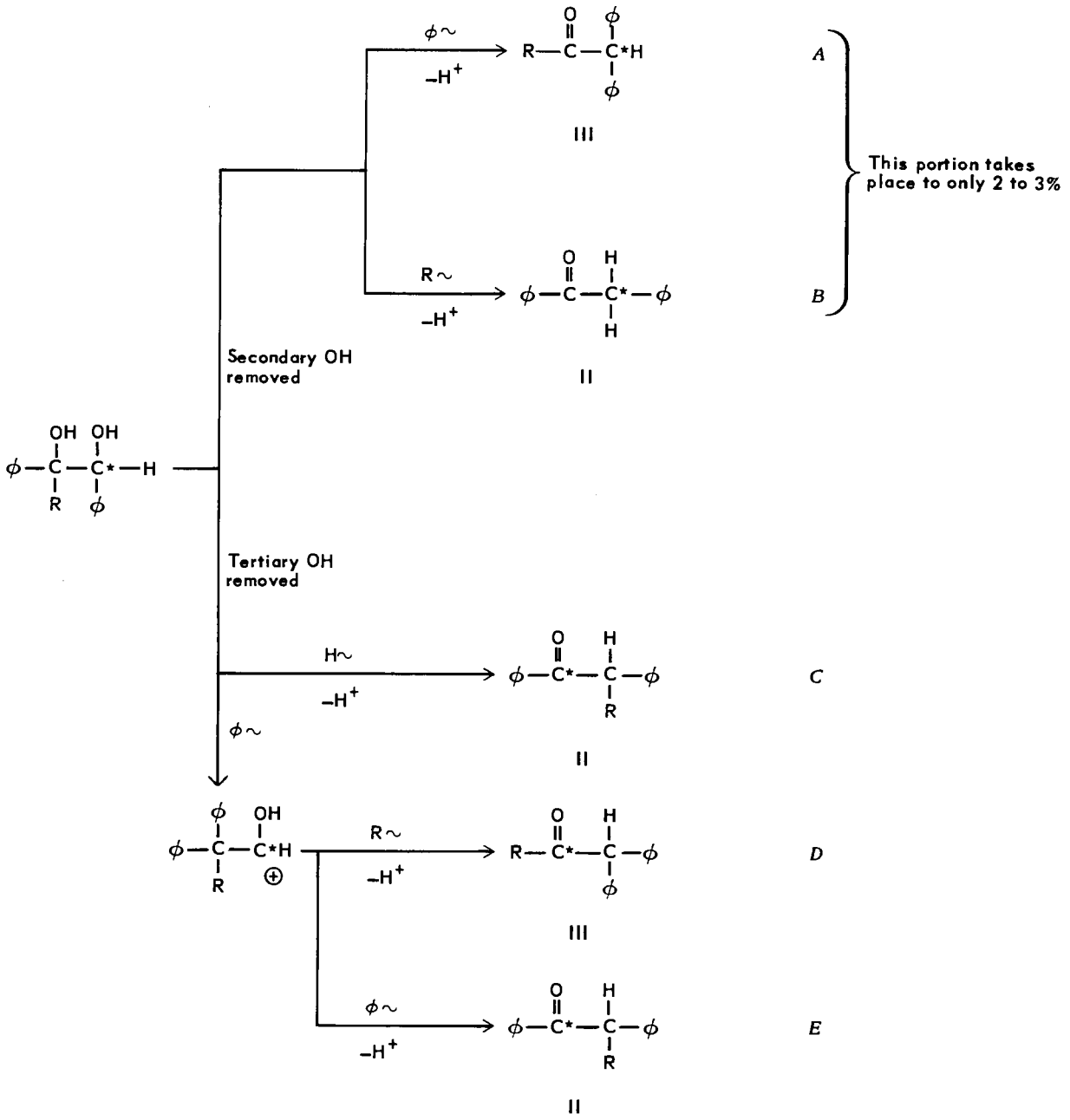

R = *o*-tolyl

Compound *C* cannot be distinguished from compound *E* by chain labeling

TABLE 12. REARRANGEMENT IN FORMIC ACID

Glycol	*p*-Tolyldesoxy-benzoin Yield (%)	*p*-Tolylbenz-hydryl Ketone Yield (%)	Total Yield (%)
α-Form	87.8	11.6	99.4
β-Form	88.4	12.4	100.8

Experiments designed to distinguish between phenyl and hydrogen migration are in progress.

ISOTOPE FRACTIONATION STUDIES

Examination of the Isotope Effect in the Condensation of *o*-Benzoylbenzoic Acid-carboxyl-C^{14} to Anthraquinone-9-C^{14}

G. A. Ropp

In the past, two C^{14} "reverse isotope effects" which had been reported from other laboratories[5] were examined in this laboratory. In each case no evidence of a reverse isotope effect was found.[6] Apparently, the original conclusions[5] resulted from failure to take the necessary precautions in assaying the radioactive compounds.

More recently, another reverse isotope effect was reported in the sulfuric acid condensation[7] of *o*-benzoylbenzoic acid-carboxyl-C^{14} to anthraquinone-9-C^{14} at 80°C. Upon examination of the experimental section of this paper it was concluded that an *apparent* reverse isotope effect might have resulted from an isotopic dilution after synthesis of the starting material.

In the work under discussion,[7] *o*-benzylbenzoic acid-carboxyl-C^{14} (I) was oxidized to *o*-benzoylbenzoic acid-carboxyl-C^{14} (II), which was then diluted severalfold with the corresponding unlabeled acid and recrystallized from 15% aqueous ethanol. It is possible that, in spite of recrystallization, the diluted acid (II) could have retained some of the unoxidized, several-times-more-radioactive acid (I). There is reason[8] to suppose that the cyclization reaction of acid I to form anthrone –

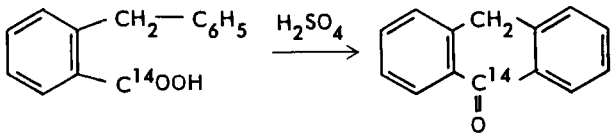

should be more rapid than the cyclization of acid II to form anthraquinone. Hence, the reaction of sulfuric acid with acid II, containing some several-times-more-radioactive acid I, might yield a crude product which at 12% reaction would contain a higher percentage of anthrone and, therefore, more activity per unit weight than at 100% reaction. If recrystallization of the crude anthraquinone samples from alcohol failed to remove all the impurity, anthrone, then the higher concentration of anthrone impurity remaining in the product of 12% reaction could account for the apparent reverse isotope effect.

To test this explanation, samples of very pure acid II have been synthesized by a process in which radiochemically pure acid I was prepared and diluted *before* oxidation to acid II. In Table 13 data are reported from two runs which were entirely independent and which employed benzoylbenzoic acid samples prepared by separate syntheses. A *normal* isotope effect corresponding to a value of k_{12}/k_{14} of about 1.03 to 1.04 is indicated. All assays were performed by wet combustion followed by radioassay of the resulting $C^{14}O_2$ in a stainless steel ion chamber with the vibrating-reed electrometer.[9]

Study of C^{13} Isotope Fractionation in Brominative Decarboxylation of 3,5-Dibromo-4-hydroxybenzoic Acid

E. Grovenstein[10] G. A. Ropp

Certain studies[11] have indicated that brominative decarboxylation of 3,5-dibromo-4-hydroxybenzoic

[5] A. Roe and E. L. Albenesius, *J. Am. Chem. Soc.* 74, 2402 (1952); Abstracts of Papers, 124th Meeting of the American Chemical Society, Chicago, Ill., Sept. 6–11, 1953, pp 65–0 to 67–0.

[6] G. A. Ropp *et. al.*, *J. Am. Chem. Soc.* 76, 1710 (1954).

[7] W. H. Stevens and D. A. Crowder, *Can. J. Chem.*, 32, 792 (1954).

[8] F. C. Whitmore, *Organic Chemistry*, p 868, Van Nostrand, New York, 1937. It is known that the keto group of acids such as *o*-benzoylbenzoic acid retards cyclization in sulfuric acid. In hydrogen fluoride as a condensing agent, *o*-benzylbenzoic acid is cyclized but *o*-benzoylbenzoic acid is not.

[9] O. K. Neville, *J. Am. Chem. Soc.* 70, 3501 (1948); V. F. Raaen and G. A. Ropp, *Anal. Chem.* 25, 174 (1953).

[10] Research participant, summer 1954, from chemistry department, Georgia Institute of Technology.

[11] E. Grovenstein, unpublished work.

TABLE 13. ASSAY DATA FOR THE STUDY OF C^{14} FRACTIONATION IN CYCLIZATION OF o-BENZOYLBENZOIC ACID-CARBOXYL-C^{14}

Compound	Activity (μc per mole)	
	Run 1	Run 2
Benzylbenzoic acid: Intermediate in synthesis		3.345 ± 0.02
Benzoylbenzoic acid: Acid used in the reaction	6.95 ± 0.01	3.36 ± 0.01
Anthraquinone: Product from ~100% reaction	6.89 ± 0.01	3.345 ± 0.02
Product from partial reaction	6.76 ± 0.01 (42% reaction)	3.22 ± 0.02 (16½% reaction)
Benzoylbenzoic acid: Recovered unreacted acid	7.11 ± 0.03	3.39 ± 0.01

acid at 25°C in acetic acid follows the course described by the following equations:

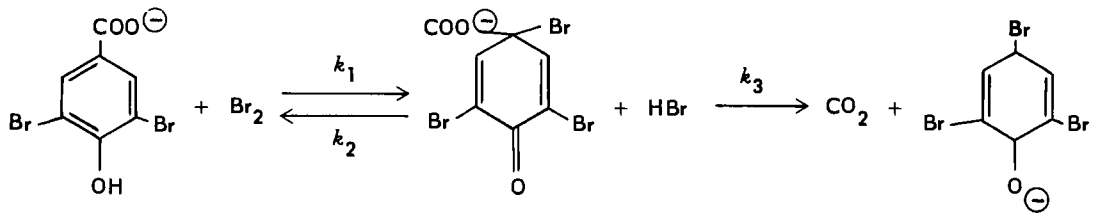

I II

In the presence of added bromide ions (and to a lesser extent, added hydrogen ions) the reaction rate is much slower, indicating that the equilibrium is shifted in favor of I over the intermediate II. Probably, k_1 is largely rate-controlling in the absence of added bromide ions, and k_2 is unimportant under these conditions. This suggested that k_3 could become more important in controlling the reaction rate as the concentration of bromide ions was increased. Therefore, this reaction was selected as an interesting case for study of isotope fractionation of the natural C^{13} present to the extent of 1% in the carbon of the carboxyl group. Since step k_1 does not involve altering of bonds to the carboxyl group, it was predicted that no isotope fractionation would be evident in the isotopic composition of the evolved carbon dioxide as long as k_1 was rate-controlling, that is, in the absence of added bromide or hydrogen ions. However, it was predicted also that addition of bromide ions should cause fractionation in the evolved carbon dioxide, since k_3 should become more and more important in controlling the over-all rate as the bromide ion concentration is increased and since k_3 involves cleavage of a bond to the labeled atom.

Experimentally, the study involved simply a determination of the isotopic composition of the carbon dioxide at different percentages of reaction in the absence of added reagents, then with perchloric acid added, and finally with sodium iodide added. Carbon dioxide from the reaction was purified by passage through stannous chloride crystals and through a U-trap cooled with dry ice–acetone. The purified gas was collected in a U-tube cooled in liquid nitrogen, and air was removed from the frozen carbon dioxide with a pump. Finally, the frozen gas was expanded and sealed in a glass bulb. Gas samples were submitted to Consolidated Engineering Corporation for determination of the ratio, R, of C^{13} to C^{12}. The data reported in Table 14 show that the predictions made from the postulated mechanism are borne out.

TABLE 14. C^{13} FRACTIONATION OBSERVED UNDER SEVERAL SETS OF REACTION CONDITIONS FOR BROMINATIVE DECARBOXYLATION OF 3,5-DIBROMO-4-HYDROXYBENZOIC ACID

Condition	Reaction (%) Represented By $C^{13}O_2$	R/R_{100}	k_{12}/k_{13}
Nothing added	12.5 to 25	1.00	1.00
	75 to 100	1.007	1.008
0.3 *N* HBr added	10.5 to 23	0.967	1.042
	51 to 73	1.003	
0.3 *N* $HClO_4$ added	10 to 21	0.993	1.009
	88 to 100	1.030	1.013

As predicted, the only appreciable fraction (k_{12}/k_{13} = 1.042) occurs in the presence of added HBr. A lesser degree of fractionation (k_{12}/k_{13} = ~1.01) results when $HClO_4$ is added. It is also interesting that the sample of carbon dioxide collected after 75% reaction showed a value of k_{12}/k_{13} of about 1.01, even for the run with no added reagents. This was probably caused by the fact that at 75% reaction some concentration of HBr had developed in the solution as a result of earlier reaction.

CHEMICAL PHYSICS

X-RAY DIFFRACTOMETER FOR LIQUID STUDIES

P. C. Sharrah M. D. Danford
H. A. Levy R. D. Ellison
P. Agron M. A. Bredig

The construction of an x-ray diffractometer designed specifically for studies on the structure of liquids was completed in recent months. The diffraction pattern from the horizontal surface of the liquid sample is obtained with a divergent beam technique similar to the Bragg-Brentano flat-sample system frequently used on powder samples. The instrument provides for simultaneous angular motion of the x-ray tube and the detector on arms moving about a horizontal axis lying in the liquid surface. This makes it possible to work with liquids with a free surface where sample-holder absorption and scattering are eliminated. A small furnace for work with molten materials is included in the design. Monochromatic x radiation, essential to good work with liquids, is obtained through the use of a bent-crystal monochromator mounted on the arm with the detector. A scintillation detector and a molybdenum target x-ray tube are in use in the system. Preliminary measurements on liquid mercury are reported.

Introduction. – The x-ray diffraction patterns produced by liquids can be studied to gain information about the spatial distribution of atoms within the liquid under study. The formal approach to this problem, introduced and developed by Zernike and Prins[1] and by Debye and Menke,[2] requires an accurately determined intensity pattern over a wide range of the scattering angle ϕ or the variable $s = 4\pi (\sin \phi/2)/\lambda$, where λ is the wavelength of the radiation used. Strictly monochromatic radiation produced by crystal-reflected characteristic radiation is required if the occurrence of extraneous peaks and other irregularities in the diffraction pattern are to be avoided.

An excellent review article[3] describes the method and presents the results obtained on liquid elements up to 1943. Further work on several liquid elements has been carried out.[4] Further fundamental mathematical aspects[5] of the problem of interpreting the experimental data and the sources of errors[6] have been discussed.

Description of Diffractometer. – The apparatus described here is designed to obtain diffraction patterns from the free surface of a liquid by the use of counting techniques. The Bragg-Brentano focusing arrangement commonly used in powder spectrometers is applied. Figure 20 shows schematically the arrangement of the x-ray tube X, sample HH, and detector arm with monochromator M and detector D; and Fig. 21 shows a photograph of the equipment. The arm containing the molybdenum target x-ray tube and the arm containing the monochromator and detector are rotated at the same angular rate and in opposite directions about a horizontal axis A lying in the surface HH of the free liquid. The monochromator is of the reflection focusing type and consists of a bent and ground NaCl crystal reflecting from (200) planes.

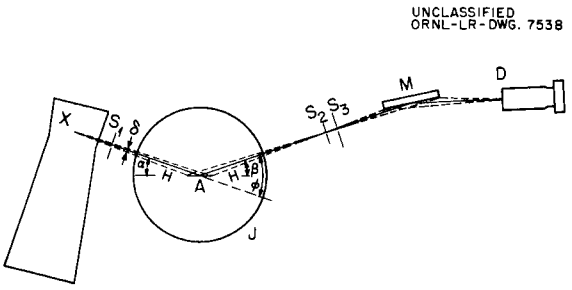

Fig. 20. Geometrical Arrangement of the X-Ray Diffractometer for Liquid Studies.

The detector consists of a sodium iodide–thallium-activated scintillation crystal and a photomultiplier tube used in conjunction with a linear amplifier

[1] F. Zernike and J. A. Prins, *Z. Physik* **41**, 184 (1927).

[2] P. Debye and H. Menke, *Ergebn. Techn. Rontgenkde.* Series II (1931).

[3] N. S. Gingrich, *Revs. Mod. Phys.* **15**, 90 (1943).

[4] J. A. Campbell and J. H. Hildebrand, *J. Chem. Phys.* **11**, 330, 334 (1943); H. Hendus, *Z. Naturforsch.* **2A**, 505 (1947); H. Hendus, *Z. Naturforsch.* **3A**, 416 (1948); W. L. Gordon, C. H. Shaw, and J. G. Daunt, *Phys. Rev.* **96**, 1444 (1954); R. Buschert, I. G. Geib, and K. Lark-Horovitz, *Bull. Am. Phys. Soc.* **30**, No. 1, 18 (1955); H. Hendus and H. Müller, *Z. Naturforsch.* **10A**, 254 (1955).

[5] J. Waser and V. Schomaker, *Revs. Mod. Phys.* **25**, 671 (1953).

[6] C. Finbak, *Acta Chem. Scand.* **3**, 1279, 1293 (1949); E. Kanda and T. Sugawara, *Sci. Rep. Res. Inst., Tohoku Univ.* **3**, 34 (1951); T. Sugawara, *Sci. Rep. Res. Inst., Tohoku Univ.* **3**, 39 (1951).

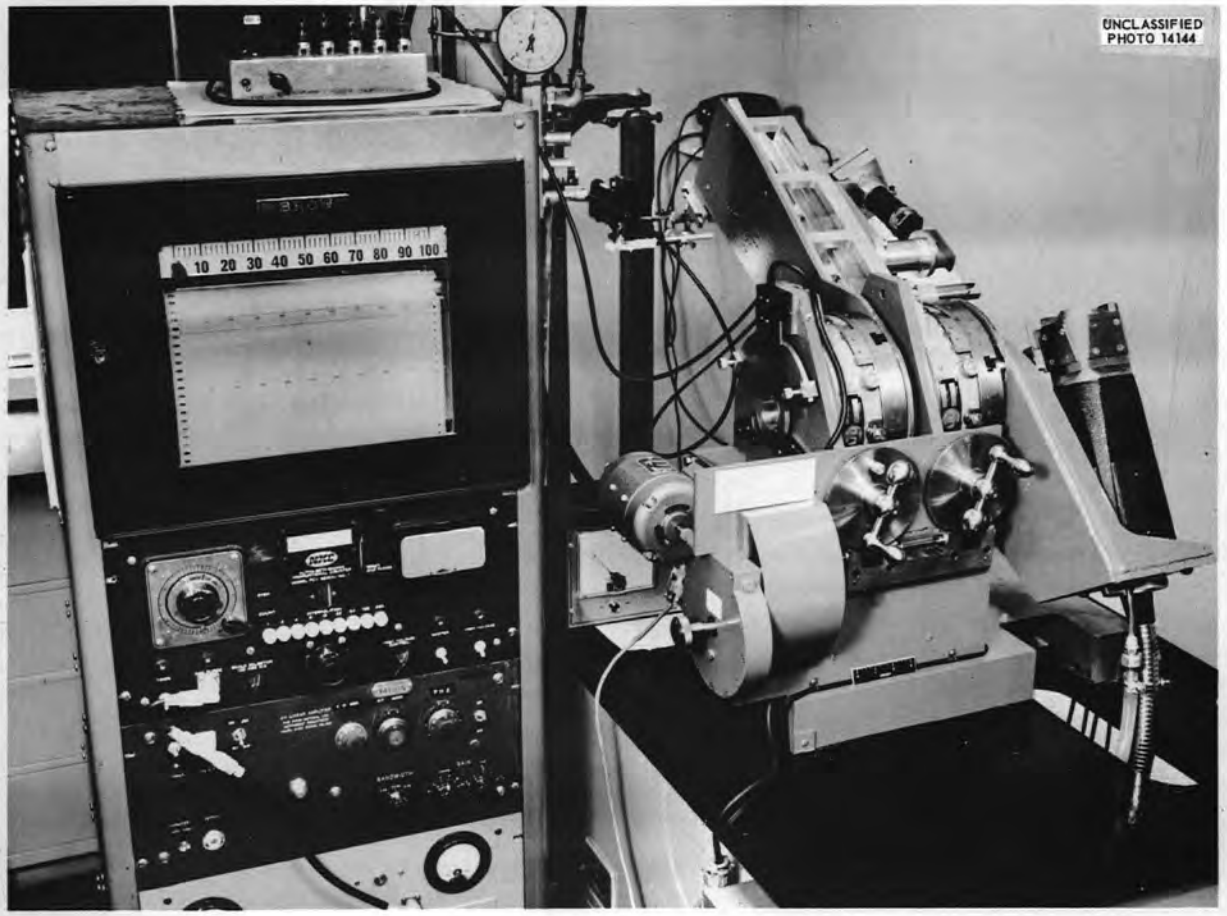

Fig. 21. Photograph of Diffractometer.

and a differential discriminator. The discriminator is set so that it counts essentially only the pulses due to the K alpha radiation, thus reducing the background and the contribution due to the half wavelength radiation reflected as second order by the monochromator.

Preliminary Results. – The apparatus has been put into operation and was thoroughly aligned and tested through the use of a powdered nickel sample. Further patterns have been obtained from aqueous uranyl fluoride solutions and from liquid mercury. The intensity pattern and Fourier analysis for liquid mercury are shown in Figs. 22 and 23. The intensity curve represents the average of several runs with different beam divergences used over the appropriate angular ranges. The curve shown has been corrected for polarization and is seen to follow the shape of the square of the atomic form factor for mercury in a quite satisfactory manner. It has been possible to obtain data which appear to be reliable to a somewhat larger value of the variable s than previously reported, the data for values of $s \leqq 14.45$ being used in the analysis. The Fourier analysis curve is proportional to $r[\rho(r) - \rho_0]$, where $\rho(r)$ is the radial atomic density function, and ρ_0 is the macroscopic average density. Full details of this study will be reported at a later time.

HIGH-SPEED COMPUTATION OF THE ABSORPTION CORRECTION USED IN DIFFRACTION STUDIES

W. R. Busing H. A. Levy

In order to obtain accurate intensity measurements in x-ray or neutron diffraction, it is necessary to divide the observed intensity by a factor, A, which corrects for the absorption within the sample.

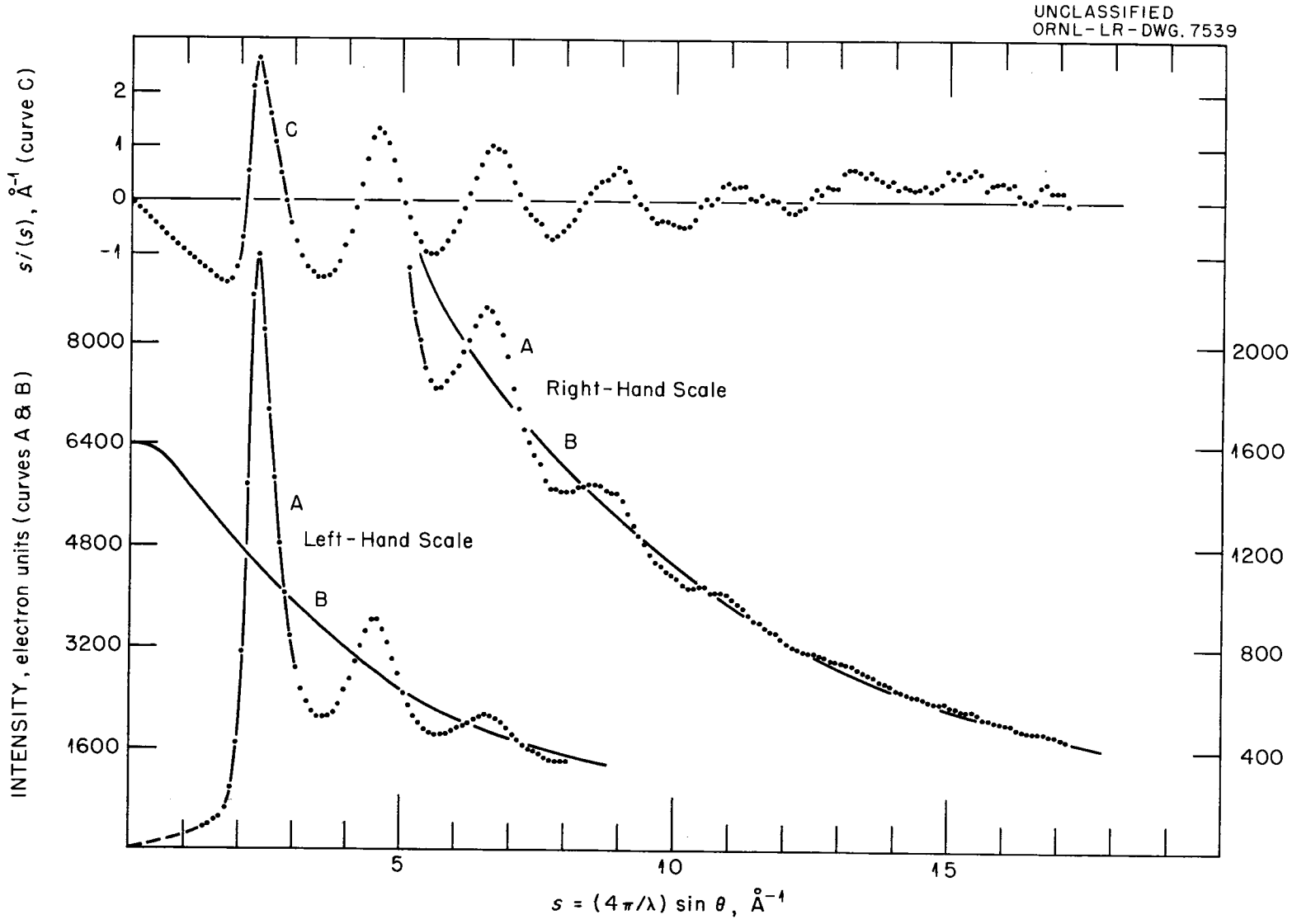

Fig. 22. Intensity Pattern (A), f^2 curve (B), and Reduced Intensity Function $s[(I/Nf^2) - 1]$ (C) for Liquid Mercury.

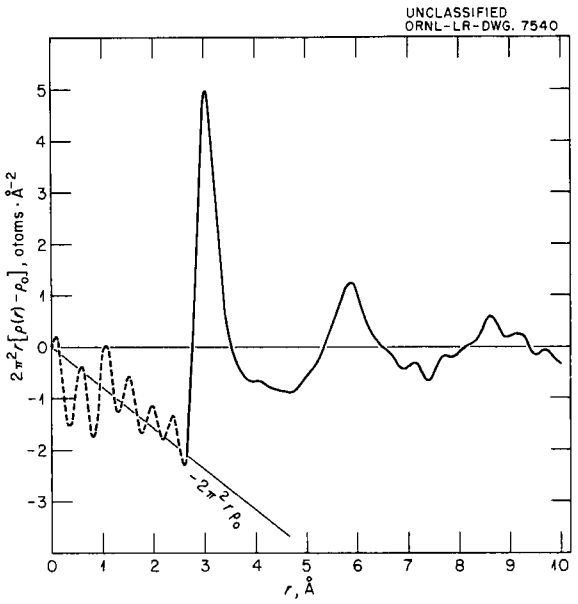

Fig. 23. The Distribution Function $2\pi^2 r[\rho(r) - \rho_0]$ for Liquid Mercury. This function is the sine Fourier transform of curve C, Fig. 22; the straight line is the function $(-2\pi^2 r\rho_0)$.

Tabulated values of A are available[7] for cylindrical samples, but there are several reasons why it may not be possible or desirable to use a sample of this form. Single crystals may be difficult to shape, or shaping them may waste a large fraction of the available material. Moreover, a given cylindrical sample may be used in only one orientation. For these reasons a program has been devised which enables the high-speed electronic computer, the Oracle, to calculate A for samples of arbitrary shape. The only requirements are that it be possible to approximate the sample surface with planes and that there be no re-entrant angles between these planes. The program to be described has been designed for zonal reflections only, but the principles can be extended to apply to a more general routine.

The shape of the sample is read into the computer as the coefficients of n equations for the planes which approximate its n faces. The signs of these coefficients are chosen so that the n inequalities

$$a_i x + b_i y + c_i z > d_i$$

are satisfied if the point (xyz) lies within the sample. The coordinate axes are chosen so that the z axis parallels the zone axis and the xz plane is a reference plane with respect to which interplanar angles are specified. In practice, a toolmaker's microscope has been used to measure the oriented sample, so that the required coefficients can be determined.

Figure 24 shows a cross section of the sample at a fixed value of z, together with one layer of a three-dimensional array of points embracing the entire crystal. The program is designed to calculate the absorption for diffraction at those points of the array which lie within the sample. It then averages the results for all such points. The Bragg angle and interplanar angle for each reflection are read into the computer, which then calculates α, β, $\sin\alpha$, $\cos\alpha$, $\sin\beta$, and $\cos\beta$. The angles α and β measure the reverse direction of the primary beam and the forward direction of the diffracted beam with respect to the reference plane, as shown in the figure.

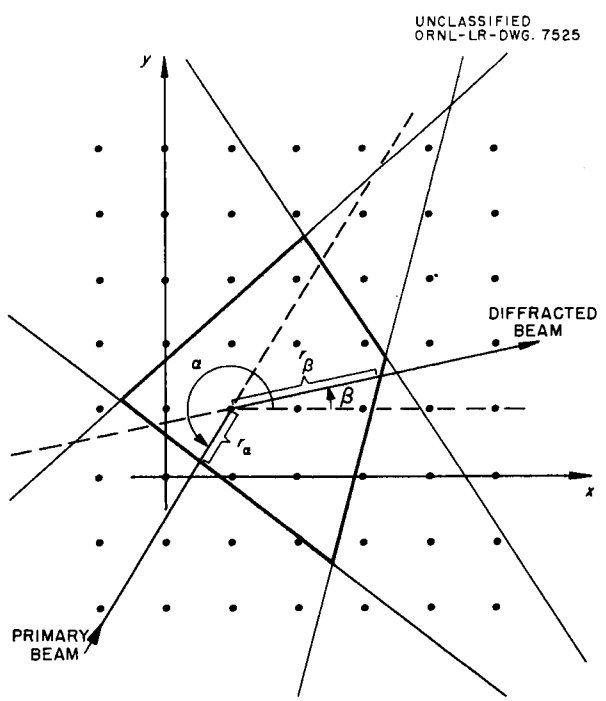

Fig. 24. Geometry of the Absorption Calculation.

[7] W. H. Bragg, M. Laue, and C. Herman (eds.), *Internationale Tabellen zur Bestimmung von Kristallstrukturen*, vol II, p 584, Borntraeger, Berlin, 1935.

The computer then begins to scan the array one point at a time. Each point is first tested to determine whether its coordinates satisfy the n inequalities which describe the sample. Failure of any one of these tests results in rejection of the point because it is outside the sample, and the computer proceeds to the next point.

If a point is found to be inside the sample, however, the computer calculates the path length, $r_\alpha + r_\beta$, in the following way. The value of r_α is found by first calculating n values of $r_{\alpha i}$, where

$$r_{\alpha i} = \frac{a_i x + b_i y + c_i z - d_i}{a_i \cos \alpha + b_i \sin \alpha} .$$

The quantities $r_{\alpha i}$ are the distances from the point of diffraction to each of the n faces or their extensions measured along the primary beam in its reverse direction. The desired distance, r_α, is simply the smallest positive $r_{\alpha i}$. The value of r_β is found in a similar way. Computation time is minimized, since the denominators in the expressions for $r_{\alpha i}$ are the same for all points of the array and since the numerators have been calculated in the tests mentioned above.

The transmission, $\exp[-\mu(r_\alpha + r_\beta)]$, is evaluated for each point, and the absorption correction, A, is the average of these exponentials over the array of points within the sample. The process is repeated for each reflection of interest.

Table 15 shows how the calculated absorption correction for a given reflection depends on the fineness of the grid used. The number of points accepted and the machine time required are also listed. In practice it was found that about 600 points gave sufficient accuracy in a reasonable amount of time.

TABLE 15. ABSORPTION CORRECTION FACTOR, *A*, FOR THE (305) REFLECTION OF $Ca(OH)_2$

Number of Points	Calculated A	Machine Time (sec)
56	0.8134	5
186	0.8157	12.5
466	0.8181	27.5
906	0.8204	53
1556	0.8212	89

NEUTRON DIFFRACTION STUDY OF $Ca(OH)_2$

W. R. Busing H. A. Levy

X-ray studies[8-10] of $Ca(OH)_2$ have shown that it has a hexagonal layer structure with space group D_{3d}^3-$P\bar{3}m$ (the CdI_2 arrangement), and Bernal and Megaw[11] have postulated that the hydrogen atoms lie on the threefold axes which pass through the oxygen atoms, so that the OH dipoles are perpendicular to the layers. A single-crystal neutron diffraction study of $Ca(OH)_2$ at room temperature has been completed, and the results are in good agreement with this structure.

Crystals of $Ca(OH)_2$ were prepared by diffusion-precipitation from NaOH and $CaCl_2$ solutions,[12] and 53 reflections of the $h0l$ zone were studied. No special shaping of the samples was required, since the absorption correction for each measurement was calculated as described elsewhere ("High-Speed Computation of the Absorption Correction Used in Diffraction Studies," this report). Comparison of the results with those from powder measurements indicated that for some crystals the strong reflections showed rather severe extinction. This problem was almost completely eliminated by using crystals which were grown rapidly and which were visibly imperfect.

The signs of the structure factors were determined initially from the postulated structure, and two-dimensional Fourier projections were calculated with and without an artificial temperature factor. Finally, the method of least squares was used to determine the best values of the two position parameters, the six temperature-factor coefficients, and the scale factor. These results are given in Table 16, together with the probable errors which were determined in the usual way.[13] The conventional discrepancy factor

$$\frac{\Sigma \, ||F_{obs}| - |F_{calc}||}{\Sigma \, |F_{obs}|}$$

[8] C. E. Tilley, *Mineralog. Mag.* **23**, 419 (1933).

[9] H. E. Petch and H. D. Megaw, *J. Opt. Soc. Amer.* **44**, 744 (1954).

[10] H. E. Petch, *Bull. Am. Phys. Soc.* **30**, No. 4, 9 (1955).

[11] J. D. Bernal and H. D. Megaw, *Proc. Roy. Soc. (London)* **A151**, 384 (1935).

[12] F. W. Ashton and R. Wilson, *Am. J. Sci.* **13**, Series 5, 209 (1927).

[13] H. C. Plummer, *Probability and Frequency*, chap. III, MacMillan, London, 1940.

TABLE 16. PARAMETERS OF $Ca(OH)_2$ AS DETERMINED FROM THE INTENSITIES OF 53 REFLECTIONS, USING THE METHOD OF LEAST SQUARES

z (O)	0.2349 ±0.00024
z (H)	0.4257 ±0.00036
OH distance	0.934 ±0.002 Å
B (Ca, perpendicular to c axis)	0.73 ±0.06 Å^2
B (Ca, parallel to c axis)	1.62 ±0.09 Å^2
B (O, perpendicular)	0.78 ±0.04 Å^2
B (O, parallel)	0.84 ±0.05 Å^2
B (H, perpendicular)	4.02 ±0.11 Å^2
B (H, parallel)	1.74 ±0.12 Å^2

is 4.5%, all reflections included. All these calculations were made with the aid of the Oracle.

The relative values of the temperature-factor coefficients show that the motion of the hydrogen atoms is predominantly perpendicular to the c axis. This is to be expected, since the other motion requires stretching of the O-H bond.

The calcium motion, on the other hand, has its largest component parallel to the c axis. Each calcium ion is surrounded by oxygen atoms at the corners of an octahedron which is somewhat compressed along the c axis. These oxygen atoms are thus in positions which, by ion contact, would tend to restrict the motion of calcium along the c axis less severely than along the layers.

The OH distance of 0.934 Å is somewhat shorter than that found in other molecules and crystals. This maybe the correct bond length for an ionic hydroxide, but it is also possible[14] that, because of the large thermal motion, the apparent OH distance really represents the projection of a somewhat longer link having an appreciable average inclination to the c axis. For this reason the measurements are presently being repeated at −140°C.

SURFACE IONIZATION OF ALKALI METALS AND HALIDES ON TUNGSTEN AND PLATINUM

S. Datz E. H. Taylor

The experimental study of surface ionization of the alkali metals and the potassium halides on tungsten, platinum, and an alloy consisting of 92% Pt, 8% W has been completed and is being written up for publication. This work originated in the observation, made in the course of applying molecular beam techniques to chemical kinetics, that platinum and tungsten showed quite different surface ionization efficiencies for KBr.

The ionization efficiencies of the alkali metals on tungsten follow the Saha-Langmuir equation if no reflection of the incident atoms is assumed. On platinum, reflection of incident atoms appears to occur for all the alkalies except sodium, which follows the Saha-Langmuir equation. The fraction reflected varies with the element and with temperature, from about 40% for potassium to about 10% for cesium at 1600°K. The behavior of the alloy is similar to that of platinum.

The potassium halides likewise follow the Saha-Langmuir equation on tungsten, behaving as if they dissociated on the surface to the alkali metal. On platinum, the ionization is generally much lower, being relatively constant, about as follows, between 1300 and 2000°K: KF, 28%; KCl, 0.10%; KBr, 0.12%. The ionization yield from KI over this range varies from 0.5% at 1300°K to 1.5% at 2000°K. The behavior of the alloy is more complex, in general being much like platinum at low temperatures and rising sharply to high efficiencies at higher temperatures.

Apparatus for the exploitation of these observations in the study of vapor pressures of mixtures of alkali halides is nearing completion.

PARAMAGNETIC RESONANCE STUDIES OF ELECTRIC DISCHARGE PRODUCTS

R. Livingston H. Zeldes

An effort has been made to increase the accuracy and reliability of quantitative measurements of numbers of unpaired electrons in samples examined by the paramagnetic resonance method. The basic approach has been to compare the area under the absorption curve of the unknown material with the area under the curve of a sample containing a known number of unpaired electrons. A series of reference standards has been made from the hydrazyl radical (α,α-diphenyl β-picryl hydrazyl). The series was made and calibrated by sealing a number of single crystalline pieces of hydrazyl in individual capillaries, cross-comparing the samples on the paramagnetic resonance spectrometer to determine the relative sizes, and then

[14] E. G. Cox, D. W. J. Cruickshank, and J. A. S. Smith, *Nature* **175**, 766 (1955).

analyzing a few of the crystals spectrophotometrically to determine the absolute amount of hydrazyl present. This indirect assay method was used, since the individual hydrazyl samples were too small to be weighed directly. Nineteen standards were made that ranged in size from 1.4 to 55 μg. Three of the above were forfeited for the spectrophotometric assay. The assay was made at the peak of the visible absorption of hydrazyl, 520 mμ, with benzene as a solvent, and the photometer calibration was made from a weighed sample of hydrazyl (about 1 mg). The hydrazyl used was several years old. A new preparation of hydrazyl made by R. Weeks was compared spectrophotometrically with the old hydrazyl and was found to have 95.1% of the strength of the old hydrazyl. This is within the accuracy of the weighing of the 1-mg samples that were compared and indicates with reasonable confidence that the number of unpaired electrons can be deduced from the weight of the individual crystals of hydrazyl and the molecular weight.

The comparison of the various hydrazyl samples was made by comparing heights of the absorption curves viewed on the oscilloscope of the paramagnetic resonance spectrometer, keeping all experimental parameters of the spectrometer constant. The line widths of the various samples were assumed to be the same. Kikuchi and Cohen[15] have reported a small anisotropy in the g factor of hydrazyl. In the course of the calibration work it was discovered that there was a very pronounced anisotropy in the line width as well. To minimize this effect the samples were rotated to give maximum intensity of absorption (sharpest line). This is, at best, a compromise, and for more accurate work the series will have to be recalibrated. The present series is known to an accuracy of about ±20%.

The measurement of unknown samples has been made by comparing the intensity of absorption for the unknown with an appropriately sized reference sample of hydrazyl. In both cases the magnet sweep width of the spectrometer is measured to obtain a scale factor for the area, and, in addition, the mean widths of the unknown and the hydrazyl are separately determined from planimeter tracings of photographs made of the oscilloscope at calibrated sweep widths. This gives another scale factor, so that a comparison of intensities (which can be made rapidly) effectively gives the comparison of areas (which is time consuming if photographs are taken each time). At present, the accuracy for broad lines (say, 100 gauss width at half height) is about a factor of 2. With further effort this can be improved, and for sharp lines the method is capable of considerable refinement. The principal merit at present is that once the mean width of an unknown is measured from a photograph, subsequent analyses can be made very rapidly.

Free-radical samples prepared by Ghormley and described in the last semiannual report[16] were assayed by the above method. A sample, prepared by passing hydrogen through an electric discharge, mixing the products of the discharge with oxygen, and then condensing the products in a liquid-nitrogen trap, was found to contain 1.4×10^{17} unpaired electrons. Ghormley found 0.986 mg of H_2O_2 to be present in the warmed sample. A different preparation of the same radical, formed by passing water vapor through an electric discharge and condensing the products, was found to contain 5.6×10^{17} unpaired electrons, and his assay on this material showed 4.86 mg of H_2O_2 to be present; H_2O_2 concentrations in excess of 60% have been made by this method.[17] If the radical is assumed to be HO_2 and is assumed to contain about 60% H_2O_2, then the samples contained roughly 0.4 wt % HO_2. Although the paramagnetic observations do not distinguish between, say, OH and HO_2, infrared spectroscopy evidence[18] has been presented for the presence of HO_2. Paramagnetic resonance observations made at 9,000 and 23,000 Mc and measurements made on the product prepared under greatly different conditions indicate that the observed asymmetric broad line is a single radical species. The absorption line, which contains a pronounced shoulder, can be derived from a sharper, symmetric line that has a g factor anisotropy and is averaged over all angles, as would be the case in the glass-like product

[15] C. Kikuchi and V. W. Cohen, *Phys. Rev.* **93**, 394 (1954).

[16] J. A. Ghormley, R. Livingston, and H. Zeldes, *Chem. Semiann. Prog. Rep. Dec. 20, 1954*, ORNL-1832, p 48.

[17] R. A. Jones and C. A. Winkler, *Can. J. Chem.* **29**, 1010 (1951).

[18] P. A. Giguère, *J. Chem. Phys.* **22**, 2085 (1954).

studied. This would require some residual, unquenched, orbital angular momentum which is reasonable for either HO_2 or OH. Any hyperfine structure effects would probably be very small and completely masked by the averaging of the anisotropy over all angles.

PARAMAGNETIC RESONANCE STUDIES ON ATOMIC HYDROGEN

H. Zeldes R. Livingston

Some of the properties of atomic hydrogen formed in H_2SO_4, H_3PO_4, and $HClO_4$ by irradiation at 77°K with gamma rays have been studied by the paramagnetic resonance method. A cryostat has been constructed, and measurements have been made on the rate at which the atomic hydrogen disappears as the above substances are warmed. In general, the rate at a given temperature depends on the concentration as well as the nature of the acid. The data appear to fit a second-order rate function. The atomic hydrogen generally disappears at a temperature lower than that for other unpaired electron species in the samples. The above results and all the earlier results on atomic hydrogen have been presented at a Faraday Society meeting and will be published soon.[19]

Since atomic hydrogen disappears from warmed samples separately from other observed paramagnetic species, it has been decided to attempt a calorimetric measurement of the heat evolved from a sample that is assayed for actual atomic hydrogen content by the paramagnetic resonance method. E. R. Van Artsdalen and his group have been consulted and will do the calorimetric part of the study. The hydrogen assay will be made by refining the method described earlier in this report. Although the method will probably not give a unique answer on the fate of the atomic hydrogen, it should supply helpful information. For example, the second-order rate data strongly suggest combination of H atoms to form H_2 molecules. If such is the case, the calorimetric measurement should show a large heat effect characteristic of such a reaction.

MICROWAVE SPECTROSCOPY

A. Weinberger R. Livingston

A new microwave spectrometer has been assembled by C. Burrus from Duke University as part of the cooperative program of measuring nuclear moments. The spectrometer operates at 195,000 Mc at the $J = 0 \rightarrow 1$ transition of DI. Work is now starting on the developing of a microsynthesis of DI, so that the moment determinations of short-lived iodine isotopes can be continued. This new approach, in lieu of the earlier CH_3I method used on I^{131}, is being started in the hope of developing a faster, simpler technique.

[19] R. Livingston, H. Zeldes, and E. H. Taylor, paper presented at meeting of Faraday Society, April 4, 1955; to be published in *Discussions Faraday Soc.*

CHEMISTRY OF SEPARATION PROCESSES

FUNDAMENTAL STUDIES ON ION-EXCHANGE RESINS

G. E. Myers G. E. Boyd

Investigations were continued into the nature of the interaction between ionogenic groups on the exchanger and the exchanging groups, that is, into the basis of the exchange selectivity phenomena. Isopiestic measurements were made upon several resins of differing structures containing ions of different size and structure. Results for some of the systems studied are discussed below.

Osmotic Coefficients of Strong-Base Anion Exchangers and the Structure of the Exchange Ion

In the previous report[1] isopiestically obtained osmotic coefficients were presented for a number of monovalent salt forms of the weakly cross-linked (0.5% DVB) strong-base anion exchanger, Dowex 1. Since that time considerable care has been employed to ensure by quantitative analyses that each resin had been completely converted to the particular salt form. The great necessity for such analyses does not appear to have been appreciated in the past by other workers in the field, but it is regarded by the present authors as an inescapable part of ion-exchange studies. Data for the following salt forms of Dowex 1, for example, had to be discarded in view of analytical results: HCO_3^-, CN^-, HSO_4^-, and NO_2^-.

Preliminary analysis of the data at the time of the previous report indicated that most of the salt forms obeyed Eq. 1 over a considerable concentration range:

$$\phi = \phi_0 + \frac{am}{1 + bm}, \tag{1}$$

where ϕ_0, a, and b are parameters specific for each salt form, m is the molality of the internal resin phase, and ϕ is the osmotic coefficient. Since it appeared that certain relationships might exist between the parameters a and b and between the parameter a and the size of the exchange ions, least-squares analyses of the data have been carried out so as to increase our knowledge of the accuracy of those parameters.[2] Table 17 presents the resultant parameters, along with their standard deviations for the various salt forms of Dowex 1 and of Dowex 2, calculated upon the basis of the first eight experimental values for each salt form. The data for Dowex 2 were obtained much earlier.[3]

The possibility exists that the first, that is, the lowest, concentration point of some of the salt forms could be slightly in error due to a small and unmeasurable swelling-pressure term. Consequently, the analyses were repeated, employing only the eight experimental points succeeding the first; the resultant parameters appear in Table 18 and may be seen to differ considerably from those in Table 17. Figure 25 presents the experimental osmotic coefficients for Dowex 1, with curves calculated from the parameters of Table 17. The parameters of Table 18 result in osmotic curves which, in some cases, deviate seriously from the neglected first point and sometimes in a direction opposite to that expected from the effect of a pressure term. In view of this and of the greater regularity in the parameters to be discussed below, the parameters of Table 17 will be chosen as a basis for discussion. This discrepancy, however, demonstrates the danger in attaching great significance to the absolute values of these parameters.

Figures 26 and 27 are plots of $a^{1/3}$ vs b and ionic radii, respectively, for Dowex 2, each containing values from Tables 17 and 18 and from the calculations of Soldano and Larson,[3] who assumed ϕ_0 to be zero in every case. While the points employing the parameters of Table 18 are rather scattered, those from Table 17 and from Solando and Larson indicate $a^{1/3}$ to be a linear function of b and of ionic radii. The linearity is extremely good for the Table 17 values.

Figures 28 and 29 present plots of $a^{1/3}$ vs b and r, respectively, employing only the parameters of Table 17. Values of r for ions other than the halogen and hydroxyl ions are measures of interatomic distance within the complex ions and are

[1] G. E. Myers and G. E. Boyd, *Chem. Semiann. Prog. Rep. Dec. 20, 1954*, ORNL-1832, p 61.

[2] The authors wish to express their appreciation to the Mathematics Panel, and to J. Z. Hearon in particular, for the considerable aid given in making the necessary calculations.

[3] B. Soldano and Q. V. Larson, *J. Am. Chem. Soc.* 77, 1331 (1955).

TABLE 17. OSMOTIC PARAMETERS

Ion	a		$a^{1/3}$		b		ϕ_0	
				Dowex 1				
ClO_3^-	0.0417	(0.011)*	0.345	(0.031)	0.0099	(0.0095)	0.113	(0.071)
BrO_3^-	0.3202	(0.0718)	0.684	(0.051)	0.1249	(0.0271)	−0.202	(0.144)
IO_3^-	0.7734	(0.0510)	0.918	(0.0202)	0.1555	(0.0112)	−0.524	(0.073)
NO_3^-	0.0603	(0.0073)	0.397	(0.016)	0.0092	(0.0050)	0.031	(0.041)
$H_2PO_4^-$	0.2778	(0.057)	0.651	(0.045)	0.0654	(0.0207)	−0.057	(0.137)
SCN^-	0.0247	(0.0031)	0.291	(0.012)	−0.0102	(0.0025)	−0.152	(0.035)
CNO^-	0.7284	(0.0479)	0.900	(0.020)	0.0937	(0.0093)	−0.751	(0.081)
$C_2H_3O_2^-$	0.6383	(0.0493)	0.860	(0.022)	0.0630	(0.0106)	−0.252	(0.085)
Br^-	0.0491	(0.0064)	0.366	(0.016)	−0.0006	(0.0044)	0.053	(0.043)
Cl^-	0.0849	(0.0115)	0.440	(0.020)	0.0073	(0.0064)	0.177	(0.056)
OH^-	0.4794	(0.0942)	0.782	(0.051)	0.0870	(0.0228)	−0.539	(0.194)
F^-	0.6345	(0.0744)	0.860	(0.034)	0.1364	(0.0178)	−0.307	(0.118)
HSO_3^-	0.4264	(0.0561)	0.752	(0.033)	0.0377	(0.0137)	−0.416	(0.127)
				Dowex 2				
I^-	0.0148	(0.0044)	0.246	(0.024)	−0.0116	(0.0047)	−0.062	(0.061)
Br^-	0.0548	(0.0125)	0.380	(0.029)	0.0113	(0.0092)	0.045	(0.072)
Cl^-	0.1124	(0.0128)	0.483	(0.018)	0.0307	(0.0071)	0.118	(0.048)
F^-	0.4810	(0.0718)	0.784	(0.039)	0.0824	(0.0196)	0.010	(0.131)

*Figures in parentheses represent standard deviations.

taken from the paper of Cobble.[4] It is apparent from Fig. 28 that the linearity observed for the simple halogen forms of Dowex 2 does not extend to the more complex ionic forms of Dowex 1. Only a general trend appears to relate a and b here. Figure 29 indicates that $a^{1/3}$ is linearly related to ion size for the simple halogen salts of Dowex 1. However, the more complex salts do not follow this same relationship, although the halogenate ions appear to follow another of opposite slope. It is worthy of mention that equally "linear" curves may be obtained by plotting $a^{1/3}$ for the Dowex 1 salts against r^3 or $1/r$.

Thus it may be concluded that the previous tentative results are confirmed by the quantitative analysis of the osmotic data. There does appear, then, to be some relation between the thermodynamic osmotic coefficients of ion-exchange resins and the size and structure of the exchanging ions. The exact nature of that relation, however, is not yet clear.

Osmotic Coefficients of Multivalent Cation Forms of Strong-Acid Exchanger

A natural extension of previous studies of ionic interaction in exchangers is to the effect of ion charge and ion size for multivalent exchange ions. Consequently, Figs. 30, 31, and 32 present measured osmotic coefficients plotted against resin concentration for numerous di- and trivalent cation salt forms of weakly cross-linked (0.5% DVB) Dowex 50 exchanger.[5] Smooth curves are

[4] J. W. Cobble, *J. Chem. Phys.* 21, 1443 (1953).

[5] The assistance of H. Templeton in the experimental portion of these researches is gratefully acknowledged.

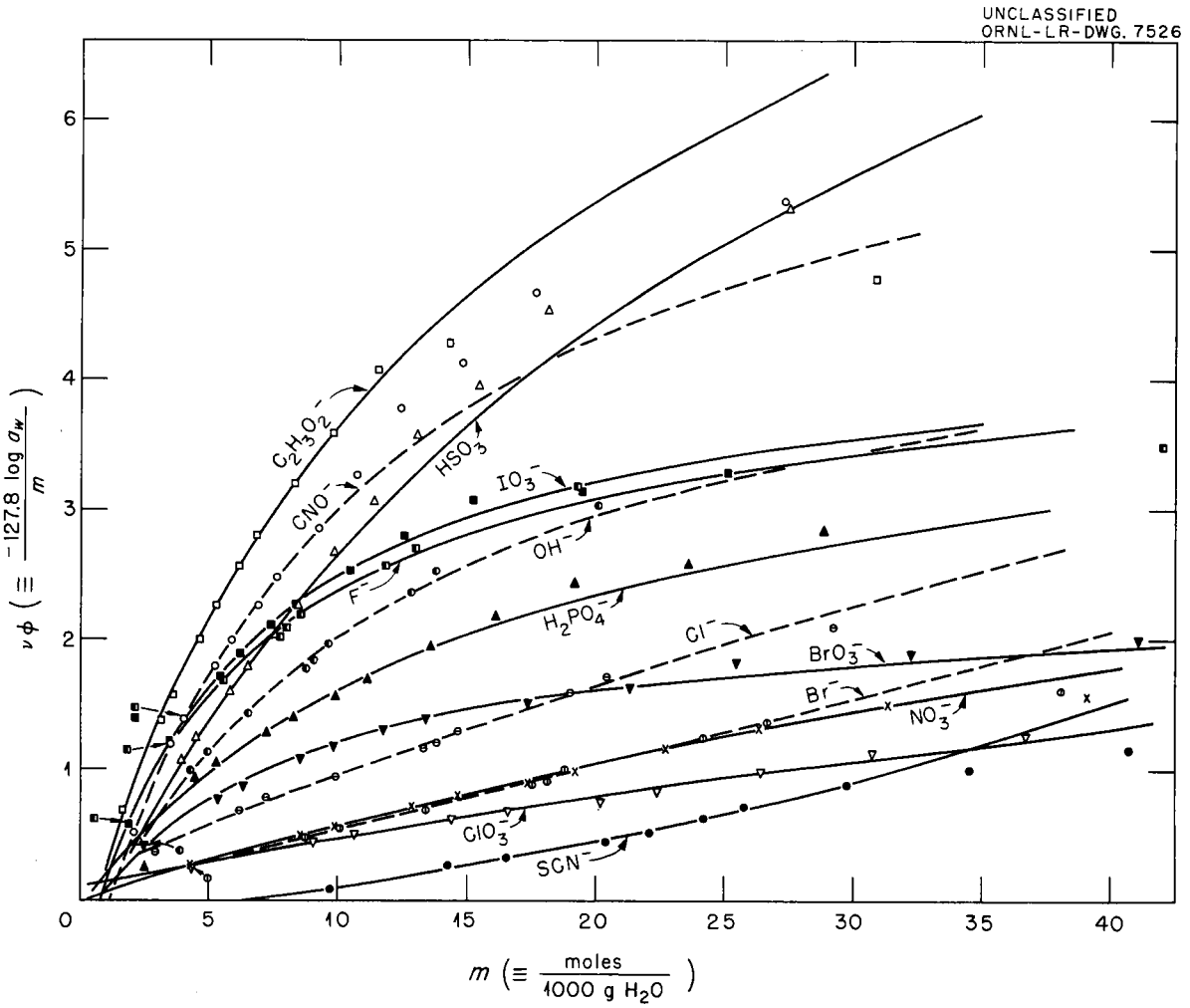

Fig. 25. Osmotic Coefficients of Monovalent Salts of ½% DVB Dowex 1.

drawn through the experimental points. It is perhaps noteworthy that Be^{++}, Fe^{+++}, and Hg^{++} are not included here, since analyses of these forms indicated appreciable hydrolysis to have occurred.

With concentrations expressed as equivalents per 1000 g of water, the osmotic curves cover generally the same region as do those for a series of monovalent salt forms of the same resin.[3] However, most of the multivalent salt forms exhibit an inflection point in their osmotic curves at a moderate concentration (i.e., ~5 *N*). In contrast, such inflections appear to occur with only the more highly associated univalent salt forms of Dowex 50 and at relatively higher concentrations. In view of the inflections, the osmotic curves of Figs. 30–32 would obey a relation such as Eq. 1 over only a relatively short concentration range. Consequently, no attempt has been made to fit these data to Eq. 1, and they can thus be discussed only in a qualitative sense.

Table 19 lists the multivalent ions in the approximate order of decreasing osmotic coefficients, that is, of increased association with the sulfonate groups of the resin. This order is compared in the table with values of the ionic radii and free energies of hydration. It may be seen that within the alkaline-earth series there is, as might be expected, a general correlation of the osmotic

TABLE 18. OSMOTIC PARAMETERS CALCULATED BY OMITTING LOWEST CONCENTRATION POINT

Ion	a	$a^{1/3}$	b	ϕ_0
		Dowex 1		
ClO_3^-	0.0224	0.280	−0.0068	0.276
BrO_3^-	0.5500	0.820	0.1904	−0.666
IO_3^-	0.5677	0.828	0.1095	−0.191
NO_3^-	0.0456	0.356	−0.002	0.130
$H_2PO_4^-$	0.1393	0.518	0.0150	0.388
SCN^-	0.0428	0.350	0.0018	−0.346
CNO^-	0.4354	0.758	0.0346	−0.144
$C_2H_3O_2^-$	0.7520	0.910	0.0817	−0.489
BF_4^-	0.1120	0.482	0.0403	−1.198
$Ag(CN)_2^-$	0.0186	0.265	−0.0075	−0.014
Br^-	0.0363	0.331	−0.0091	0.157
Cl^-	0.0584	0.388	−0.0070	0.336
OH^-	0.2350	0.617	0.0241	0.119
HSO_3^-	0.2600	0.688	−0.0014	0.081
		Dowex 2		
Br^-	0.0327	0.320	−0.0051	0.206
Cl^-	0.0998	0.464	0.0232	0.164
F^-	0.2080	0.592	−0.0006	0.644
I^-	0.0170	0.257	−0.0090	−0.085

coefficient with both the other ion properties. Comparing all the divalent ions, there appears to be no consistent correlation with ionic radii. With regard to the hydration free energies, a consistent and reasonable pattern may exist, the energies decreasing with increased association with the resin, except for Cu^{++} and Pb^{++}. It seems reasonable to assume that these two ions would be associated with the polysulfonate ion to an abnormal degree. For the trivalent cations, data are needed on more salt forms before any conclusions may be drawn.

Moisture Isotherms of Sulfonium-Type Anion Exchangers

Previous studies upon anion exchangers have involved the polystyrene quaternary ammonium-type resins, for example, Dowex 1. However,

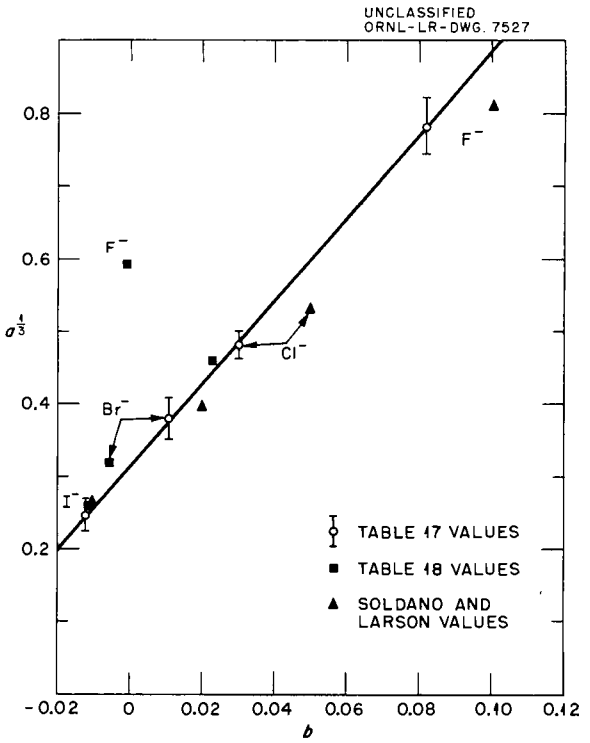

Fig. 26. Relation Between Parameters of Osmotic Equation for Dowex 2 Salt Forms.

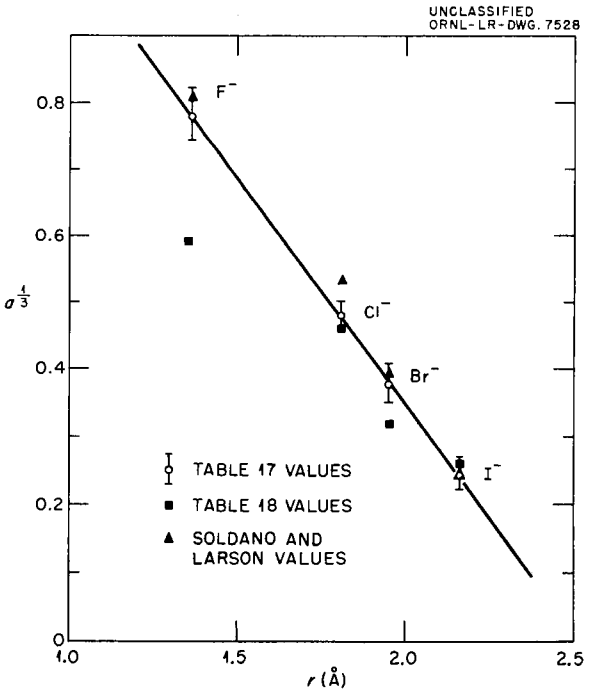

Fig. 27. Relation Between Osmotic Parameter and Ion Size for Dowex 2 Salt Forms.

TABLE 19. IONIC RADII AND FREE ENERGIES OF HYDRATION OF MULTIVALENT IONS

Ion	Ionic Radii[a] (Å)	$-\Delta F_{hyd}$ (kcal/mole)[b]
Co^{++}	0.72	
Zn^{++}	0.74 (0.88)[c]	466
Mg^{++}	0.65 (0.82)	434
Ni^{++}	0.70	
Al^{+++}	0.50 (0.72)	1087
Cu^{++}	0.8	480
Cr^{+++}	0.63 (0.81)	1445
Mn^{++}	0.80	421
Cd^{++}	0.97 (1.14)	413
Ca^{++}	0.99 (1.18)	363
La^{+++}	1.15 (1.39)	768
Sr^{++}	1.13 (1.32)	334
Ba^{++}	1.35 (1.53)	304
Pb^{++}	0.9	350

[a]L. Pauling, *Nature of the Chemical Bond*, 2d ed., p 346, Cornell University Press, Ithaca, 1940.

[b]W. M. Latimer, *J. Chem. Phys.* 23, 90 (1955).

[c]Figures in parentheses are Pauling's "univalent" radii.

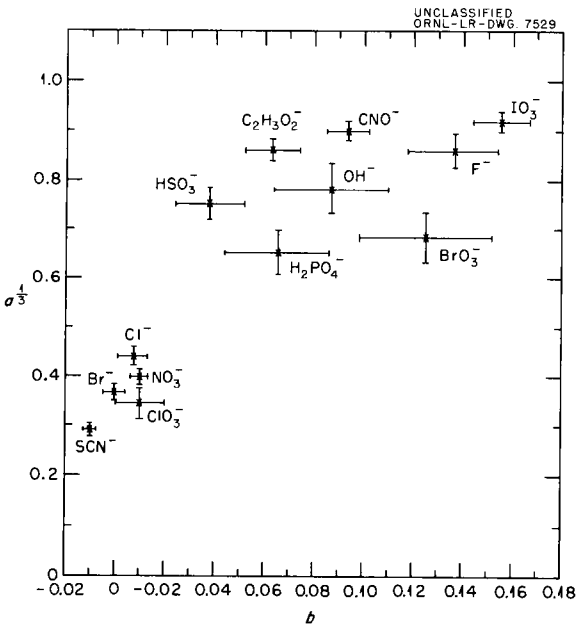

Fig. 28. Relation Between Parameters of Osmotic Equation for Dowex 1 Salt Forms.

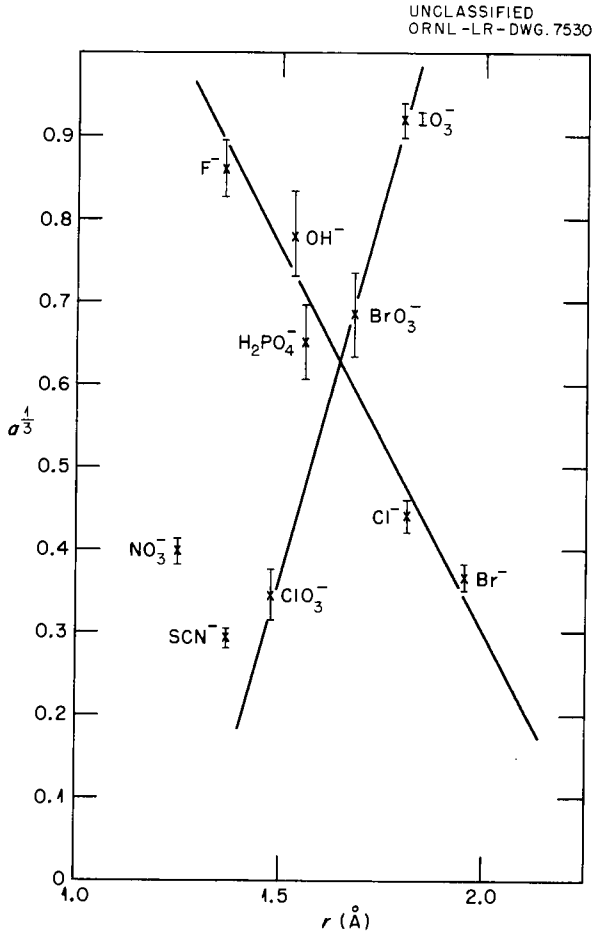

Fig. 29. Relation Between Osmotic Parameter and Ion Size for Dowex 1 Salt Forms.

isopiestic data have now been obtained for a number of monovalent salt forms of a phenol-formaldehyde sulfonium-type resin, Stamex S-44.[6] The structures of Dowex 1 and Stamex S-44 are compared in Fig. 33, and the moisture isotherms of salt forms of the latter are shown in Figs. 34 and 35. It should be pointed out that analyses of the various salt forms for complete conversion have not been completed, and the data are presented here with that reservation.

Since the degree of cross-linking of the Stamex resin is unknown and is probably greater than that corresponding to ½% DVB, it is necessary to present the data as moisture isotherms rather than as osmotic curves. However, the Stamex isotherms may be compared qualitatively with

[6]Dutch patent No. 72245, April 15, 1953.

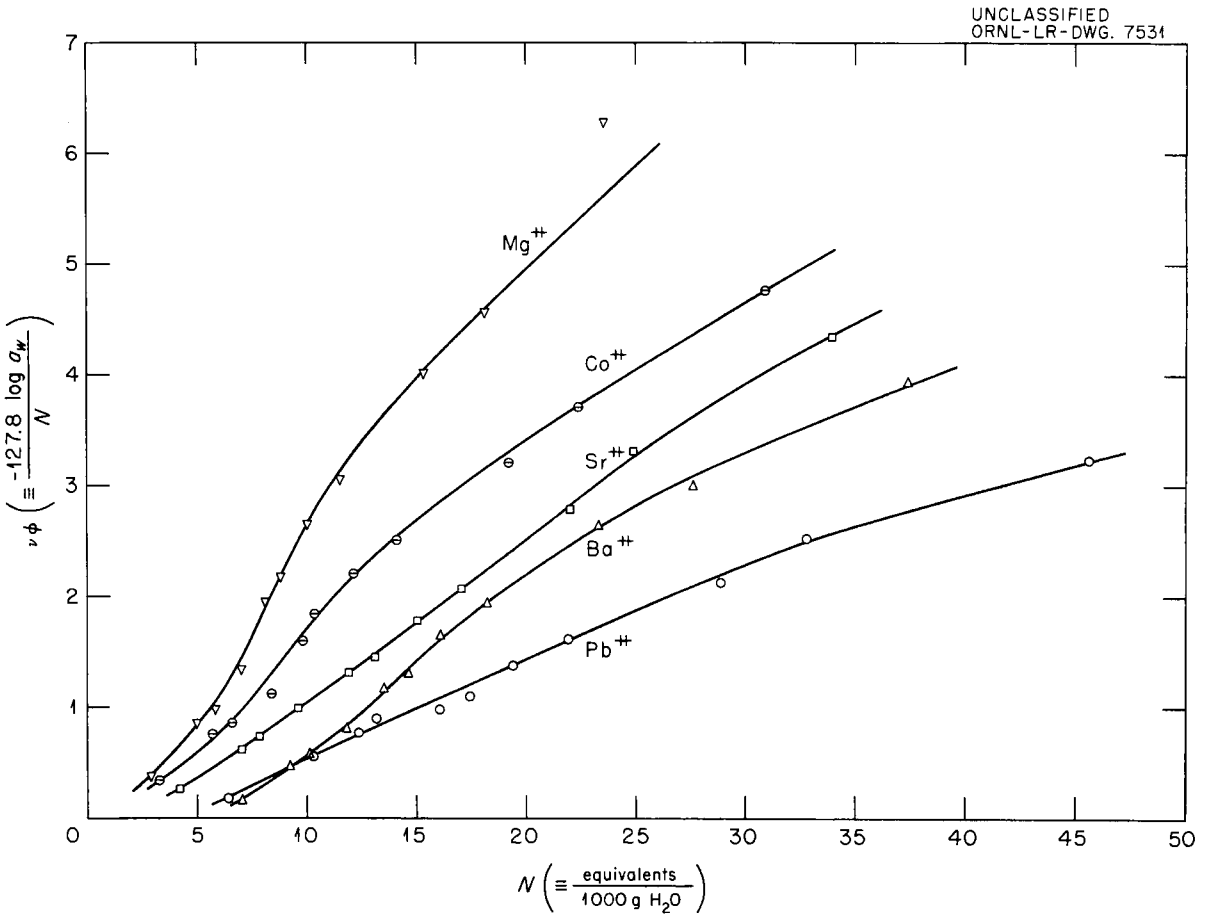

Fig. 30. Osmotic Coefficients of Alkaline-Earth Cation Forms of ½% DVB Dowex 50.

the Dowex 1 osmotic curves in Fig. 25. Such comparison shows the sequence of ions to be the same within the halogens and the halogenates for both resins. Intercomparison between all the ions, however, shows the ClO_3^- and NO_3^- to have reversed positions in Stamex relative to Dowex 1. It would seem, therefore, that no great degree of specific interaction exists between the various anions and the quaternary ammonium or sulfonium ionogenic groups.

Figure 34 contains, in addition to the isotherms for the halogen forms of Stamex S-44, the isotherms for the F^- and Br^- forms of 6% DVB Dowex 1. Although the Stamex forms possess much more water than the cross-linked Dowex 1, they lack the visible swelling and the very large upswing in moisture content typical of weakly cross-linked resins at high humidities. These apparently contradictory facts may be explained if the Stamex resin is assumed to be relatively highly cross-linked and the sulfonium group to be considerably more hydrated than the very nonpolar quaternary ammonium group of Dowex 1.

INTERACTION BETWEEN TRIBUTYL PHOSPHATE SOLVENT AND MONOVALENT ELECTROLYTE SOLUTES

W. H. Baldwin B. A. Soldano

The relationship between the structure of an organic solvent and its ability to extract electrolytes has remained largely empirical.[7] Efforts

[7] C. E. Higgins, W. H. Baldwin, and J. M. Ruth, *Organo-Phosphorus Compounds for Solvent Extraction*, ORNL-1338 (July 24, 1952).

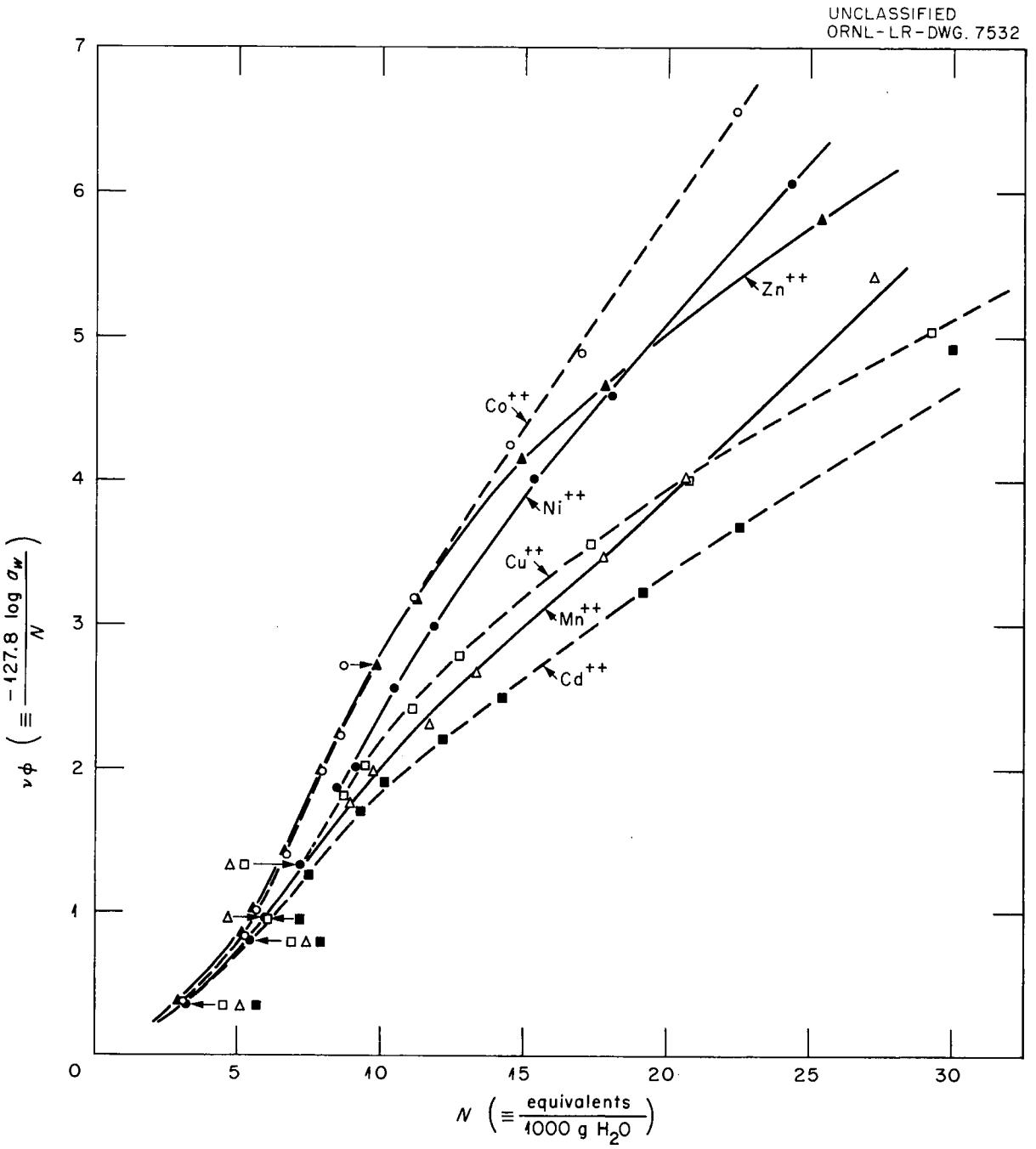

Fig. 31. Osmotic Coefficients of Divalent Transition Cation Forms of ½% DVB Dowex 50.

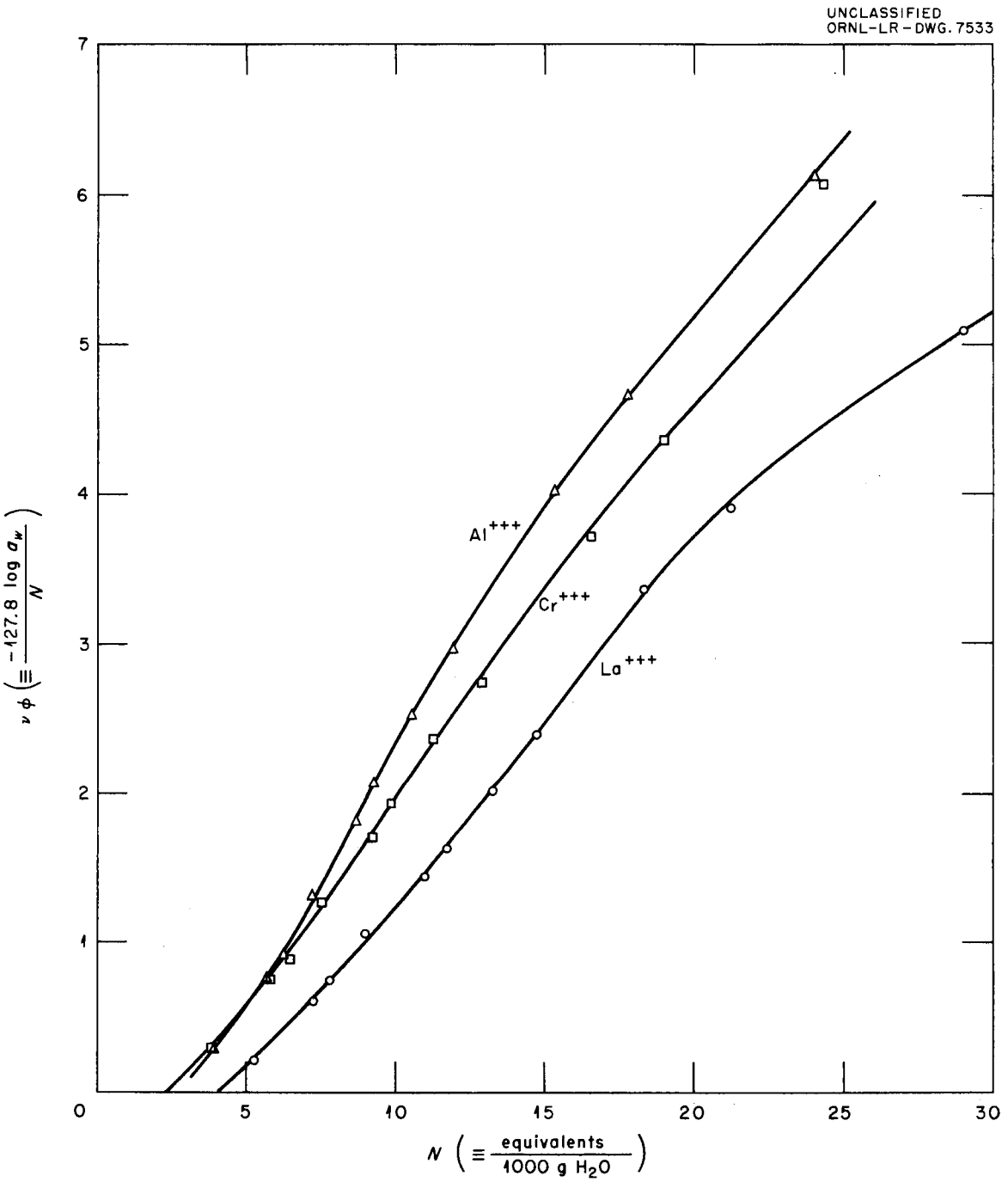

Figs. 32. Osmotic Coefficients of Trivalent Cation Forms of ½% DVB Dowex 50.

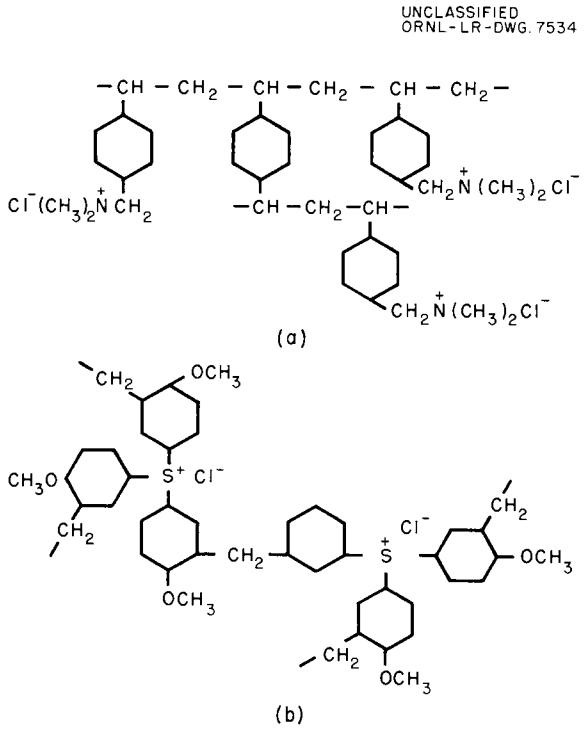

Fig. 33. (a) Dowex 1 Anion Exchanger; (b) Stamex S-44 Anion Exchanger.

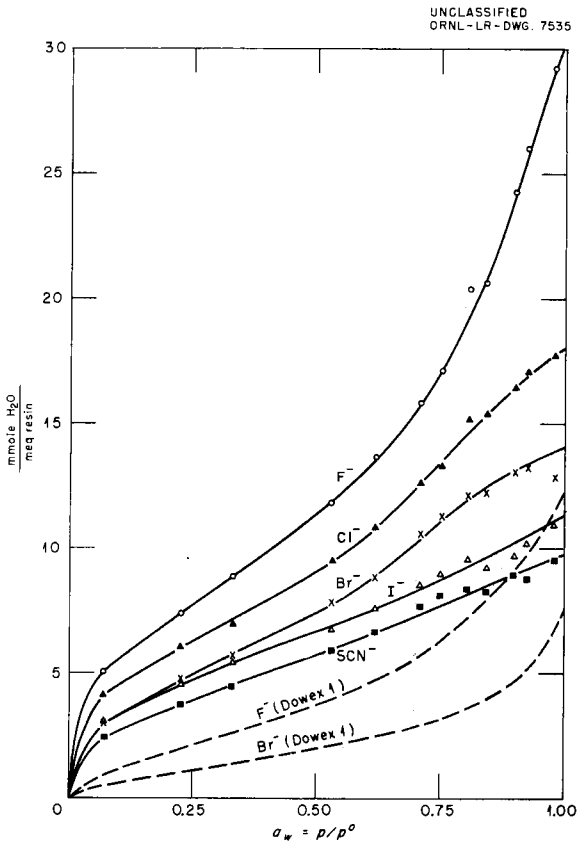

Fig. 34. Moisture Isothems for Monovalent Anion Forms of Stamex S-44 Anion Exchanger and for Two Forms of Dowex 1.

have recently been devoted to obtaining a fundamental expression for the distribution of electrolytes between water and organic solvents. The problems involved in the physical chemistry of such systems are basically as follows: (1) characterization of the forces involved in the primary hydration of salts, and (2) determination of the role of the nonaqueous solvent in modifying the first effect.

The following parameters were investigated in the laboratory: (1) the distribution of monovalent salts between tributyl phosphate and water as a function of concentration, (2) the effects of anions on the behavior of these systems, (3) the water in the organic phase as a function of the salt concentration, and (4) the refractive index of the organic mixtures.

The approach consisted in applying the Scatchard-Hildebrand theory[8] for regular nonaqueous systems, with the main difference being the omission of the inherent assumption that the energy density for a mixture is related to a geometric mean of the energy terms of the pure components, namely,

$$\left[\left(\frac{\Delta E_1{}^{v}}{v_1}\right)^{1/2} - \left(\frac{\Delta E_2{}^{v}}{v_2}\right)^{1/2}\right]^2 .$$

In this approach the primary interaction term for two components consisting of (1) monohydrated tributyl phosphate and (2) the primary hydrated salt is initially treated as an empirical constant.

Equating the chemical potential of the primary hydrated salt species in both phases, it can be

[8] J. H. Hildebrand and R. L. Scott, *Solubility of Non-Electrolytes*, 3d ed., p 119, Reinhold, New York, 1950.

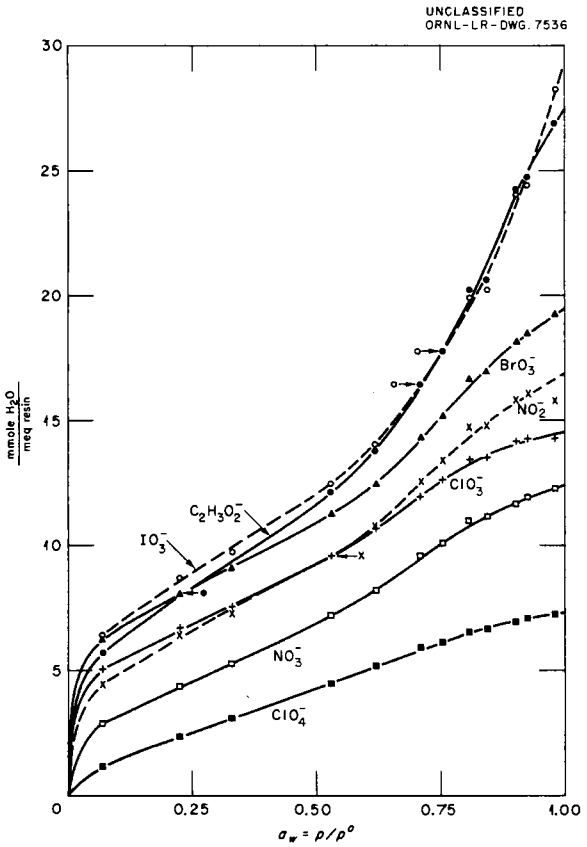

Fig. 35. Moisture Isotherms for Monovalent Anion Forms of Stamex S-44 Anion Exchanger.

written, thermodynamically, that for monovalent ions:

$$2 \log m\gamma_{\pm} - 0.0156mn\phi = K_1 + K_2\,\sigma_1^2 + \frac{\sigma_1}{2.3}\left(1 - \frac{V_S}{V_T}\right) + \log \sigma_2 ,$$

where

ϕ = osmotic coefficient of electrolyte,

$m\gamma_{\pm}$ = activity of electrolyte in aqueous phase,

K_1 = term to account for change in standard state,

K_2 = primary interaction term = $E_{11} + E_{22} - 2E_{12}$,

σ_1 = volume fraction of monohydrated solvent,

σ_2 = volume fraction of hydrated electrolyte in the organic phase,

n = primary hydration number – an empirical constant normally used to characterize strong aqueous salt interactions,

V_S = volume of hydrated salt (i.e., $HCl \cdot 4H_2O$),

V_T = volume of tributyl phosphate $\cdot H_2O$.

Distribution data obtained from two different concentrations were used to determine values of K_1 and K_2. The equation was then tested by comparison with the data obtained at other concentrations.

The above equation was sufficient for handling systems such as HCl up to 9 N. When applied to a series of monovalent ions, several qualitative conclusions became apparent: (1) for chloride salts at most concentrations, the amount of water in the organic phase at equilibrium is sufficient to satisfy the requirements implied in the equation; (2) for the bromides and iodides, however, this is not the case. Any realistic interaction term K_2 must involve a continuous change in the number of water molecules per equivalent of electrolyte in the organic phase.

The values of K_2 in the equation (for HCl, K_2 = 1.86) are large enough to strongly suggest that this term primarily reflects the results of hydrogen bonding[9] and the effects of changing environment on this bond. Moreover, for the esters in general and tributyl phosphate in particular, the hydrogen bond is basic in characterizing such solution properties as the effects of salts and the thermal effects on the solubility of esters in aqueous solutions. Viscosity adequately reflects the hydrogen bonding ability.

A simple plot of the viscosity of water against the log of the ester solubility at corresponding temperatures reveals a simple linearity from 0 to 60°C. This relationship holds for the carboxylate esters up to six carbon atoms and for tributyl phosphate, with 12 carbon atoms.

The slopes of the curves for each ester, when compared against the number of carbon atoms in the ester, show a simple structural relationship (Fig. 36). Such a plot reveals decreasing or increasing solubility with temperature, essentially revealing the complexity of the ester. Ketones, on the other hand, have slopes that are independent of the size of the ketone. This indicates the

[9] L. J. Thompson and F. A. Long, *J. Am. Chem. Soc.* 76, 5886 (1954).

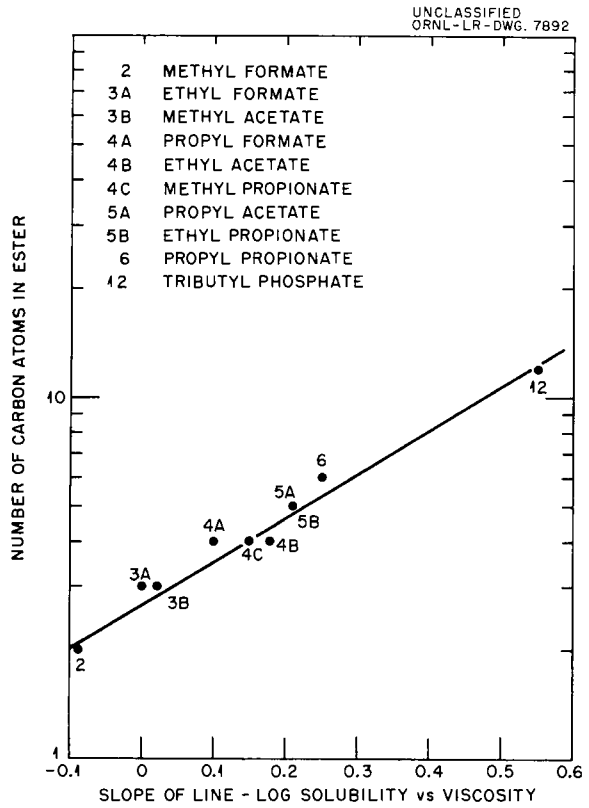

Fig. 36. Relation of Size of Ester to Solubility in Water and Viscosity of Water.

hydrogen bonding ability to be independent of size. It is planned to continue work in this direction.

P^{32} IN NEUTRON-IRRADIATED KH_2PO_4

W. H. Baldwin C. E. Higgins

Sources of P^{32} are important for the preparation of labeled organophosphorus compounds. Sources are readily available from n,γ reactions on phosphorus-containing compounds. It has been noted, however, that the P^{32} may appear in several chemical forms.[10] The classical precipitation methods proved unsatisfactory for the identification of components formed in KH_2PO_4 by neutron irradiation.[10] Selective elution from anion-exchange resin has proved very useful for the separation and identification of mixtures containing phosphorus polyacids.[11] It was believed that this would provide more useful information about irradiated KH_2PO_4 than was currently available, and the assumption proved to be true.

In addition to the P^{32} being present in orthophosphate (69% by phosphomolybdate precipitation and elution from resin), four other components were detected (see Table 20). Pyrophosphate and triphosphate were identified by coelution with carriers. Two other components remain unknown. It has been established, however, that these unknowns are not phosphite, hypophosphate, tetraphosphate, trimetaphosphate, nor tetrametaphosphate.

TABLE 20. DISTRIBUTION OF P^{32} IN NEUTRON-IRRADIATED KH_2PO_4

	Amount (%) After Irradiation	Amount (%) After Irradiation and After 24 hr at 175°C
Orthophosphate	69	96.3
Pyrophosphate	3.4	0.2
Triphosphate	14.9	1.1
Fraction IV	8.0	1.2
Fraction V	4.6	0.4

Moreover, it was shown in confirmation of the report of Borland *et al.*[10] that heating at 175°C reduced the amounts of the nonorthophosphate components (see Table 20).

DISTRIBUTION OF NEPTUNIUM IN THE PUREX METAL-RECOVERY PROCESS

G. W. Parker W. J. Martin
P. M. Lantz G. E. Creek

Recent interest in the behavior of neptunium in the Purex metal-recovery solvent extraction process being operated for the recovery of low g/T plutonium and uranium was initiated in an effort to develop a method which would permit isolation of several grams of this important element from one of the process waste streams.

Very preliminary comparisons of the distribution of neptunium tracers in a countercurrent batch-type contactor, in which flowsheet proportions

[10] J. W. Borland, A. J. MacKinzie, and W. L. Hill, *Ind. Eng. Chem.* 44, 2726 (1952).

[11] C. E. Higgins and W. H. Baldwin, paper submitted for publication in *Anal. Chem.*

of feed and solvent were used, gave an almost quantitative distribution in favor of the aqueous phase. From this, it is inferred that instead of forming an extractable state, for example, Np(IV) analogous to Pu(IV), or Np(VI) analogous to U(VI), the neptunium exists predominantly in the more stable pentavalent state.

Subsequent analyses of actual plant process streams revealed a decidedly different distribution from that predicted. Current studies show this behavior to be the result of a number of complex variables in the process, as well as subtle differences in behavior exhibited between laboratory batch tests and countercurrent plant streams.

Metal-Recovery Flow Plan

The metal-recovery continuous dissolver is operated so that it produces a uniform feed containing 2 moles of nitric acid, 1 mole of uranium, and about ¼ mole of aluminum nitrate per liter, with small amounts of mercury nitrate. The solvent is 30% tributyl phosphate in a kerosene-type hydrocarbon diluent which becomes saturated with uranium when it contains about 120 g/liter. The uranium loading is designed to reach 70% in the plant. To extract both uranium and plutonium from the feed (IAF), three to four volumes of solvent are contacted countercurrent in a pulse column (IA) at about 70°C. The fission products are essentially removed in the aqueous (IAW) stream. Plutonium is preferentially stripped out of the enriched solvent in the next column (IB) with a quantity of ferrous sulfamate–sulfamic acid mixture (0.04 and 0.08 *M*, respectively) equivalent to 20% of the volume of the enriched solvent by reducing plutonium to the trivalent state. The uranium is next stripped from the solvent with 6.6 volumes of water in the IC column, forming a high pH, dilute uranium solution (ICU) which is then reconcentrated by evaporation. The plutonium (IBP) is further processed by an additional extraction (IIA column) and stripping (IIB column) and is then isolated by adsorption as Pu(III) on a cation exchanger.

Trial Material Balances of Neptunium Through Typical Plant Runs

On the basis of numerous batch-type distribution experiments and neptunium valence determinations, it was generally expected that a relatively large fraction of the neptunium would appear in the first column raffinate or waste, the IAW stream; however, repeated TTA extraction-type analyses of in-stream samples and large holding-tank composites conclusively showed that only 8 to 10% of the total neptunium was present. This led to the further sampling of all the available streams and resulted in the trial material balance given in Table 21. In the feed, approximately 90% of the calculated product

$$U^{238}(n,2n)U^{237} \xrightarrow{\beta^-} Np^{237}$$

was found. This corresponds to a value of about 0.25% of the amount of plutonium. The total percentage of neptunium found in all the dividing streams – IAW waste, IBP plutonium, and IDF uranium – was slightly more than 30%, leaving a discrepancy of about 70%.

When the results of lengthy, duplicate analyses were finally accepted, no additional runs for which a more successful material balance might have been attempted were available. Instead, only a special aqueous waste concentrate was being run which resulted in the trial balance given in Table 22. The sum of the percentages in the dividing streams is greater than 100%; however, an error of 20% (the limit of the accuracy of the analysis) in one or more analyses could account for this. At the same time, some solution volumes were being adjusted, causing an additional source of error.

In this run the neptunium split evenly between the uranium and plutonium streams, while the total uranium in the feed was about 10% of that in a normal run. This observation lends some weight to the theory that most of the neptunium is following the uranium through the process and should subsequently appear in the recovered uranium being reprocessed at the diffusion plants.

Extraction Studies. – In an effort first to anticipate and later to account for the disappearance of neptunium in the plant, distribution coefficients of neptunium in various states were determined, as shown in Fig. 37. From this it is apparent that the Np(VI) is considerably more extractable than Np(IV), which, in turn, is far more extractable than Np(V). An additional effect, observed but not fully investigated, is the decrease in Np(IV) and (VI) extraction with increasing uranium loading, coupled with the higher extractability in fresh solvent, which leads to speculation that neptunium may simply reflux in the first column.

TABLE 21. TRIAL NEPTUNIUM MATERIAL BALANCE FOR URANIUM FEED

Process Solution	Description of Stream	Np^{237} Analysis (counts/min/ml)	Relative Volume	Total Np (relative counts/min)	Total* (%)	
IAF	Uranium feed (400 g/T)	270	100	27,000	100	
IAW	Fission-product waste, $Al(NO_3)_3$, etc.	15	145	2,175		7.8
IDF	Uranium stream to ID column	23	100	2,300		8.5
ICW	Solvent from IC column	1	422	422		1.6
IDW	Final uranium column waste	1	150	150	0.06	
IEUC	Uranium product concentrate	23	72.2	1,660	6.15	
IBP	Pu(III) product from IIB column	52	67	3,484		12.9
IIAW	Final plutonium column waste	2	93	186	0.07	
IIBW	Solvent from plutonium column	12	20	240	0.09	
IIBP	Pu(III) to ion-exchange column	230	5.1	1,173	4.34	
IIBPW	Ion-exchange plutonium waste	1	5.1	5.1	0.0	
				Total material balance		30.8
				Deficiency		69.2

*Figures in right column include those in the left column.

TABLE 22. TRIAL NEPTUNIUM MATERIAL BALANCE FOR SPECIAL WASTE FEED

Process Solution	Description of Stream	Np^{237} Analysis (counts/min/ml)	Relative Volume	Total Np (relative counts/min)	Total* (%)	
IAF	Uranium feed (400 g/T)	115	100	11,500	100	
IAW	Fission-product waste, $Al(NO_3)_3$, etc.	5	145	725		6.3
IDF	Uranium stream to ID column	71	100	7,100		61.8
ICW	Solvent from IC column	1	422	422		3.7
IDW	Final uranium column waste	0	150	0	0	
IEUC	Uranium product concentrate	5	72.2	361	3.14	
IBP	Pu(III) product from IIB column	105	67	7,035		61.2
IIAW	Final plutonium column waste	5	93	465	4.04	
IIBW	Solvent from plutonium column	1	20	20	0.17	
IIBP	Pu(III) to ion-exchange column	5	5.1	25.5	0.22	
IIBPW	Ion-exchange plutonium waste	11	5.1	56.1	0.5	
				Total material balance		133.0
				Excess		33.0

*Figures in right column include those in the left column.

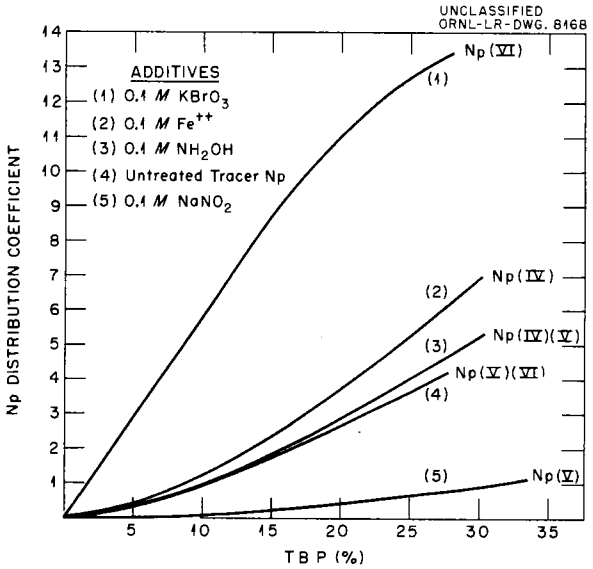

Fig. 37. Neptunium Distribution Coefficients in 2 *M* HNO_3–0.44 *M* $Al(NO_3)_3$.

Another possible explanation suggested is that the very low acid strength (~0.0004 *M*) of the IC uranium strip, together with neptunium in the tetravalent state, might lead to hydrolytic precipitation (as with plutonium) in the ICU evaporator. In contrast to this, all efforts in the laboratory have failed to hydrolyze Np(IV) in this way, and a hot, strong nitric acid wash of the ICU concentrator failed to produce any neptunium.

Effect of Time. – Studies of the extraction of Np(VI) have shown a significant time dependency. To illustrate this effect, typical extractions of Np(IV) and Np(VI) are described in Fig. 38. These point out the favorable distribution coefficient of Np(VI) for the solvent in the presence of $KMnO_4$ or MnO_2, followed by solvent reduction to Np(V) and the resulting redistribution into the aqueous phase. Neptunium(IV) in the presence of ferrous sulfamate shows poor extraction and no time dependence at room temperature.

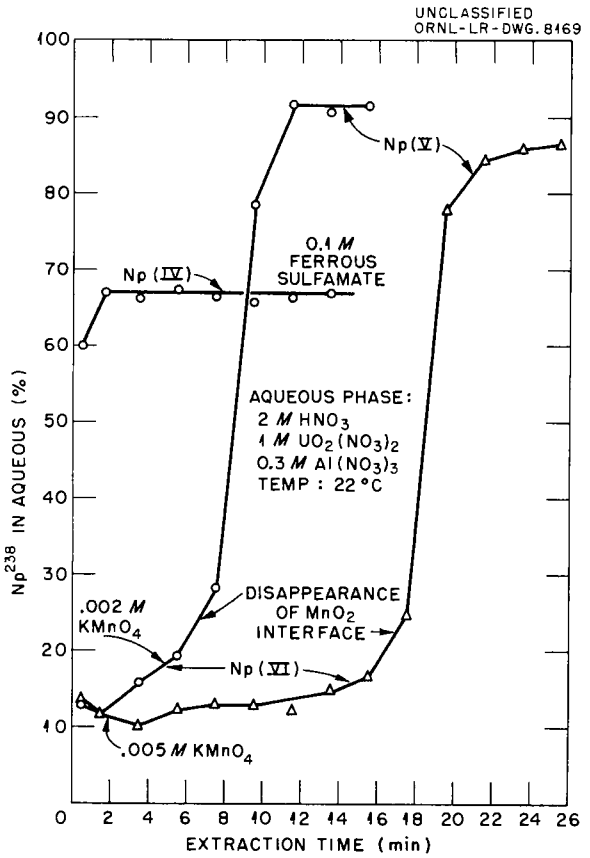

Fig. 38. Time Dependence of Neptunium Extraction with 30% TBP.

Discussion

For future work, several new sampling points between columns have been made available to improve material balance or to pinpoint the source of the anomolous behavior. Efforts to adjust the process slightly to make neptunium recovery more practical, such as by stabilizing the Np(V) and thus causing it to appear completely in the IAW stream, as well as a search for other possible means of one-stream concentration are being expended.

RADIATION CHEMISTRY

RADIATION STUDIES ON NITRATE SOLUTIONS

J. W. Boyle H. A. Mahlman

Effect of Acidity on the Decomposition of Nitrate Solutions

Recently, attention has been directed to the radiation chemistry of nitrate solutions in an attempt to elucidate a mechanism for the formation of molecular nitrogen. Figure 39 shows the production of nitrite ion when a 5 *M* solution of $NaNO_3$ (reagent-grade Baker and Adamson) is subjected to Co^{60} gamma-ray irradiation. The dependence of nitrite formation on pH suggested experiments that would ascertain if nitrite ion were an intermediate in the mechanism of molecular nitrogen formation. If nitrite ion were a precursor of molecular nitrogen, then the basic solution might exhibit a greater yield of molecular nitrogen than the acid solution.

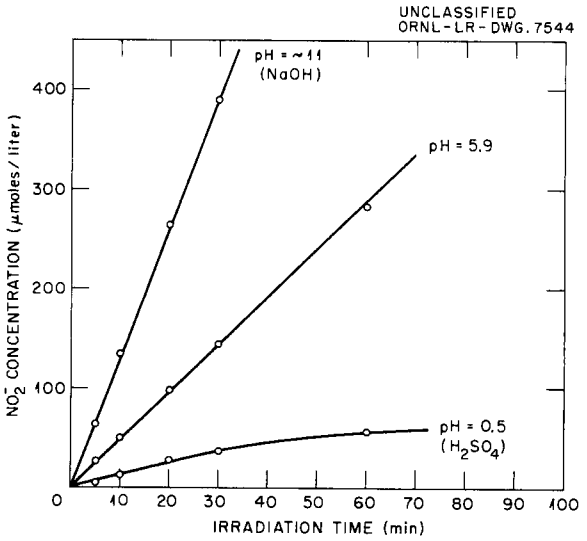

Fig. 39. pH Dependence of Nitrite Ion Production in the Gamma Irradiation of 5 *M* $NaNO_3$ Solutions.

Degassed samples of 5 *M* $NaNO_3$ at pH 0.5, 5.9, and approximately 11 were irradiated in hole 10 in the ORNL Graphite Reactor, and the solutions were analyzed for H_2, O_2, N_2, CO_2, N_2O, NO_2 (ref. 1), and NO_2^-. The results are listed in Table 23. No NO_2 was detectable. The amount of CO_2 was low (~2.5 μl) in all samples. The amount of N_2O was estimated to be approximately 0.02 μl.

From the data it may be concluded that the molecular hydrogen yield remains constant within experimental error throughout the pH range investigated. The lack of NO_2^- formation in highly acid solutions probably results from the rapid oxidation of NO_2^- by the peroxide produced in the decomposition of water. Good stoichiometry between NO_2^-, H_2, and O_2 was observed in all samples. There appeared to be no correlation between the yield of molecular nitrogen and the yield of nitrite ion. Thus it was concluded that molecular nitrogen is probably not produced from nitrite ion.

Effect of Temperature on the Reactor Decomposition of Nitrate Solutions

Studies of the reactor decomposition of $Th(NO_3)_4$ solutions containing enriched uranyl sulfate have

[1] J. W. Boyle, *HRP Quar. Prog. Rep. April 30, 1954*, ORNL-1753, p 147.

TABLE 23. REACTOR IRRADIATION OF 5 *M* $NaNO_3$ SOLUTIONS AT SEVERAL ACIDITIES

Sample No.	pH	G_{H_2}	G_{O_2}	G_{N_2}	$G_{NO_2^-}$ calc	$G_{NO_2^-}$ meas
1	0.5 (H_2SO_4)	0.0709	0.0359	0.00109	~0	
2	5.9	0.0690	0.63	0.00088	1.20	1.21
3	~11.0 (NaOH)	0.0750	1.224	≦0.0014*	2.36	2.33

*The large volumes of accompanying gases made absolute measurements of nitrogen subject to considerable error.

been extended to 250°C. Degassed samples were individually irradiated at constant reactor power in hole 12 of the ORNL Graphite Reactor for 15, 30, or 45 min. The samples were 2.73 or 1.45 *m* in thorium and 0.0128 *M* in uranyl sulfate. The energy input was calculated from the thermal-neutron flux determined by Mn^{55} monitors. In samples containing 0.136 *M* enriched uranyl sulfate, 99.2% of the energy input resulted from fission. In samples containing 0.0128 *M* enriched uranyl sulfate, 92.7% of the energy resulted from fission.

The data are tabulated in Table 24. The yields of hydrogen and nitrogen are presented graphically in Fig. 40, where G_{N_2} and G_{H_2} are plotted against the dose at the experimental temperatures. The nitrogen yield appears to be independent of temperature and decreases slightly with increasing dose.

The hydrogen yield appears to increase slightly with increasing temperature but at any given temperature decreases with dose. The sample containing 1000 g of thorium per liter (7.59 *m*) and 0.0128 *M* enriched uranyl sulfate was prepared by adding the calculated weights of uranyl sulfate solution, crystalline thorium nitrate, and water into a pressure-tested quartz ampoule. The sample was degassed and irradiated in hole 12 for 5 min at 250°C.

The yields of nitrogen in the reactor decomposition of thorium nitrate solutions at 250°C increase with increasing nitrate concentration, as shown in Fig. 41.

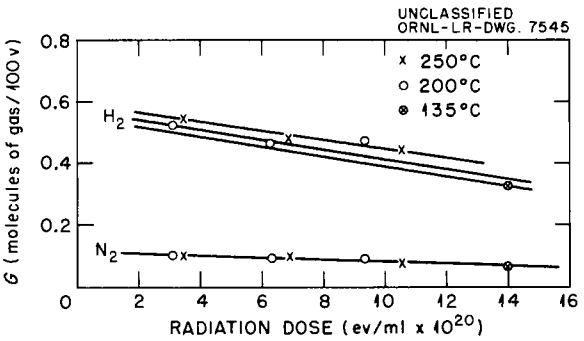

Fig. 40. Production of Hydrogen and Nitrogen in the Reactor Irradiation of 2.73 *m* $Th(NO_3)_4$ Solutions at Elevated Temperatures.

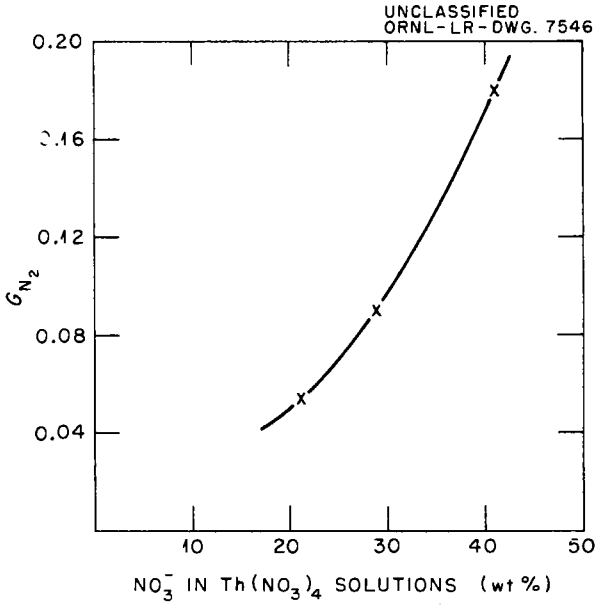

Fig. 41. Nitrogen Yield as a Function of $[NO_3^-]$ at 250°C.

TABLE 24. REACTOR IRRADIATION OF THORIUM NITRATE SOLUTIONS AT ELEVATED TEMPERATURES

$Th(NO_3)_4$ (*m*)	UO_2SO_4 (*M*)	Irradiation Time (min)	Temperature (°C)	Total Energy (ev per ml of soln)	Volume of H_2, STP (cc per ml of soln)	Volume of N_2, STP (cc per ml of soln)	H_2 Produced (molecules per 100 ev)	N_2 Produced (molecules per 100 ev)	Volume of O_2, STP (cc per ml of soln)	O_2 Produced (molecules per 100 ev)
7.59	0.0128	30	250	6.91×10^{20}	0.0224	0.0458	0.09	0.180	0.00627	0.0024
2.73	0.0128	15	200	3.12×10^{20}	0.060	0.0118	0.52	0.100	0.0426	0.367
2.73	0.0128	30	200	6.29×10^{20}	0.106	0.0212	0.46	0.090	0.0873	0.373
2.73	0.0128	45	200	9.38×10^{20}	0.165	0.0310	0.47	0.089	0.145	0.415
2.73	0.0128	15	250	3.22×10^{20}	0.0642	0.0119	0.54	0.100	0.0366	0.305
2.73	0.0128	30	250	6.94×10^{20}	0.125	0.0240	0.48	0.093	0.0936	0.362
2.73	0.0128	45	250	1.05×10^{21}	0.171	0.0304	0.44	0.078	0.144	0.369
1.45	0.0128	30	250	6.83×10^{20}	0.198	0.0136	0.78	0.054	0.103	0.405
2.73	0.136	5	135	1.40×10^{21}	0.174	0.0330	0.33	0.062	0.169	0.324

Effect of Acidity on Nitrite Formation in Concentrated Nitrate Solutions

When aqueous solutions are irradiated, the water decomposes to yield H and OH free radicals and H_2 and H_2O_2 (or O_2) molecules. The H and OH radicals may not be present in equal number; so three equations may be used to express the proper stoichiometry:[2]

$$(F) \qquad 2H_2O \rightsquigarrow H_2 + H_2O_2$$

$$(R) \qquad H_2O \rightsquigarrow H + OH$$

$$(E) \qquad 2H_2O \rightsquigarrow H + H + H_2O_2$$

One of the effects of the radicals from reactions *R* and *E* in nitrate solutions will be the reduction of NO_3^- by H to produce NO_2^-:

$$(1) \qquad NO_3^- + H \longrightarrow NO_2 + OH^-$$

$$(2) \qquad 2NO_2 + H_2O \longrightarrow NO_3^- + NO_2^- + 2H^+$$

In concentrated solutions, a fourth type of radiation effect may result from the direct action of radiation on the solute present. The energy causing decomposition of NO_3^- by direct action includes that energy absorbed directly by the NO_3^- ion and also the energy transferred to the NO_3^- ion from excited water molecules. The over-all direct action reaction on $NaNO_3$ may be written as equation *D*:

$$(D) \qquad 2NaNO_3 \rightsquigarrow 2NaNO_2 + O_2$$

Until the magnitudes of the NO_2^- yields due to radical and direct action are determined, a proposed mechanism for NO_2^- formation is not warranted.

The nitrite yield in 5 *M* $NaNO_3$ solutions irradiated with Co^{60} gamma rays was studied over the pH range 0.5 to 13.55. The measured 100-ev yields of NO_2^- are presented in curve a, Fig. 42. The solutions were sparged with helium gas during the irradiation. It is likely that two different phenomena (see curves b and c), both of which are pH dependent, are involved in the production of NO_2^-. Curve b shows a steady increase in NO_2^- yield with increase in pH over the entire pH range studied. No satisfactory explanation for the slope of curve b is available at this time. Curve c, obtained by subtracting b from a, is insensitive to pH changes up to pH 11.0.

[2] A. O. Allen, *Radiation Research* 1, 85 (1954).

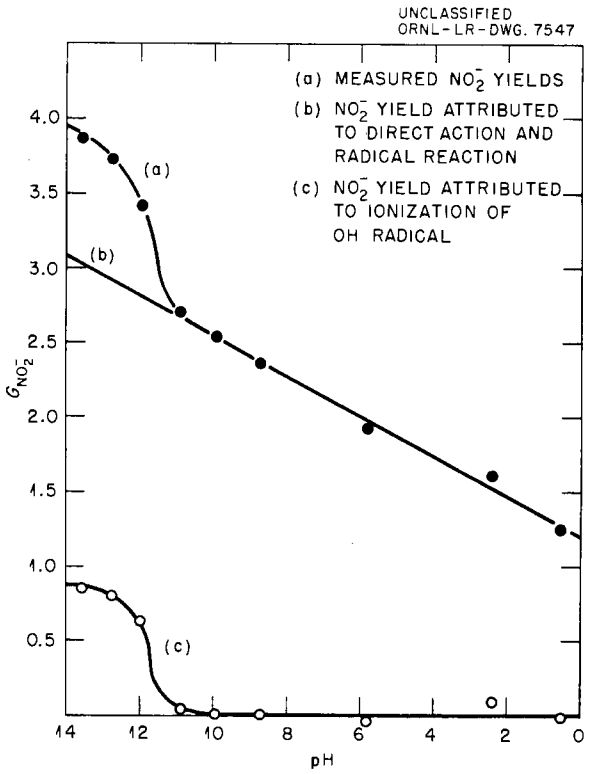

Fig. 42. NO_2^- Yields from Co^{60} Gamma Rays in Helium-sparged 5 *M* $NaNO_3$ Solutions as a Function of pH.

A marked increase in the NO_2^- yield is noted between a pH of 11.0 and 13.0. This increase is postulated to be due to the ionization of the OH radical:

$$(3) \qquad OH \longrightarrow H^+ + O^-$$

The ionization of OH, in effect, converts a strong oxidizing agent, the OH radical, into a reducing agent, O^-, and thereby affects the NO_2^- yield. The O^- may reduce some nitrate by reacting with $NaNO_3$, as in Eq. 4:

$$(4) \qquad NaNO_3 + O^- \longrightarrow NaNO_2 + O_2^-$$

Theoretically, if the degree of ionization of OH were plotted as a function of pH, a curve the shape of curve c would be produced. The break observed does occur at the pH predicted from thermodynamic calculations.[3] Curve c would indicate an equilibrium constant *K* for the OH radical of about

[3] E. J. Hart, S. Gordon, and D. A. Hutchison, *J. Am. Chem. Soc.* 75, 6165 (1953).

2×10^{-12}, and at 25°C a ΔF equal to 16,150 cal. The above thermodynamic calculations[3] indicated a $K = 2.3 \times 10^{-12}$ and a ΔF at 25°C = 16,050 cal.

RADIATION CHEMISTRY OF CERIC ION

T. J. Sworski

Effect of Thallous Ion

Thallous ion enhances the rate of ceric ion reduction by cobalt gamma radiation in 0.8 *N* sulfuric acid from a yield of 2.45 molecules per 100 ev to a yield of 7.85 molecules per 100 ev. The thallous-enhanced yield for reduction of ceric ion is independent of thallous ion concentration (10^{-2} to 10^{-5} *M*), as shown in Fig. 43.

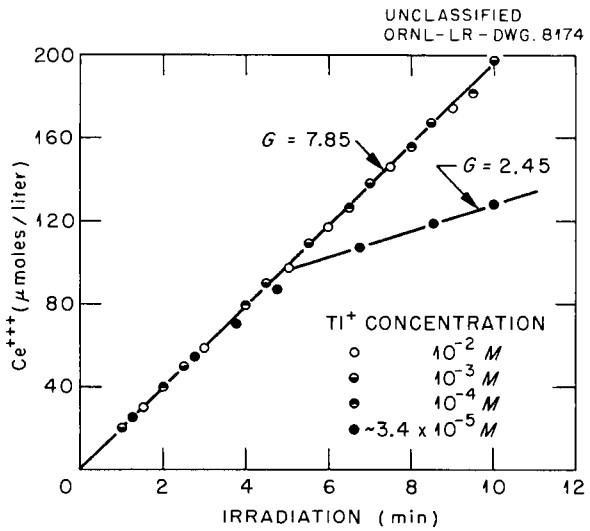

Fig. 43. Effect of Thallous Ion Concentration on the Reduction by Cobalt Gamma Radiation of a 2×10^{-4} *M* Ceric Ion Solution in 0.8 *N* Sulfuric Acid.

In the decomposition of water by ionizing radiation, the formation of the intermediate H, OH, H_2, and H_2O_2 may be expressed[4] by the following equations:

$$(F) \qquad 2H_2O \longrightarrow H_2 + H_2O_2$$

$$(E) \qquad 2H_2O \longrightarrow 2H + H_2O_2$$

$$(R) \qquad H_2O \longrightarrow H + OH$$

[4] A. O. Allen, *Radiation Research* 1, 87 (1954).

The rate of ceric ion reduction in 0.8 *N* sulfuric acid has been postulated[4] to be equal to $2F + 4E$, according to a mechanism in which H atom reduces ceric ion and OH radical oxidizes cerous ion, with no resultant contribution from reaction *R*.

It is proposed here that thallous ion enhances the reduction of ceric ion by reaction with OH radical according to reaction 1 to form Tl(II), which is capable of reducing ceric ion according to reaction 2:

$$(1) \qquad OH + Tl^{+} \longrightarrow OH^{-} + Tl^{++}$$

$$(2) \qquad Tl^{++} + Ce^{4+} \longrightarrow Tl^{+++} + Ce^{+++}$$

On the basis of this mechanism, the thallous-enhanced yield for ceric ion reduction is equal to $2F + 4E + 2R$. The kinetics of this reaction are under detailed investigation. Thallous ion is much more reactive than cerous ion toward OH radical, as evidenced by the sharp break in the rate of ceric ion reduction upon thallous ion depletion (see Fig. 43).

Thallous ion decreases the yield of "molecular" H_2O_2 in a similar manner, as reported for bromide ion[5] and chloride ion.[6] The rate of formation of H_2O_2 in air-saturated 0.8 *N* sulfuric acid is dependent upon the thallous ion concentration, as shown in Fig. 44. This effect of thallous ion is

[5] T. J. Sworski, *J. Am. Chem. Soc.* 76, 4687 (1954).
[6] T. J. Sworski, *Radiation Research* 2, 26 (1955).

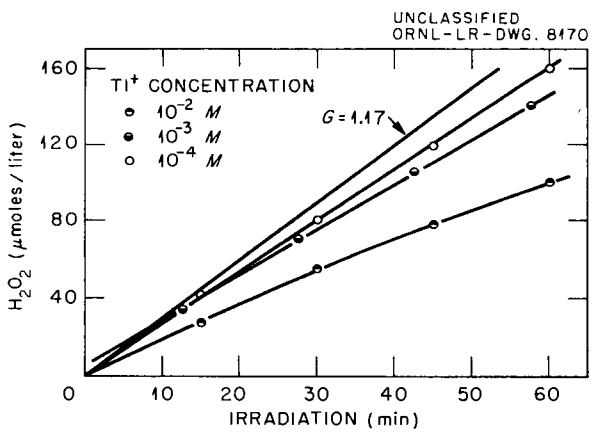

Fig. 44. Effect of Thallous Ion Concentration on the Formation of Hydrogen Peroxide in Air-saturated 0.8 *N* Sulfuric Acid by Cobalt Gamma Radiation.

consistent with the sequence of reactions 1 and 3:

$$(3) \quad Tl^{++} + H_2O_2 \longrightarrow Tl^{+} + H^{+} + HO_2$$

Spectrophotometric analyses of the thallous ion solutions showed no change in the absorption spectrum of the thallous ion upon irradiation. Purification of the 10^{-2} *M* thallous ion solution by the method employed for sulfuric acid solutions by Allen and Holroyd[7] did not alter the curvature shown in Fig. 44.

Direct Action of Cobalt Gamma Radiation

Nitrate ion enhances[8] the rate of ceric ion reduction. It has been proposed[9] that in nitrate solutions the reduction of ceric ion is enhanced through reactions of OH radical with nitrate ion. Figure 45 shows that nitrate ion enhances the rate of ceric ion reduction, when thallous ion is present, by the same amount as when thallous ion is absent. This is interpreted as conclusive experimental evidence that enhancement of ceric ion reduction by nitrate ion is not attributable to OH radical reactions but is attributable, rather, to the direct action of gamma radiation on the nitrate ion. This direct action is considered as resulting from excitation-energy diffusion to the nitrate ion, with resultant decomposition to nitrite ion, as in the photochemical decomposition of nitrate ion. Studies in this system are being continued.

[7] A. O. Allen and R. A. Holroyd, paper presented at the 127th National Meeting of the American Chemical Society, Cincinnati, March 27 to April 7, 1955.

[8] W. H Sullivan and A. Savolainen, *Oak Ridge National Laboratory Status and Progress Report, October 1954*, ORNL-1805 (Nov. 7, 1954).

[9] G. E. Challenger and B. J. Masters, *J. Am. Chem. Soc.* 77, 1063 (1955).

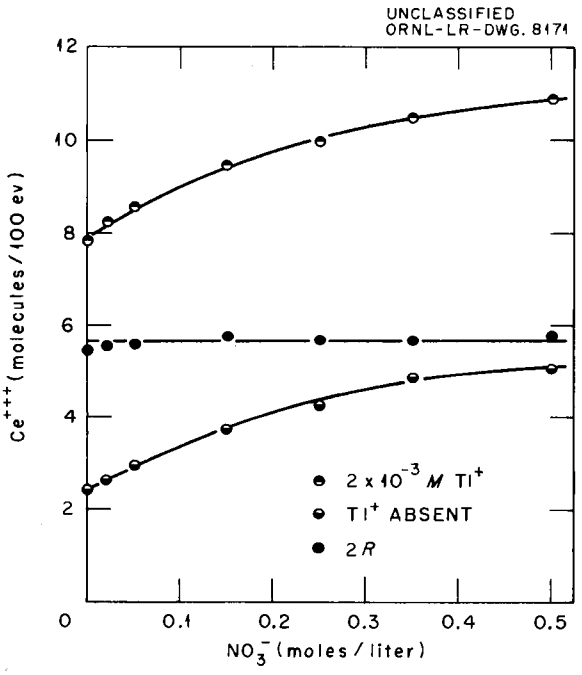

Fig. 45. Effect of Nitrate Ion Concentration on the Reduction of Ceric Ion by Cobalt Gamma Radiation in 0.8 *N* Sulfuric Acid.

Radiation Chemistry of Sulfuric Acid

Figure 46 shows the yield for ceric ion reduction, both in the presence and absence of thallous ion, in sulfuric acid solutions as a function of the electron fraction of sulfuric acid. The lines extending beyond the experimental points in Fig. 46 are based on the present working hypothesis of the author for this system. In the absence of ceric ion, sulfur dioxide has been reported[10] as a measurable product in the decomposition of concentrated sulfuric acid solutions by cobalt gamma radiation.

[10] C. J. Hochanadel, J. A. Ghormley, and T. J. Sworski, *J. Am. Chem. Soc.* 77 (to be published).

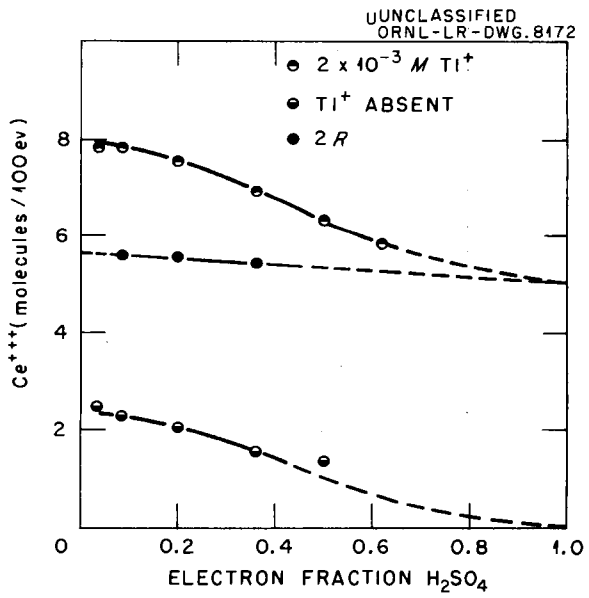

Fig. 46. Reduction of Ceric Ion as a Function of Electron Fraction of H_2SO_4.

In 20.0 *N* sulfuric acid (about 62% electron fraction sulfuric acid), there is a postirradiation effect in the reduction of ceric ion, as shown in Fig. 47. This postirradiation effect is interpreted as resulting from the inability of the oxidizing radicals to oxidize cerous ion, which inability results in radical combination. With thallous ion present, no postirradiation effect is present, since, evidently, the oxidation of thallous ion by the oxidizing radicals can still occur. This interpretation is consonant with the mechanism[11] presented for the photooxidation of water by ceric ion, where the oxidation-reduction potential of the cerous-ceric couple is higher in 0.8 *N* perchloric acid than in 0.8 *N* sulfuric acid. Studies in the radiation chemistry of sulfuric acid are continuing.

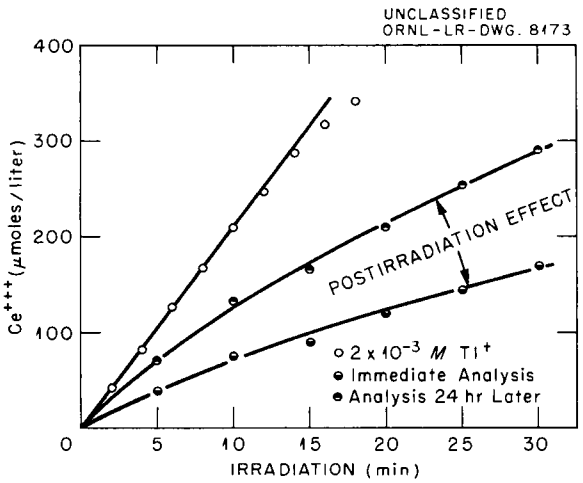

Fig. 47. Reduction of Ceric Ion in 20.0 *N* Sulfuric Acid by Cobalt Gamma Radiation.

RADIATION CHEMISTRY OF ORGANIC SUBSTANCES

J. G. Burr, Jr.

The radiation decomposition of several substituted butanes is under investigation. The quantities which are being determined are the yield and composition of the gaseous products, the yield of those liquid and solid products which can be feasibly measured, and the amount of starting material which disappears by all processes. It is hoped that careful examination of such data will provide some knowledge of the influences governing the breakdown pattern of aliphatic hydrocarbons and provide some information about the reaction mechanisms.

Since the radiation stability of tri-*n*-butyl phosphate is of practical interest in some of the Laboratory's operations, it has been chosen as the first substance to be studied, and most of the data presented here are concerned with the radiation chemistry of this material. Some preliminary data on the radiation chemistry of di-*n*-butyl carbonate are included for comparison.

The radiations were carried out in a water-jacketed glass cell with a thin window. This cell was attached to a closed evacuated system of known volume. Electrons from a Van de Graaff generator were used as a radiation source. The materials were degassed by refluxing *in vacuo*, and, following the radiation, the product gases were removed from the cell system with a Toepler pump. Repeated refluxing and pumping were necessary to recover the more soluble gaseous products (about 30% of the gaseous products were found to remain dissolved in the irradiated liquid). The data thus obtained are summarized in Table 25. In this table the entry labeled "prompt gas" refers to the products found in the gas phase during and after the radiation, excluding those which remained dissolved in the liquid. The evolution of this material was found to be linear with dose up through doses of 10^{23} ev. The gas analyses reported in Table 25 were obtained by mass spectrometer analysis. Interpretation of the mass pattern required the solution of a system of 20 simultaneous equations for the 15 listed components; these solutions were obtained as least-mean-squares fits, with the assistance of the Oracle. In addition, the gas fraction nonvolatile at liquid-nitrogen temperatures (this includes everything but hydrogen, methane, and carbon monoxide) was isolated, and its infrared spectra were examined; the quantitative interpretation of these spectra is not yet complete.

In the case of the tributyl phosphate, it is further proposed to determine the acidity of the irradiated material (this should be an indication of the amounts of mono- and dibutyl phosphates formed) and also to determine the total disappearance of reactant by isotope dilution techniques.

Since a comparison of the hydrocarbon products is one of the most interesting results of these

[11] T. J. Sworski, *J. Am. Chem. Soc.* 77, 1074 (1955).

TABLE 25. COMPOSITION AND YIELDS OF GASES FROM IRRADIATION OF BUTYL ESTERS

	Tributyl Phosphate		Dibutyl Carbonate
	Run 1	Run 2	
Voltage, Mev	1.66	1.66	1.66
Current, μa	5	5	5
Time, min	30	30	25
Prompt gas	1.29[a]	1.27	1.81
Total gas	1.96	1.92	2.82
Methane	0.053[b]	0.031[b]	0.030[b]
Ethane	0.061	0.045	0.066
Ethylene	0.087	0.085	0.109
Propane	0.094	0.091	0.116
Propylene	0.019	0.015	0.036
n-Butane	0.196	0.217	0.029
Isobutane	0.034	0.046	0.003
Isobutene	0.004	0.007	0
1-Butene	0.023	0	0.013
2-Butene	0.212	0.258	0.004
C_5 hydrocarbons	Trace	Trace	0
Carbon dioxide	0	0	1.35
Hydrogen	1.15	1.12	1.06
Water, % of total gas	1.62	1.07	0.07
Nitrogen, % of total gas	2.70[c]	4.30[c]	0[c]

[a]Except where noted, all numbers such as these are *G* values (molecules of gas formed per 100 ev absorbed).

[b]The *G* values for the gas constituents have been calculated on a nitrogen-free, water-free basis for the gas.

[c]These values represent the sum of nitrogen and carbon monoxide. The mass spectrometer does not distinguish accurately between these two substances.

experiments, the yields of these products have been recalculated on a hydrogen-free, nitrogen-free, and water-free basis. The values are shown in Table 26 (as percentage composition).

Some interesting aspects of these results may be briefly mentioned. The butane/isobutane ratio in the products from tributyl phosphate is about 6.0. This means that about 17% isomerization of the butyl group has occurred during the decomposition. The equilibrium value of this ratio in isomerization reactions known to occur through positive ions is about 5.0, representing 20% isomerization of *n*-butane. This correlation might be adduced as evidence that separation of the butyl groups during the radiation decomposition must occur as positive butyl ions, $C_4H_9^+$, rather than as butyl radicals whose lifetimes might be expected to be too short to allow appreciable isomerization.

TABLE 26. RELATIVE GASEOUS HYDROCARBON YIELDS FROM IRRADIATION OF BUTYL ESTERS

	Tributyl Phosphate		Dibutyl Carbonate
	Run 1	Run 2	
Methane	6.90	3.86	7.28
Ethane	7.70	6.38	16.15
Ethylene	11.07	10.57	26.90
Propane	12.02	13.00	28.60
Propylene	2.48	2.42	8.95
n-Butane	25.00	26.92	7.22
Isobutane	4.46	4.32	0.62
Isobutene	0.46	0.44	0
1-Butene	2.86	0	3.26
2-Butene	27.05	32.00	0.97

It can be seen from Table 26 that the principal gaseous hydrocarbon products in the decomposition of tributyl phosphate are intact four-carbon fragments. This implies that a major process in the decomposition of tributyl phosphate is fission of the butyl-group–oxygen bond, with breakdown of the butyl group playing a relatively less important part. On the other hand, in the decomposition of dibutyl carbonate, intact four-carbon fragments compose only a very small percentage of the products. It is apparent here that breakdown of the butyl group is almost the exclusive source of the gaseous hydrocarbon products. An over-all conclusion is that the nature of the prosthetic group (carbonate or phosphate) bound to butane exerts a profound effect on the radiation-induced breakdown of the butane molecule.

Since tributyl phosphate is used in solvent extraction processes where it is exposed to considerable amounts of radiation, it is interesting to attempt an estimate of the tributyl phosphate destroyed during the extraction process. If every hydrogen molecule produced is considered to represent two tributyl phosphate molecules changed, and if every molecule of the other products is considered to represent one tributyl phosphate molecule changed, then the observed G value for gas production represents 1.7 g of tributyl phosphate changed per hour per 1000 curies of 1-Mev beta radiation. The gas production is then about 100 cc/hr. The former value is a minimum value, since, undoubtedly, tributyl phosphate must decompose to some extent by processes which do not form gaseous products.

GAS-PHASE IRRADIATION

S. C. Lind

A. C. Stewart P. S. Rudolph

The analyses of the CO polymerization induced[12] by alpha particles, both in the presence and absence of krypton, indicate that the only gaseous product is CO_2. These analyses and the ratio of 3 for the decrease in pressure of the CO to increase in pressure of the CO_2 ($-\Delta P_{CO}/+\Delta P_{CO_2}$) for the CO + Kr reaction are in agreement with the previous work[12,13] on this polymerization. In the reaction of pure CO, $-\Delta P_{CO}/+\Delta P_{CO_2}$ is 3.4. This high value appears to be due to a discrepancy in the analysis.

The polymerization of HCN and of HCN mixed with Kr, A, or He was studied. No analytical data are yet available, hence the following treatment of data is tentative. (It has been tentatively decided to have these analyses performed by mass spectrographic means rather than by the previously used chemical methods.)

The preliminary statement[14] that the inert gases seemed to have little effect on the velocity of the polymerization of HCN does not appear correct in the light of more thorough but still incomplete treatment of the data. When log P vs $e^{-\lambda t}$, where P is the pressure of the HCN and $e^{-\lambda t}$ is the fraction of radon remaining, was plotted, a straight line with a sudden break indicated little effect of the inert gas. The line resulting from a similar plot, where P is the pressure of the HCN plus the equivalent pressure of the inert gas, was just as straight as the line in the previous case. The velocity constants, proportional to the slope of this line and corrected to a 2-cm sphere, are given in Table 27. Included in this table are the efficiencies of the inert gas ions in causing polymerization, assuming that the only mechanism is charge transfer.

TABLE 27. COMPARISON OF THE VELOCITY CONSTANTS OF THE HCN RADIOLYSIS WITH AND WITHOUT INERT GASES

Reaction	$(k\mu/\lambda)$ HCN	$(k\mu/\lambda)$ HCN + Inert Gas	Efficiency of Inert Ions (%)
HCN	89		
HCN + Kr	112	71	62
HCN + A	101	76	67
HCN + He	115	85	91

The value 89 for pure HCN agrees well with the published value[15] of 93 when the deviation of HCN from ideal gas behavior is taken into account.

[12] S. C. Lind, P. S. Rudolph, and A. C. Stewart, *Chem. Semiann. Prog. Rep. Dec. 20, 1954*, ORNL-1832, p 80.

[13] S. C. Lind and D. C. Bardwell, *J. Am. Chem. Soc.* 47, 2675 (1925).

[14] F. T. Howard and W. H Sullivan, *Oak Ridge National Laboratory Status and Progress Report, February 1955*, ORNL-1867, p 23 (March 7, 1955).

[15] S. C. Lind, D. C. Bardwell, and J. H. Perry, *J. Am. Chem. Soc.* 48, 1562 (1926).

Lind and Bardwell[16] found the velocity constant for HCN + N_2 and HCN + Xe to be equal to 85.

The polymerization of benzene vapors at 100°C is in progress. The velocity constant for this reaction is 36.1, compared with 40.4 calculated from the data of Mund and Bogaert.[17] Both values are based on total pressure drops and are corrected to 2-cm spheres. The ion yield in both cases for comparable time periods is about 1. The decrease in the C_6H_6 pressure was accompanied by the evolution of a gas. After the reaction had run for five days, the pressure in the reaction vessel increased slowly. The polymer, on first formation, was a yellow liquid which turned dark brown and finally changed into a white solid.

[16] S. C. Lind and D. C. Bardwell, *J. Am. Chem. Soc.* **48**, 1580 (1926).

[17] W. Mund and E. Bogaert, *Bull. soc. chim. Belges* **34**, 410 (1925).

REACTOR CHEMISTRY

INVESTIGATION OF THE ALKALI OR ALKALINE-EARTH OXIDE–URANIUM TRIOXIDE–CARBON DIOXIDE–WATER PHASE EQUILIBRIA AT HIGH TEMPERATURE

F. J. Loprest W. L. Marshall
C. H. Secoy

An investigation was started on the phase equilibria at high temperature of the systems alkali or alkaline-earth oxide–uranium trioxide–carbon dioxide–water. The purpose of this work was to explore the various alkaline uranium systems and to evaluate their potentialities as suitable aqueous homogeneous reactor fuels. The results reported here are of a preliminary nature. It was desired to survey several systems before obtaining extensive data on any one.

Among the systems investigated, namely, the Na_2O-UO_3-CO_2-H_2O, the MgO-UO_3-CO_2-H_2O, and the Li_2O-UO_3-CO_2-H_2O, emphasis at the present time is placed on the lithium system, since it appears to be the most promising of the three for a reactor fuel. Systems involving the other alkali or alkaline-earth oxides did not appear desirable, either because the neutron absorption cross section of the metal oxides appeared to be too high or because work at low temperature indicated unsatisfactory solubilities to be expected at high temperature.

There have been a few exploratory studies made on the Na_2O-UO_3-CO_2-H_2O system at high temperature (100 to 250°C) by Wright and Gill,[1] Blake *et al.*,[2] and a cursory examination by Bidwell *et al.*[3] The sodium system did not appear feasible for dissolving appreciable quantities of uranium at high temperature.

Several recent, rather thorough, investigations[4–6] have dealt with these systems at low temperature. Blake *et al.* have reported that as much as 320 g of uranium per liter can be dissolved at 25°C in the Na_2O-UO_3-CO_2-H_2O system. Bachelet *et al.* have studied the Li_2O-UO_3-CO_2-H_2O and MgO-UO_3-CO_2-H_2O systems, among others, and state that appreciable solubilities of the order of 1 to 2 *M* of compounds such as $Li_4UO_2(CO_3)_3$ and $Mg_2UO_2(CO_3)_3$ can be obtained in the temperature range 25 to 60°C. However, they state that hydrolysis occurs above approximately 50 to 75°C, with subsequent precipitation of a uranium compound. It was the intention here to attempt to prevent this precipitation by the use of carbon dioxide gas pressure.

Experimental

Uranium trioxide was obtained from the Mallinckrodt Chemical Works. It was water-washed at room temperature and finally at 250°C in order to remove as much nitrate impurity as possible (NO_3^-, <24 ppm). Baker and Adamson reagent-grade sodium carbonate and lithium carbonate and Merck reagent-grade magnesium carbonate were used as starting alkali or alkaline-earth materials. Commercial-grade dry ice was used for producing the CO_2 pressure on the system under study. Water-pumped, commercial-grade tank oxygen was used for oxygen addition; in some of the early work, Baker and Adamson cp 30% H_2O_2 was used for oxygen addition. The use of H_2O_2 was discontinued, since it was observed to form highly colored soluble complexes of questionable stability and thus to complicate the solubility relationships.

$Mg_2UO_2(CO_3)_3$ and $Li_4UO_2(CO_3)_3$ were prepared in aqueous solutions at low temperature according to the methods of Bachelet *et al.*[6] High solubilities at room temperature and up to approximately 100°C were obtained; these values verified a few of the observations of Bachelet *et al.*

The soluble $Li_4UO_2(CO_3)_3$ did not crystallize when the solution was concentrated by evaporation to approximately 2.0 to 2.5 *M*, in accordance with Bachelet's observations. The soluble

[1] H. W. Wright and J. S. Gill, *HRP Quar. Prog. Rep. Aug. 15, 1951*, ORNL-1121, p 120.

[2] C. A. Blake *et al.*, Oak Ridge National Laboratory, private communication (1951).

[3] R. W. Bidwell *et al.*, Los Alamos, private communication (1951).

[4] C. A. Blake *et al.*, *Studies in the Carbonate-Uranium System. Part I. Investigations in the Four Component System UO_3-Na_2O-CO_2-H_2O*, AECD-3280 (Dec. 14, 1951); *Part III. Spectrophotometric Investigation of the Carbonate-Uranyl Complexes*, Y-794 (Aug. 20, 1951).

[5] K. B. Brown and J. M. Schmitt, *Studies in the Carbonate-Uranium System. Part II. The Solubility of Sodium Uranyl Tricarbonate in Solutions of Certain Sodium Salts*, AECD-3229 (Oct. 20, 1950).

[6] M. Bachelet *et al.*, *Bull. soc. chim. France* 19, 55–60 (1952); 19, 565–569 (1952); 21, 173–179 (1954).

$Mg_2UO_2(CO_3)_3$, however, did form clear yellow needle crystals after concentration of a dilute solution by evaporation at 75 to 80°C to approximately 2 *M* and after the solution was cooled to room temperature and seeded.

The apparatus and thermostat controllers for solubility determination at high temperature are described in another report.[7] The present apparatus included a few modifications (Fig. 48). Commercial high-pressure stainless steel valves and other equipment were used exclusively. A second capillary tubing connection was added to the solubility bomb, thus providing both a capillary solution sampling tube and a tube opening into the vapor phase for addition or removal of gas and vapor.

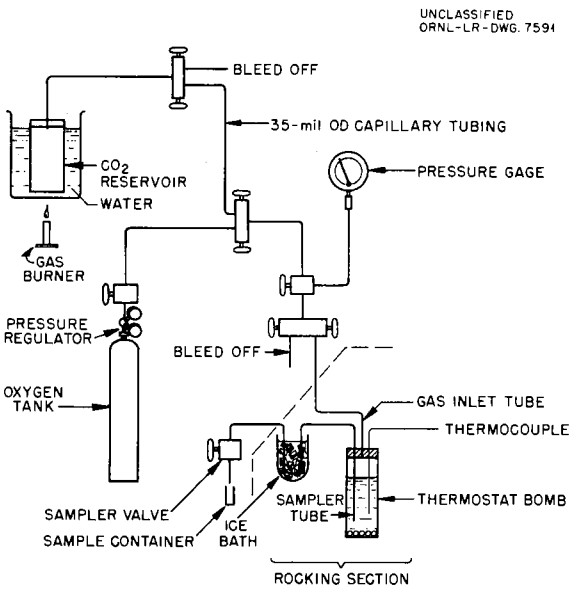

Fig. 48. Schematic Diagram of Solubility Apparatus.

Since the critical pressure of liquid carbon dioxide at the critical temperature (31°C) is 1071 psi, whereas total pressures of 3000 psi were contemplated in these investigations, the usual tank liquid CO_2 could not be used to obtain these pressures, at least not at room temperature. Therefore, a bomb was constructed to which a weighed amount of dry ice was added, and the bomb was heated in a water bath above the critical temperature of CO_2. This bomb, containing a high pressure of CO_2 and connected to a pressure gage and to the thermostat bomb by a series of valves, was used to achieve the desired pressures on the system under consideration.

The procedure for making a run was as follows. Weighed amounts of UO_3 hydrate and either Na_2CO_3, Li_2CO_3, or $MgCO_3$ were added to a 100-cc-capacity pressure bomb. A 60-cc volume of distilled water, which had been purified further by use of an ion-exchange column, was added to the bomb. The bomb head was screwed down, and the unit was placed in the thermostat, which was rocked by means of a hydrogenation apparatus rocker. The temperature was raised to 75 to 100°C, and 50 ± 5 psi of oxygen pressure was added to the system from an oxygen tank and regulator. The temperature was raised to a given value, and the desired CO_2 pressure was placed on the system from the CO_2 bomb reservoir. The thermostat was rocked for a sufficient length of time, the unit stopped, the thermostat rotated from the horizontal to the vertical position, and a solution sample obtained in the manner described.[7] The total pressure on the system could be varied by adding additional CO_2 or bleeding off the vapor phase.

Uranium was determined in most samples colorimetrically by the basic peroxide method.[8] In the case of UO_3 and UO_2CO_3 solubilities in H_2O, the uranium concentrations were too low, and therefore the more sensitive method of Yoe, Will, and Black[9] was used. A few uranium samples were analyzed potentiometrically. Lithium was determined by D. Fornwalt of the Analytical Chemistry Division by use of a flame spectrophotometric method. Carbonate was determined by decomposition with acid and adsorption of the liberated CO_2 by Ascarite. An approximate method for estimating CO_2 in the liquid samples involved the trapping of the sample in a 3-mm pyrex tube 1 m in length at 1 atm pressure. Comparison of the volumes of the liquid and

[7] W. L. Marshall, *The pH of UO_3-H_2SO_4-H_2O Mixtures at 25°C and Its Application to the Determination of the Solubility of UO_3 in Sulfuric Acid at Elevated Temperatures*, ORNL-1797 (1954).

[8] C. J. Rodden (Editor-in-Chief), *Analytical Chemistry of the Manhattan Project*, p 93, McGraw-Hill, New York, 1950.

[9] J. H. Yoe, F. Will, III, and R. A. Black, *Anal. Chem.* 25, 1200 (1953).

gas phases permitted an estimation of the amount of CO_2 in excess of that which is in combined form in the liquid phase.

The Systems UO_3-H_2O and UO_2CO_3-H_2O

The solubility of UO_3 was determined at various temperatures on one batch of 3 g of solid oxide (Table 28). The average values for the indicated temperatures are listed in the last column of the table.

An attempt to measure the effect of CO_2 pressure on the solubility of UO_3 indicated that UO_3 was converted to a different solid phase, probably UO_2CO_3, at total pressures in excess of 860 psi (the minimum CO_2 pressure necessary for conversion was not determined). The solubility determinations were erratic but indicated that the solubility of the new phase is of the same order of magnitude as the solubility of UO_3 in pure water.

The System (MO or M_2O)-UO_3-CO_2-H_2O – General Discussion

The weight percentages of the components MO or M_2O, UO_3, and H_2O in the liquid phase (except when noted), the total mixture, and the solid phase are expressed, with the CO_2 content being completely neglected. These data, therefore, represent points on a Jänecke projection of points in the quaternary isothermal, isobaric tetrahedron on the MO- or M_2O-UO_3-H_2O face. The tie lines on this projection can be extrapolated to solid-phase compositions that express the true ratio of three of the components but do not give any information about the fourth component, CO_2. Some supporting observations provide the basis for an estimate of the CO_2 content of the liquid and solid phases. The composition of the vapor phase at a constant total pressure and temperature can be assumed to be fixed, since the vapor pressure of water probably does not vary much.

TABLE 28. SOLUBILITY OF UO_3 IN WATER

Temperature (°C)	Initial Mixture		Total Stirring Time (hr)	Concentration of U in Liquid Phase	
	g of UO_3	ml of H_2O		ppm	Average
250	3	50	3	16.7	
			6	12.8	
			11	16.4	
			27	19.4	
*					
250	3	60	0.25	13.3	
			2.5	12.7	
			9	14.3	
*					
290	3	60	16	19.0	
			18	17.1	18.1 (290°C)
250			3	9.9	14.4 (250°C)
*					
200	3	60	4	5.3	
			7	5.2	5.3 (200°C)
*					
175	3	60	2.5	6.4	
			5.0	6.0	6.2 (175°C)
150			1.0	6.2	
			2.0	6.4	6.3 (150°C)

*Indicates interruption of run for washing of solid.

In calculating the weight percentages in the liquid phase, two assumptions were made. The first was that the CO_2 remaining in the liquid phase, after the solution was cooled and the pressure was reduced, as described in the discussion of the sampling procedure, was stoichiometric to the M_2O and UO_3 in the liquid phase. This small weight of CO_2 was subtracted from the total weight of the sample, which was then analyzed for M and U. The second assumption concerned the densities of the liquid phase. Since a volumetric sample was analyzed, it was necessary, in the absence of density measurements, to assume that the density of the liquid was unity. Based on UO_2SO_4 densities for similar molarities,[10] these densities probably do not deviate more than +5% from unity.

In order to obtain the *absolute* weight percentages of the three components, MO or M_2O, UO_3, and H_2O, the absolute weight per cent of the fourth component, CO_2, would have to be determined in the system under equilibrium conditions. The Jänecke projection values given[11] would then be multiplied by the factor $(1.0 - X)$, where X is the weight fraction of CO_2 at equilibrium. The true weight percentages for all four components would then be obtained. At 1500 psi total pressure and at 250°C the true weight fraction of CO_2 in the solution was found to be approximately 0.018 to 0.020 in the lithium system, as obtained by the gas-liquid volume ratio method at atmospheric pressure and by assumption of the residual and stoichiometric CO_2 contents in the liquid. Therefore, the correction factor $(1 - X)$ would produce only a 1.8 to 2.0% negative correction of the values reported.[12]

The System Na_2O-UO_3-CO_2-H_2O

Table 29 lists the data obtained thus far for the Jänecke projection. The solid-phase compositions were obtained by direct analysis of the solids which had been removed from the bomb after the final sampling of the liquid phase. The solids were separated from the liquid phase by filtration, washed with two or three small portions of distilled water, allowed to dry in air, and ground in a mortar until uniform. The complete analyses of the solids, including CO_2 determination, are listed in Table 30.

In constructing the Jänecke projection (Fig. 49), the liquid phase could not be corrected for residual CO_2, since the Na_2O content of the liquid had not been determined in most cases. The solubility curve in the projection is therefore fixed by drawing a tie line between the solid phase and total mixture points and terminating it at the given value of the percentage UO_3 in the liquid phase.

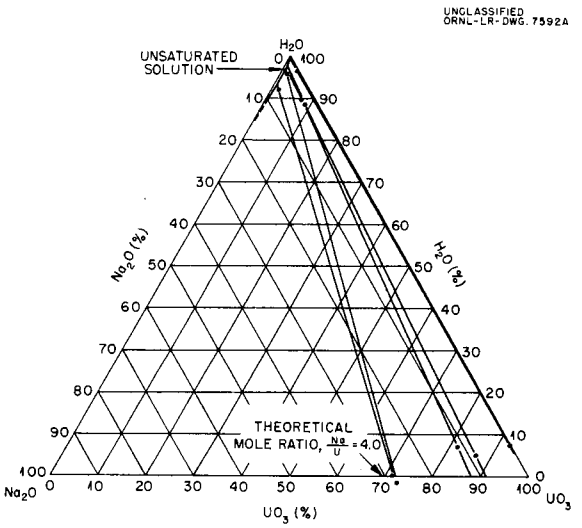

Fig. 49. The System Na_2O-UO_3-CO_2-H_2O at 250°C and at 1000 to 1600 psi CO_2 (Jänecke Projection).

Two of the solids obtained have compositions close to that of $Na_4(UO_2)(CO_3)_3$ (theoretical composition, wt %: Na_2O = 22.87, UO_3 = 52.77, CO_2 = 24.36). It appears probable, therefore, that this solid is one of the equilibrium phases at high temperature just as it is at room temperature. Two of the tie lines in the projection lie in what appears to be a two-solid-phase eutectic region. If the two solid phases involved are $Na_4(UO_2)(CO_3)_3$ and UO_2CO_3, then the deep solubility well found by Blake and co-workers at room temperature apparently is absent at 250°C.

The System MgO-UO_3-CO_2-H_2O

An unsaturated solution of magnesium uranyl carbonate (0.2154 *M* MgO and 0.07173 *M* UO_3) was prepared at room temperature according to the

[10] W. L. Marshall, *HRP Quar. Prog. Rep. Mar. 15, 1952*, ORNL-1280, p 188.

[11] Tables 29 and 34 and Figs. 50 and 54.

[12] Table 34 and Fig. 54.

TABLE 29. THE SYSTEM Na_2O-UO_3-CO_2-H_2O

Data for Jänecke projection on Na_2O-UO_3-H_2O face at 250°C

Run No.	Total Mixture (%)		Liquid[a] Phase (%)		Solid[b] Phase (%)		P_{total} (psi)	Stirring Time[c] (hr)
	UO_3	Na_2O	UO_3	Na_2O	UO_3	Na_2O		
II-44-1	3.06	0.265	0.00				580	1
2			0.00		92.48	0.00	1600	2
II-39-1[d]	8.78	2.53	0.135				820	3
2			0.192		83.36	11.05	1250	4
II-41-1	7.43	2.56	0.098	1.82			580	2
2			0.159	1.82	86.67	8.85	1100	3
II-31-1[d]	1.67	2.74	0.050				800	1
2			0.144				1000	3
3			0.169				1000	3
4			0.154				1400	4
5			0.179		73.57	28.79	1300	2
II-43-1	19.54	6.02	0.126				580	
2			0.166				1400	
II-35-1[d]	1.63	6.36	0.159				780	2
2			0.179		71.47	28.27	1000	3

[a]Analytical data uncorrected for residual CO_2.
[b]By analysis of washed, dried solids.
[c]Not cumulative.
[d]Initial pressure of O_2 introduced at 100°C was 200 psi; in all other runs it was 50 psi.

TABLE 30. ANALYSES OF DRIED WASHED SOLIDS

Run No.	UO_3 (%)	Na_2O (%)	CO_2 (%)
II-44-2	91.80	0.004	0.74
II-41-3	83.16	8.49	4.04
II-39-2	81.33	10.78	2.43
II-35-2	55.20	21.83	22.77
II-31-5	56.48	22.10	23.23

directions given by Bachelet *et al.*[13] This solution was employed in run A IX 25. For run B IX 27, solid $MgCO_3$ and UO_3 were mixed with water. The data for these runs are listed in Table 31.

[13]M. Bachelet *et al.*, *Bull. soc. chim. France* 19, 55–60 (1952); 19, 565–569 (1952); 21, 173–179 (1954).

These two runs cover only a small portion of the dilute region of the phase diagram. Much more extensive investigation is planned for this system, although the apparently very low solubility of $MgCO_3$ seemed to indicate that there may not be any appreciable solubility of uranium at high temperatures.

The System Li_2O-UO_3-CO_2-H_2O

A preliminary measurement of solubility relations in the system Li_2O-CO_2-H_2O at various CO_2 pressures at 250°C was made, and the data are recorded in Table 32 and are plotted in Fig. 50. It is seen that the rate of change of the solubility with pressure appears to fall off at about 1000 psi total pressure to a constant low value at higher pressures. Moreover, plots of the Li_2O and UO_3 contents in the liquid phase and of the Li/U mole

TABLE 31. THE SYSTEM $MgO-UO_3-CO_2-H_2O$

Agitation time was 2 hr

Run No.	Total Mixture (%)		UO_3 in Liquid Phase (%)	Temperature (°C)	Total Pressure (psi)
	MgO	UO_3			
A IX 25	0.869	2.052	0.0039	250	1500
			0.0012	150	1000
			0.0015	100	880
			0.0026	100	220
B IX 27	0.438	3.107	<0.004	250	1600
			<0.004	250	720

TABLE 32. THE SYSTEM $Li_2O-CO_2-H_2O$, SOLUBILITIES

Run No.	Total Pressure* (psi)	Weight Per Cent As Li_2CO_3	Weight Per Cent As Li_2O on Jänecke Projection
IX-38-1	625 (no CO_2)	0.241	0.0973
IX-38-2	625 (no CO_2)	0.235	0.0952
IX-38-3	1600	1.26	0.511
IX-38-4	1430	1.21	0.490
IX-38-5	1310	1.14	0.460
IX-38-6	1225	1.07	0.434
IX-38-7	1190	1.08	0.435
IX-38-8	1050	1.02	0.411
IX-38-9	960	0.964	0.390

*$H_2O + CO_2 + 50$ psi of O_2.

ratio (Figs. 51,52,53) exhibit, with some scattering of points, a similar behavior.

Table 33 contains the data thus far obtained in this investigation. The solid-phase compositions are the Jänecke projections. The liquid-phase compositions, as listed in the table and plotted in Figs. 51 and 52, have not been corrected for residual CO_2.

In considering Figs. 51 and 52, it is seen that the UO_3 and Li_2O content of the liquid phases at pressures above 1100 psi roughly appears to be one of two constant sets of values. For example, at 1500 psi for runs IX-33 and II-52, values of Li_2O = 1.08% and UO_3 = 3.37% may be read from the figure, and, likewise, for runs II-48 and II-58, values of Li_2O = 0.80% and UO_3 = 2.04% may be obtained. These values may be corrected for residual CO_2, and they are listed in Table 34. The data in Table 34 are plotted in Fig. 54. The existence of three solid phases is tentatively postulated, and this is consistent with the experimental observations. The postulated solids may be: I = Li_2CO_3, II = a lithium uranyl carbonate with mole ratio of Li/U probably 2 or less, and

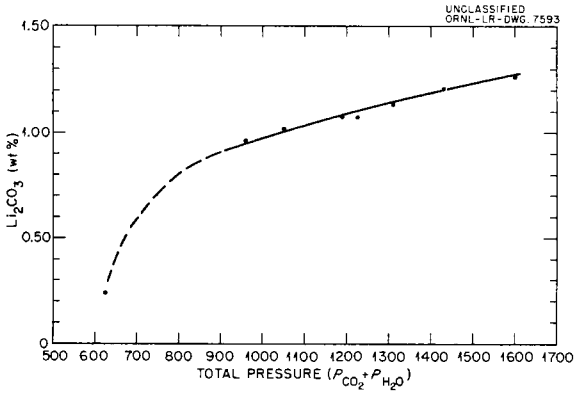

Fig. 50. Per Cent of Li_2CO_3 in Liquid Phase; System Li_2O-CO_2-H_2O.

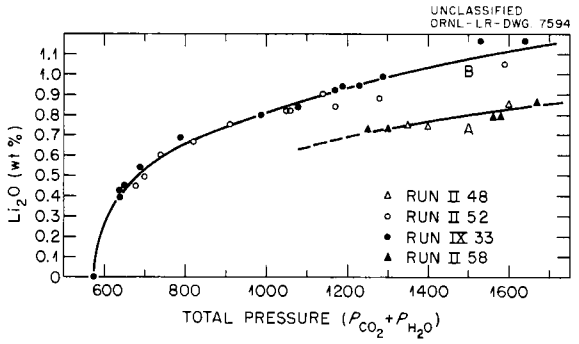

Fig. 51. Per Cent of Li_2O in Liquid Phase; System Li_2O-UO_3-CO_2-H_2O.

III = UO_2CO_3. The existence of a whole series of complex solids, such as occurs in the Na_2O-UO_3-H_2O system,[14] is, of course, possible. If this were the case, then a corresponding number of very dilute solutions saturated with respect to two solids would exist in the system.

The relatively small region of unsaturation is bounded by rather steep solubility surfaces, and, if the liquid phase is to remain unsaturated, conditions have to be maintained within rather narrow limits. It is expected that this region of unsaturation will increase as the temperature is decreased. However, at 250°C it does not appear likely that a liquid phase containing more than 4% of UO_3 or about 30 to 40 g of uranium per liter will be obtained, at least at total CO_2-H_2O pressures up to 2000 psi.

[14] J. E. Ricci and F. J. Loprest, *J. Am. Chem. Soc.*, 77, 2119, (1955).

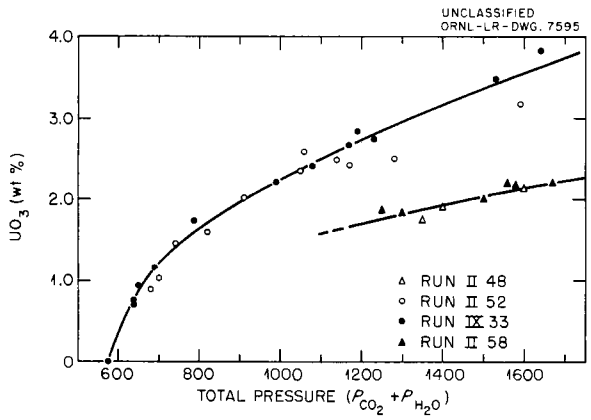

Fig. 52. Per Cent of UO_3 in Liquid Phase; System Li_2O-UO_3-CO_2-H_2O.

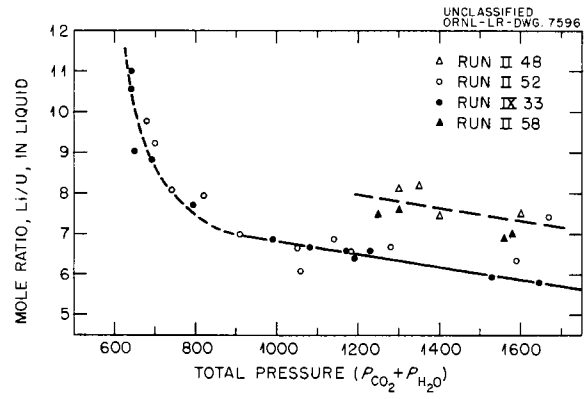

Fig. 53. Mole Ratios of Li to U in Liquid Phase; System Li_2O-UO_3-CO_2-H_2O.

Summary and Conclusions

Some preliminary solubility data for the systems Na_2O-UO_3-CO_2-H_2O, Li_2O-UO_3-CO_2-H_2O, and MgO-UO_3-CO_2-H_2O have been obtained at 250°C up to approximately 1000 psi of CO_2. On the basis of these data, some deductions about the solid phases in equilibrium with the solutions are made, and tentative phase diagrams are presented. In addition, the solubility of UO_3 or UO_2CO_3 as a function of CO_2 gas pressure and temperature from 150 to 290°C is mentioned, and an order of magnitude of solubility is given.

TABLE 33. THE SYSTEM Li_2O-UO_3-CO_2-H_2O AT 250°C

Run No.	Total Mixture[a] (%)		Liquid Phase[b] (%)		Total Pressure[c] (psi)	Agitation Time[d] (hr)	Mole Ratio Li/U in Liquid
	UO_3	Li_2O	UO_3	Li_2O			
II-48-1	3.043	0.9440	2.15	0.850	1600	1	7.57
2			1.91	0.743	1400	2	7.45
3			1.76	0.754	1350	2	8.20
4			1.76	0.753	1350	1	8.19
II-50-1	3.043	0.9435	0.061	0.131	600	2	41.1
2			0.046	0.121	600	2	50.4
3			0.421	0.323	750	1	14.7
II-52-1	8.439	2.616		0.194		1	
2			2.21	0.861	1670	1	7.46
3			3.17	1.055	1590	1	6.37
4			2.42	0.840	1170	1	6.65
5			2.50	0.905	1140	3	6.93
6			2.51	0.881	1280	3	6.72
7			2.60	0.819	1060	2	6.03
8			2.36	0.819	1050	2	6.64
9			2.05	0.753	910	1	7.03
10			1.60	0.666	820	2	7.97
11			1.44	0.603	740	1	8.02
12			1.03	0.496	700	1	9.22
13			0.89	0.451	680	1	9.70
IX-33-1	10.385	2.169	3.83	1.16	1640	4	5.80
2			3.74	1.16	1530	1	5.94
3				0.990	1340	2	
4			2.75	0.947	1230	4	6.59
5			2.85	0.947	1190	1	6.36
6			2.68	0.926	1170	1	6.62
7			2.42	0.840	1080	2	6.65
8			2.22	0.80	990	2	6.9
9			1.73	0.69	790	2	7.6
10			1.18	0.54	690	1	8.8
11			0.96	0.45	650	2	9.0
12			0.75	0.43	640	2	11.0
13			0.70	0.39	640	1	10.7
II-63-1	5.184	0.5447	0.497	0.366		1	14.1
2			0.448	0.366		4	15.6
3			0.439	0.366		2	16.0
4			0.298	0.323		1	20.7
5			0.302	0.323		2	20.5
6			0.336	0.344		3	19.6
7			0.342	0.323		1	18.1
8			0.364	0.344		1	18.1

TABLE 33 (continued)

Run No.	Total Mixture[a] (%)		Liquid Phase[b] (%)		Total Pressure[c] (psi)	Agitation Time[d] (hr)	Mole Ratio Li/U in Liquid
	UO_3	Li_2O	UO_3	Li_2O			
II-58-1	5.564	0.8480	2.17	0.797	1580	1	7.03
2			2.21	0.797	1560	2	6.90
3			2.01		1500	19	
4			1.84	0.732	1300	2	7.62
5			1.87	0.732	1250	1	7.50
II-61-1	5.204	5.206	2.234	0.797	1140		6.83

[a]Points on Jänecke projection on Li_2O-UO_3-H_2O face.
[b]Not corrected for residual CO_2 and are not points on the projection.
[c]50 psi of O_2 introduced at 100°C.
[d]Not cumulative.

TABLE 34. THE SYSTEM Li_2O-UO_3-CO_2-H_2O

Jänecke projection on Li_2O-UO_3-H_2O phase at 250°C and 1500 psi total pressure

Run No.	Total Mixture (%)		Liquid Phase[a] (%)		Extrapolated Value of Li_2O (%) at 0% H_2O	Postulated[b] Solids
	UO_3	Li_2O	UO_3	Li_2O		
	0.000	4.49		0.505	4.40	I
IX-33	10.385	2.169	3.47	1.10	13.9	I + II
II-52	8.439	2.616	3.47	1.10	23.4	I + II
II-61	5.204	5.206	3.47	1.10	68.3	I + II
II-48	3.043	0.9440	2.07	0.81	c	II + III
II-58	5.564	0.8480	2.07	0.81	c	II + III
II-63	5.184	0.5447	0.338	0.325		III

[a]Corrected for residual CO_2 content of sample on the assumption of stoichiometry; see text.
[b]I = Li_2CO_3, II = a lithium uranyl carbonate (possibly with mole ratio Li/U = 2 or less), III = UO_2CO_3.
[c]Not precise enough for accurate extrapolation.

Several experiments indicate that a small pressure of oxygen of the order of 50 psi is necessary to stabilize the U(VI) in solution and thus prevent reduction to U(IV) in type 347 stainless steel and perhaps in titanium containers at 250°C. The use of 30% H_2O_2 for stabilization of these systems resulted in the formation of highly colored soluble complexes which do not precipitate as such and which interfere with a study of the four-component system MO-UO_3-CO_2-H_2O.

At 250°C there was negligible solubility of uranium in the magnesium system. The uranium solubility in the sodium system was of the order of 1.5 g of uranium per liter, and the Na/U ratio is probably unfavorable from neutron-absorption-cross-section considerations. The lithium system seems most feasible at the present time for possible consideration as an aqueous homogeneous reactor fuel that makes use of the low-cross-section stable isotope (σ_{abs} = 0.033; 92.5%). Concentrations of ura-

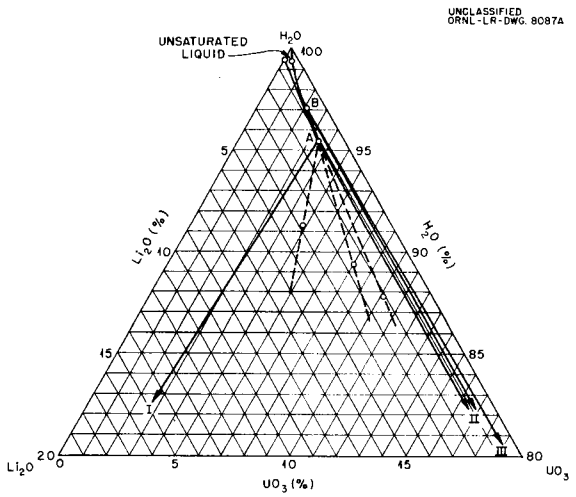

Fig. 54. The System Li_2O-UO_3-CO_2-H_2O at 250°C and at 1500 psi Total Pressure, Where $P_{total} = P_{H_2O} + P_{CO_2}$ (Jänecke Projection). A and B are invariant points.

nium as high as 20 to 25 g/liter at a mole ratio of Li/U ≅ 6 can be attained at 250°C under 1500 to 2000 psi total pressure of CO_2 and H_2O. It is possible that precipitation of UO_4 by an excess of radiation-produced H_2O_2 might be inhibited in these alkaline systems.

The next objective is to make a rather extensive study of the Li_2O-UO_3-CO_2-H_2O system at high temperature as a function of temperature and CO_2 pressure before proceeding to a further evaluation of the other systems.

THE BASE-SATURATED REGION OF THE SYSTEM CuO-UO_3-SO_3-H_2O AT 100°C

F. E. Clark R. Slusher C. H. Secoy

Study of the solid-liquid phase equilibria in the four-component system CuO-UO_3-SO_3-H_2O at 100°C in the region in which the liquid is base-saturated was almost completed. Data embracing all but a small uranium-rich region of the phase diagram from total salt concentrations as low as about 4% up to salt concentrations as high as about 25% are presented. Five points in the three-component system CuO-SO_3-H_2O were obtained, each corroborating and verifying the results of Posnjak and Tunell.[15] Experiments in the uranium portion of the phase diagram indicate that previous work done at 100°C on the three-component system UO_3-SO_3-H_2O is valid[16] and will be compatible with this four-component phase diagram.

Experimental Methods

Solutions of $CuSO_4 \cdot 5H_2O$ in a range of concentrations from 4% $CuSO_4$ through saturation at room temperature served as vehicles for adding the CuO and SO_3 components in the desired quantities; UO_3 was added, by weight, in the form of specially purified $UO_3 \cdot H_2O$.

The components, in the desired concentration, were sealed into 12-mm pyrex tubes. Approximately 7 ml of solution was found to fill each tube to not more than two-thirds its volume, including the addition of the solid component. Consequently, after equilibration, 4 to 6½ ml of liquid could be removed for analyses. The wet solids could be weighed readily in the tubes prior to their dissolution and dilution to volume; aliquots were removed for analyses. In a few instances centrifuging was necessary for a more complete separation of the liquid from the solid phase. The top of the tube was broken off, and the liquid sample was taken by decantation into a sample bottle which was quickly stoppered with a rubber stopper. Every effort was made to maintain the temperature of each experiment at 100°C up to the time of opening the tube. Samples were equilibrated in a specially insulated Precision Unitherm constant-temperature water bath, with Dow-Corning 550 fluid silicone used as the bath medium. Temperature control was maintained to ±1°C by the use of a Fenwal thermoregulator. Equilibration time varied from a minimum of 86 days for one experiment to 151 days for the majority of the tubes. This equilibration time was found necessary in past experience in this laboratory and by other workers.[15,17,18]

The analyses of the liquid samples were carried out as follows. The SO_3 analyses were made by weighing the sample aliquots in previously calibrated 500-μl pipettes and thus obtaining approximate specific-gravity values. The aliquot was

[15] E. Posnjak and G. Tunell, *Am. J. Sci.* 218, 1–34 (1929).

[16] C. H. Secoy, *et al.*, *HRP Quar. Prog. Rep. Oct. 31, 1953*, ORNL-1658, Table 19, p 90.

[17] F. E. Clark and C. H. Secoy, *HRP Quar. Prog. Rep. Oct. 31, 1954*, ORNL-1813, p 168.

[18] S. W. Young and A. E. Stearn, *J. Am. Chem. Soc.* 38, 1947–1953 (1916).

then eluted, with water, through Dowex 50 cation-exchange resin in the hydrogen form,[19,20] and the resultant quantitatively exchanged H_2SO_4 was titrated with approximately 0.1 *N* NaOH. This alkali solution had been standardized by titration against U.S. Bureau of Standards potassium acid phthalate to a pH of 8.6.

Cupric oxide was determined according to the short iodide method for copper as given in *Standard Methods of Chemical Analysis.*[21] The liquid sample was rinsed from the micropipette into a 100-ml beaker, rendered alkaline with NH_4OH, and acidified with glacial acetic acid plus six drops of excess acetic acid; 2 g of solid KI was added, and the liberated iodine was titrated with standardized sodium thiosulfate solution, starch indicator being used for determining the end point. The sodium thiosulfate solution was standardized by titrating it against weighed quantities of copper dissolved in H_2SO_4, and treating as outlined above.

Uranium trioxide was determined by potentiometric titration, employing $Ce(HSO_4)_4$ as the oxidant; this is a modification of the method described by Furman and Schoonover.[22] The uranium-containing solution was made 10 vol % H_2SO_4 and then passed slowly through a Jones reductor; the reductor was thoroughly rinsed with 10% H_2SO_4 to assure quantitative recovery of the uranium, and the reduced solution was then aerated to oxidize trivalent uranium to the tetravalent form. The uranium was then titrated with standard ceric sulfate solution, a Fisher titrimeter equipped with a gold-platinum electrode system being used to detect the end point. The ceric sulfate solution was standardized against U.S. Bureau of Standards As_2O_3 and/or weighed portions of specially purified uranium metal.

A special technique was developed to enable both the CuO and UO_3 to be determined in the same weighed aliquot of each sample. The weighed sample was rinsed into a column of Dowex 1 anion-exchange resin in the sulfate form. The CuO was quantitatively eluted from the column, with distilled water, as $CuSO_4$ into a 100-ml beaker and determined as previously mentioned. The UO_3, which had been quantitatively held in the column, was then quantitatively eluted from the ion-exchange resin with warm (70°C) sulfuric acid and determined by the accepted potentiometric method for uranium.

A special technique was also employed for analyzing the solid phase obtained in experiments 1000, 1006, 1012, 1018, and 1024. In each case the total solid phase, after being separated from the liquid phase and being weighed, was slurried with Dowex 50 cation-exchange resin in the hydrogen form. The solid phase was slowly dissolved, and the free H_2SO_4 was eluted from the resin and titrated with standard NaOH solution. In order to accomplish the elution, it was necessary to transfer the resin quantitatively to a glass column containing several centimeters of clean Dowex 50 resin in the hydrogen form and to continue rinsing until at least four to six resin volumes of water had been used as rinse water. The Cu^{++} was held on the Dowex cation resin; it was then quantitatively eluted from the resin with about six column volumes of 10% H_2SO_4 and determined for CuO, as mentioned previously.

In all cases, except in experiments 1000, 1006, 1012, 1018, and 1024, the solid phase was weighed in the stoppered tube after decantation of the liquid phase and dissolved in a minimum amount of concentrated HCl. The solution was then diluted to a convenient volume, and pipetted aliquots were removed for the SO_3 determination and for the CuO and UO_3. No difficulties were encountered in separating the CuO from the UO_3 by utilizing the anion-exchange resin, unless the concentration of HCl was in excess of that required initially to dissolve the solid phase. The SO_3 content of the solid phases obtained in the remainder of the experiments in this study was determined by precipitating the SO_3 as $BaSO_4$ according to the conventional gravimetric procedure.

Data and Discussion

The results of the analyses of the saturated liquids and the wet residues are given in terms of weight per cent in Table 35. The compositions of the synthetic mixes, known in all cases, are not given, since the linearity of the three points was so good that the third point is superfluous.

[19] O. Samuelson, *Ion Exchangers in Analytical Chemistry*, Wiley and Sons, New York, 1953.

[20] H. O. Day, Jr. *et al.*, *Anal. Chem.* 26, 611 (1954).

[21] W. W. Scott, *Standard Methods of Chemical Analysis*, 5th ed., Vol. 1, 371–372, Van Nostrand, New York, 1939.

[22] N. H. Furman and I. C. Schoonover, *J. Am. Chem. Soc.* 53, 2561–2571 (1931).

TABLE 35. ANALYSES OF SATURATED LIQUID AND WET RESIDUES IN THE SYSTEM $CuO-UO_3-SO_3-H_2O$ EQUILIBRATED AT 100°C

Sample No.	Saturated Liquid				Wet Residue			Solid Phase
	CuO (%)	UO_3 (%)	SO_3 (%)	Specific Gravity (~25°C)	CuO (%)	UO_3 (%)	SO_3 (%)	
1000	1.89	0	2.00	1.0374	19.46	0	7.92	$3CuO \cdot SO_3 \cdot 2H_2O$
1001	0.90	2.64	1.63	1.0468	25.20	0.95	9.49	$3CuO \cdot SO_3 \cdot 2H_2O$
1002	0.40	3.88	1.48	1.0532	19.41	35.82	6.85	Solid solution
1003	0.33	5.01	1.40	1.0627	10.68	49.27	4.01	Binary
1004	0.30	5.02	1.39	1.0621	6.37	52.38	2.61	Binary
1005	0.30	5.10	1.40	1.0626	4.60	57.76	1.94	Binary
1006	2.65	0	2.78	1.0541	28.89	0	11.00	$3CuO \cdot SO_3 \cdot 2H_2O$
1007	1.60	2.78	2.39	1.0639	17.41	2.61	7.36	$3CuO \cdot SO_3 \cdot 2H_2O$
1008	0.73	5.33	2.05	1.0759	19.39	13.06	7.69	Solid solution
1009	0.40	6.95	1.91	1.0889	14.56	35.05	5.66	Binary
1010	0.40	6.98	1.91	1.0894	8.10	42.78	3.49	Binary
1011	0.40	7.06	1.91	1.0892	6.76	51.83	2.86	Binary
1012	3.44	0	3.60	1.0708	41.14	0	15.81	$3CuO \cdot SO_3 \cdot 2H_2O$
1013	2.40	2.65	3.21	1.0800	23.66	3.23	9.60	$3CuO \cdot SO_3 \cdot 2H_2O$
1014	1.18	5.96	2.74	1.0968	25.05	3.90	10.28	$3CuO \cdot SO_3 \cdot 2H_2O$
1015	0.60	8.47	2.51	1.1122	21.80	31.85	8.33	Solid solution
1016	0.50	9.01	2.45	1.1185	12.36	40.90	5.14	Binary
1017	0.51	9.19	2.46	1.1195	9.67	51.98	4.02	Binary
1018	4.18	0	4.37	1.0877	32.77	0	12.63	$3CuO \cdot SO_3 \cdot 2H_2O$
1019	3.19	2.54	3.99	1.0983	17.55	2.76	8.04	$3CuO \cdot SO_3 \cdot 2H_2O$
1020	1.85	6.02	3.48	1.1128	16.25	3.72	7.91	$3CuO \cdot SO_3 \cdot 2H_2O$
1021	0.91	9.08	3.08	1.1316	23.24	24.44	9.26	Solid solution
1022	0.60	11.07	2.93	1.1478	19.80	39.72	7.61	Binary
1023	0.60	11.00	2.92	1.1478	12.55	49.12	5.18	Binary
1024	8.77	0	9.02	1.2019	27.75	0	10.77	$3CuO \cdot SO_3 \cdot 2H_2O$
1025	8.47	0.66	8.88	1.2044	34.59	0.38	13.64	$3CuO \cdot SO_3 \cdot 2H_2O$
1026	8.14	1.35	8.77	1.2070	51.67	0.33	21.67	$3CuO \cdot SO_3 \cdot 2H_2O$
1027	7.75	2.44	8.59	1.2117	29.76	1.33	12.83	$3CuO \cdot SO_3 \cdot 2H_2O$
1028	5.93	5.74	7.99	1.2245	26.32	3.95	12.28	$3CuO \cdot SO_3 \cdot 2H_2O$
1029	4.07	11.19	7.06	1.2476	31.33	5.99	13.70	$3CuO \cdot SO_3 \cdot 2H_2O$
1030	2.43	16.18	6.30	1.2807	31.30	8.86	13.68	$3CuO \cdot SO_3 \cdot 2H_2O$
1031	0.94	18.00	4.65	1.2644	15.17	41.49	9.40	Probably ternary

The synthetic mixes were prepared in five sets, as indicated in the arrangement of the table, each set consisting of variable additions, in increasing amounts, of solid $UO_3 \cdot H_2O$ to a fixed concentration of stoichiometric copper sulfate solution. The nominal concentrations of the starting $CuSO_4$ solutions were 4, 6, 8, 10, and 18% $CuSO_4$, respectively. The first member of each set contained no added $UO_3 \cdot H_2O$ and thus provided not only a starting point for each set in the quaternary system but also gave a value in the ternary system $CuO-SO_3-H_2O$. It is of interest to note, as has already been shown by Posnjak and Tunell,[15] that stoichiometric copper sulfate solutions are

not stable at 100°C over the concentration range studied and will yield a precipitate of the basic salt, $3CuO \cdot SO_3 \cdot 2H_2O$.

The nature of the liquidus surface in the portion of the quaternary system studied is shown by the projections of Fig. 55. The isobaric, isothermal diagram for such a system is perhaps most completely shown in a regular tetrahedron or by various projections of surfaces and lines to the faces of the tetrahedron. In the system under discussion, neither the usual orthogonal projection nor the Jänecke projection from the H_2O apex of the tetrahedron is satisfactory, since the surface to be projected is nearly parallel with the direction

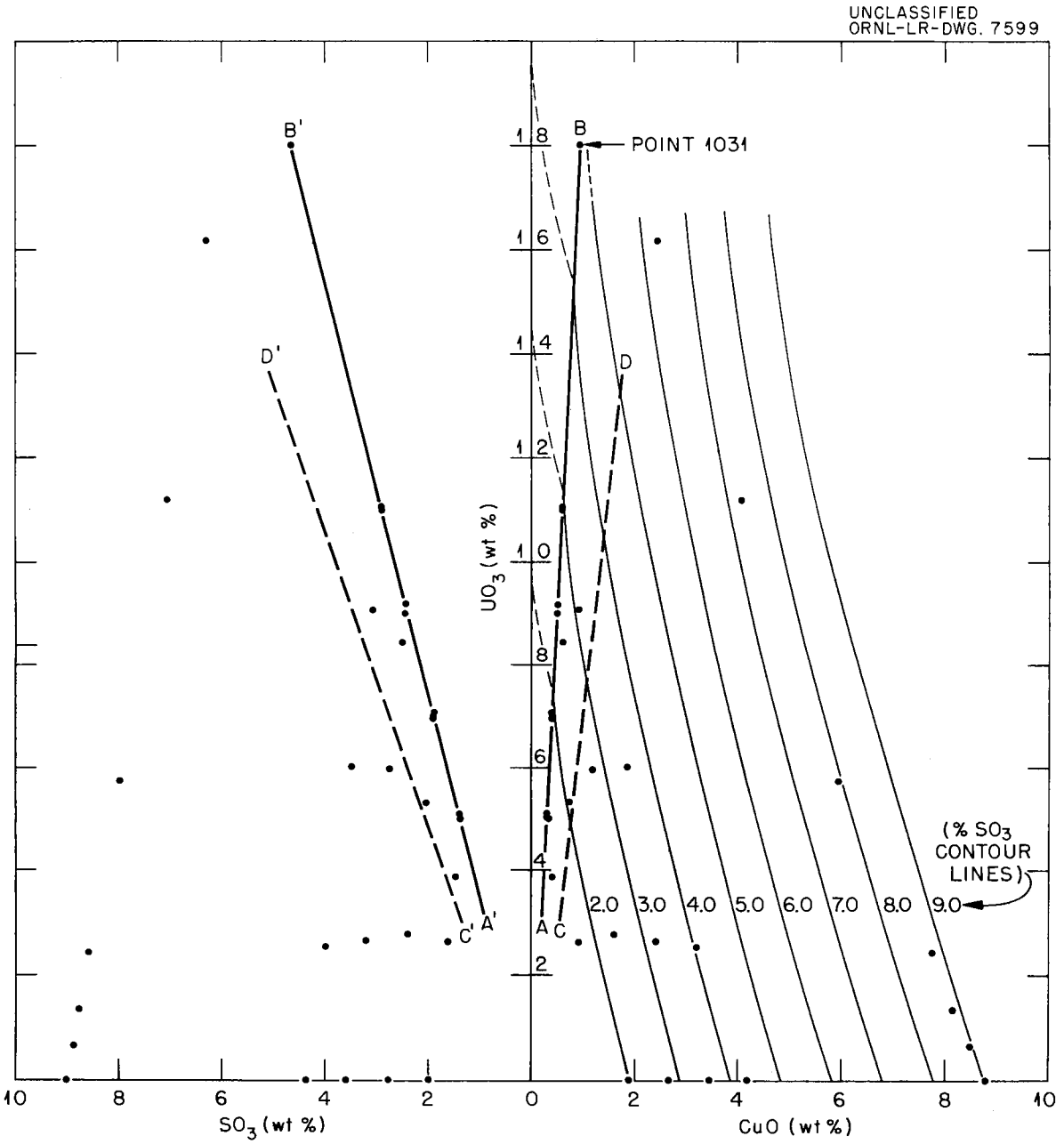

Fig. 55. Liquidus Surface in the System $CuO-UO_3-SO_3-H_2O$ at 100°C.

of projection. Therefore, in Fig. 55, projection parallel to an edge of the tetrahedron, sometimes called the Schreinemakers projection, was employed. The data have been plotted with orthogonal coordinates rather than with trilinear ones. Weight per cents are read directly from the graph, and the per cent H_2O at any pair of points (one in the UO_3-CuO projection and a corresponding point in the UO_3-SO_3 projection) may be readily obtained by subtracting the sum, $UO_3 + CuO + SO_3$, from 100.

The constant-SO_3 contour lines shown on the UO_3-CuO portion of the diagram were obtained by graphical interpolation in the following manner. Each set of data follows a smooth but arbitrary path across the liquidus surface. For each set, a smooth curve was drawn through the points obtained by plotting the per cent SO_3 against the UO_3 fraction of CuO + UO_3. Values for the per cent SO_3 at a constant UO_3 fraction read from these curves were found to give straight lines when plotted against the per cent total salt. This is equivalent to saying that the liquidus surface has no curvature if a path of constant $UO_3/(CuO + UO_3)$ ratio is followed. Values of this ratio and of the per cent total salt at constant per cent SO_3 could therefore be obtained from the graphs and the per cent of each component readily calculated.

The identities of the solids were established by a study of projections of the tie lines. Tie lines for the first two or three points of each set and for all but the last point of the most concentrated set project close to the theoretical composition of the mineral antlerite, $3CuO \cdot SO_3 \cdot 2H_2O$. Microscopic examination of these solids agreed with Posnjak and Tunell's description. Therefore the conclusion is reached that this compound is the stable solid phase in equilibrium with solutions over a major portion of the liquidus surface. This conclusion should and will be verified or disproved by obtaining the x-ray diffraction pattern for the solids.

The fact was noted that the CuO-to-SO_3 mole ratio was nearly constant and was approximately 3 in all the wet residues except the residue from tube 1031. This suggested immediately that the remaining solids were either a mixture of antlerite and $UO_3 \cdot H_2O$ (known to be the stable solid phase along the UO_3-SO_3-H_2O side of the diagram) or a series of solid solutions whose compositions could be represented by a combination of varying amounts of these two compounds. It was also noted that the composition of the liquid phase in the last two or three points of each set except the fifth was essentially constant in spite of the fact that the synthetic mix varied markedly. Furthermore, these liquid points lie on a smooth curve, line *AB* in Fig. 55. This strongly suggests that the solid is a binary mixture. In order to prove that this is the case, the algebraic equation for each tie line was solved simultaneously with the algebraic equation for the line connecting the two compounds, antlerite and $UO_3 \cdot H_2O$. The calculated intersection points are given in Table 36, and the projections of these points are shown in Fig. 56. Obviously, the compositions of all solids except the solid from tube 1031 can be accurately represented by combinations of antlerite and $UO_3 \cdot H_2O$.

Four of the liquid points falling in the region between lines *CD* (position not known accurately) and *AB* in Fig. 55 also gave solid compositions falling on the antlerite–$UO_3 \cdot H_2O$ line. These liquid points are scattered over an area and could not lie on any sensible continuous curve. The solid therefore must consist of a single phase, and the only reasonable interpretation is that it is a solid solution. The limit of solubility appears to be about 1.5 moles of $UO_3 \cdot H_2O$ to 1 mole of antlerite. Any $UO_3 \cdot H_2O$ in excess of this amount appears as a second solid phase, and the liquid points then fall on the binary line, *AB*. These conclusions must be checked by x-ray studies before they can be accepted without question.

Point 1031 does not follow the pattern established by the last points of each of the four more dilute sets in either the liquid phase or the solid. Microscopic examination of the solid indicated the probable presence of three solid phases. The liquid point 1031 probably represents a ternary in the system and therefore should lie at the intersection of three binary lines, one of which is the line *AB*. Visual observation of tubes containing compositions in this vicinity and now in the process of equilibration appears to support this interpretation. The third solid phase in the ternary may well be $5UO_3 \cdot 2SO_3 \cdot xH_2O$, the basic uranyl sulfate, previously found to exist at the higher

concentrations in the three-component system,[23] UO_3-SO_3-H_2O.

Additional compositions, now in the process of equilibration, are designed to give information at lower concentrations (2% $CuSO_4$); in the $UO_3 \cdot H_2O$ region between the binary *AB* and the UO_3 axis in Fig. 55; concerning the exact position of the line *CD*; and at higher concentrations, particularly in the region beyond the point *B*.

[23] C. H. Secoy, *et al.*, *HRP Quar. Prog. Rep. Oct. 31, 1953*, ORNL-1658, Table 19, p 90.

TABLE 36. INTERSECTION POINTS OF EXTRAPOLATED TIE LINES WITH THE LINE REPRESENTING MIXTURES OF $UO_3 \cdot H_2O$ AND $3CuO \cdot SO_3 \cdot 2H_2O$

Sample No.	Composition (%)				Solid Phase
	CuO	UO_3	SO_3	H_2O	
$3CuO \cdot SO_3 \cdot 2H_2O$	67.27	0	22.57	10.16	Theoretical composition
1000	66.23	0	23.67	10.10	$3CuO \cdot SO_3 \cdot 2H_2O$
1001	68.37	−2.05	23.45	10.23	$3CuO \cdot SO_3 \cdot 2H_2O$
1006	66.94	0	22.92	10.14	$3CuO \cdot SO_3 \cdot 2H_2O$
1007	65.41	2.09	22.46	10.14	$3CuO \cdot SO_3 \cdot 2H_2O$
1012	66.04	0	23.88	10.08	$3CuO \cdot SO_3 \cdot 2H_2O$
1013	63.99	4.33	21.73	9.95	$3CuO \cdot SO_3 \cdot 2H_2O$
1014	66.26	0.34	23.30	10.10	$3CuO \cdot SO_3 \cdot 2H_2O$
1018	67.25	0	22.59	10.16	$3CuO \cdot SO_3 \cdot 2H_2O$
1019	67.10	−1.30	24.05	10.15	$3CuO \cdot SO_3 \cdot 2H_2O$
1020	70.07	−0.488	24.47	10.34	$3CuO \cdot SO_3 \cdot 2H_2O$
1024	74.33	0	15.06	10.61	$3CuO \cdot SO_3 \cdot 2H_2O$
1025	69.66	0.41	19.62	10.31	$3CuO \cdot SO_3 \cdot 2H_2O$
1026	64.51	0.29	25.21	9.99	$3CuO \cdot SO_3 \cdot 2H_2O$
1027	69.82	−0.69	20.55	10.32	$3CuO \cdot SO_3 \cdot 2H_2O$
1028	68.38	0.26	21.13	10.23	$3CuO \cdot SO_3 \cdot 2H_2O$
1029	68.15	−1.03	22.66	10.22	$3CuO \cdot SO_3 \cdot 2H_2O$
1030	67.23	−0.25	22.86	10.16	$3CuO \cdot SO_3 \cdot 2H_2O$
1008	49.01	25.33	16.65	9.01	$3CuO \cdot SO_3 \cdot 2H_2O \cdot 0.43\ UO_3 \cdot H_2O$
1021	40.83	36.54	14.04	8.49	$3CuO \cdot SO_3 \cdot 2H_2O \cdot 0.75\ UO_3 \cdot H_2O$
1015	34.39	45.73	11.79	8.09	$3CuO \cdot SO_3 \cdot 2H_2O \cdot 1.11\ UO_3 \cdot H_2O$
1002	29.58	52.92	9.72	7.78	$3CuO \cdot SO_3 \cdot 2H_2O \cdot 1.49\ UO_3 \cdot H_2O$
1022	28.98	53.42	9.85	7.75	Binary: solid solution* + $0.04(UO_3 \cdot H_2O)$
1009	26.00	57.75	8.69	7.56	Binary: solid solution + $0.35(UO_3 \cdot H_2O)$
1016	21.13	64.48	7.13	7.26	Binary: solid solution + $1.05(UO_3 \cdot H_2O)$
1023	18.50	68.10	6.31	7.09	Binary: solid solution + $1.57(UO_3 \cdot H_2O)$
1003	15.95	71.79	5.33	6.93	Binary: solid solution + $2.25(UO_3 \cdot H_2O)$
1010	14.72	73.58	4.85	6.85	Binary: solid solution + $2.67(UO_3 \cdot H_2O)$
1017	14.38	73.98	4.82	6.82	Binary: solid solution + $2.79(UO_3 \cdot H_2O)$
1011	10.66	79.30	3.45	6.59	Binary: solid solution + $4.71(UO_3 \cdot H_2O)$
1004	9.93	80.19	3.33	6.55	Binary: solid solution + $5.24(UO_3 \cdot H_2O)$
1005	6.79	84.64	2.22	6.35	Binary: solid solution + $8.90(UO_3 \cdot H_2O)$
$UO_3 \cdot H_2O$	0	94.08	0	5.92	Theoretical composition
1031	24.05	56.15	12.36	7.44	Probably ternary

*Solid solution = $3CuO \cdot SO_3 \cdot 2H_2O \cdot 1.5(UO_3 \cdot H_2O)$.

[redacted]

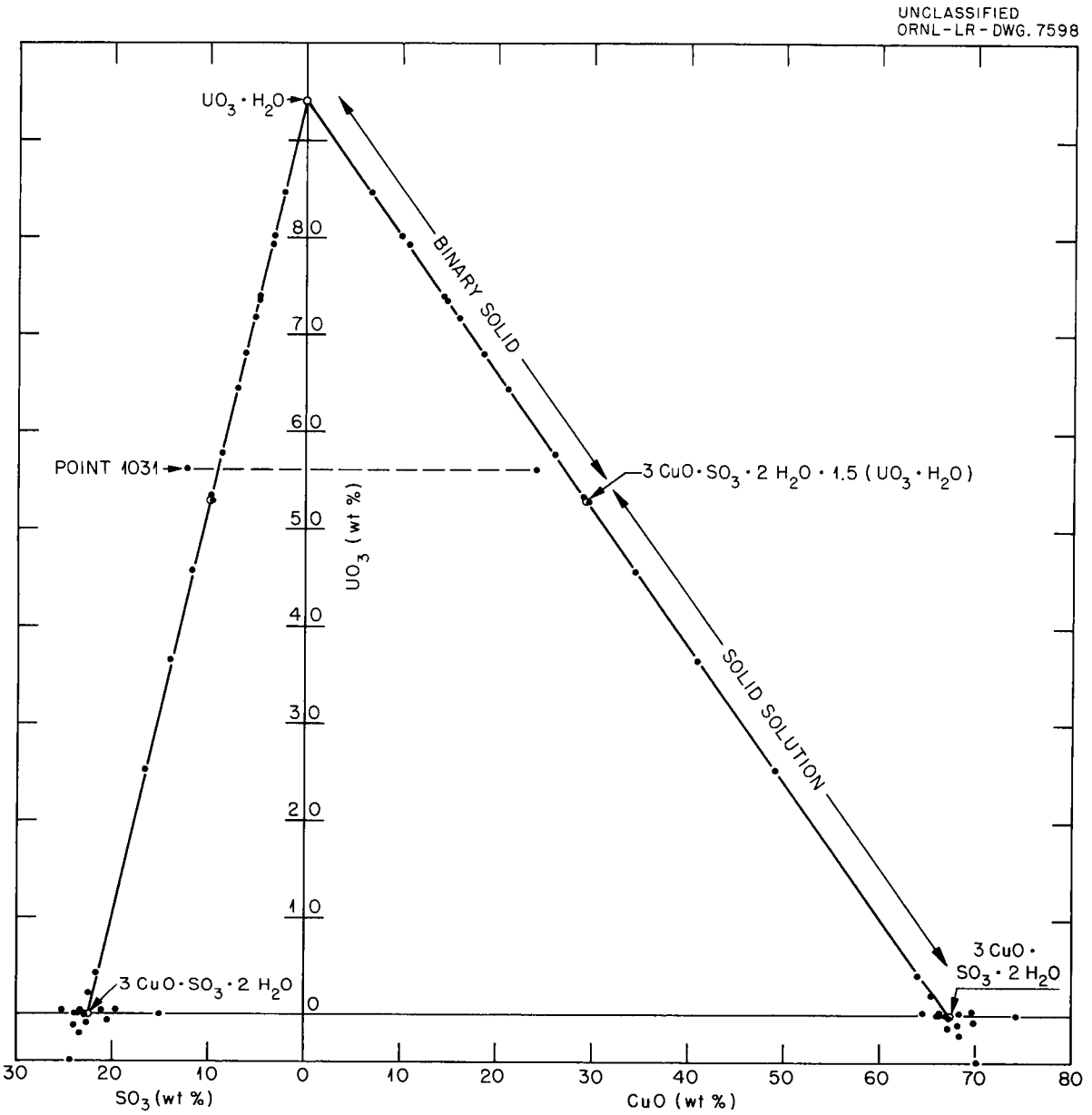

Fig. 56. Projection of the Intersection Points of the Extrapolated Tie Lines with the Line Connecting the Compositions $3CuO \cdot SO_3 \cdot 2H_2O$ and $UO_3 \cdot H_2O$.

[redacted]